Modélisation du comportement hydrodynamique des pompes pour des fluides au comportement rhéologique complexe

Lila Achour

HESAM UNIVERSITÉ

Arts et Métiers Sciences et Technologies

ECOLE DOCTORALE SCIENCES ET METIERS DE L'INGENIEUR

Laboratoire d'ingénierie des fluides et des systèmes énergétiques (LIFSE) - Campus de Paris

THÈSE

Présentée par **Lila ACHOUR**

Soutenue le 17 juillet 2023

Pour obtenir le grade de **Docteur d'HESAM Université**

Préparée à **l'Ecole Nationale Supérieure d'Arts et Métiers**

Spécialité : mécanique

Hydrodynamic behavior modeling of pumps handling fluids with complex rheological behavior

Thèse dirigée par :

Madame ACHOUR Lila

et encadrée par :

Monsieur KOUIDRI Smaïne

		Jury
M. Kacem MANSOURI	Pr, LEMI, UMB Boumerdès	Président
M. Nicolàs Rios RATKOVICH	Pr, UNIANDES Universidad de los Andes, Colombie	Rapporteur
M. Hocine TEBBICHE	Dr, MC UMMTO Tizi Ouzou	Rapporteur
M. Smaïne KOUIDRI	Pr, LIFSE, Arts et Métiers	Directeur
M. Idir BELAIDI	Pr, LEMI, UMB Boumerdès	Directeur
M. Mathieu SPECKLIN	Dr, MC LIFSE, Arts et Métiers	Co-encadrant
M. Miguel ASUAJE	Pr, Université Simón Bolivar, Venezuela	Invité

THÈSE

Praise be to Allâh through Whom good things come to pass.

Acknowledgements

I would like to thank all the people who have provided me with much-needed support, guidance, and inspiration throughout the extraordinary journey that has led me to the completion of this doctoral thesis. The most important ones, without whom I would not have been able to complete the work presented here, and to whom I, therefore, owe my deepest gratitude, are mentioned below:

First, I would like to thank my supervisor Pr Belaidi Idir, for giving me this precious opportunity to pursue a PhD and for opening up a maximum of opportunities. For his support at all levels and his caring personality toward his Ph.D. students. I will always remember and appreciate your constant attention and support.

On a more personal note, I must express my special thanks to Prof. Kouidri, my thesis supervisor at ENSAM, for giving me the valuable opportunity to learn about an interesting topic that touches on many aspects of physics. His personal dedication and passion are always my greatest motivation to push the limits and achieve breakthroughs. Most importantly, I must express my gratitude for her personal attention to all aspects of my life that allows me to pursue my research in a serene environment.

I would especially like to thank my co-supervisor, Dr. Specklin Mathieu, who accompanied me at every step of my work, advising and guiding me. I also greatly appreciate the precious time he devoted to proofreading my work and the many constructive suggestions he made.

Prof. Asuaje Miguel deserves my deep gratitude for his advice on the work I am doing, his suggestions, and his invaluable help.

I would like to thank the many people who made my secondment to LIFSE one of the most productive periods of my Ph.D. years. Pr Khelladi and Pr Bakir welcomed me with open arms in their laboratory and gave me all the support I could dream of.

Finally, I would like to express my deepest gratitude to my mother who has given me every conceivable support throughout my academic career.

Not only has my doctoral journey been extremely instructive from a scientific point of view, but it has also allowed me to make friendships across national and cultural barriers.

Résumé

Les travaux de recherche de la thèse portent sur le pompage de fluides au comportement rhéologique complexe. L'objectif de la thèse est d'effectuer une analyse exhaustive des performances et des caractéristiques d'écoulement interne d'une pompe centrifuge à volute lors du traitement d'émulsions non newtoniennes complexes. Les applications industrielles dans ce domaine sont nombreuses et peuvent inclure le pompage d'émulsions de pétrole brut, le pompage d'eaux usées, et les émulsions cosmétiques et alimentaires. Deux éléments se combinent pour expliquer la complexité de ce problème scientifique : le premier concerne la pompe et sa géométrie tridimensionnelle avec un fort couplage avec la boucle. Le second concerne le comportement rhéologique non linéaire et instable du fluide pompé, en particulier lorsque la pompe transporte une fraction réduite de la phase continue. Ces écoulements concernent des fluides au comportement non newtonien et particulièrement instable. Les connaissances nécessaires à leur compréhension sont parfois à la limite de la chimie avec des approches à l'échelle moléculaire. Dans ce travail, plusieurs approches ont été utilisées pour étudier le comportement hydrodynamique de la pompe sous écoulement d'émulsion : une approche analytique, une simulation CFD monophasique et une simulation CFD diphasique. L'approche analytique est basée sur un modèle mécaniste pour la détermination de la viscosité de l'émulsion en fonction des conditions de fonctionnement de la pompe, qui est ensuite couplé à un modèle mécaniste basé sur les différentes pertes rencontrées dans les pompes à volute. La simulation monophasique est basée sur une étude CFD dans laquelle le comportement rhéologique des émulsions a été considéré en négligeant la nature diphasique du fluide, et l'étude diphasique qui considère les deux fluides et les différentes interactions entre les phases. Les approches adoptées appartiennent à deux catégories distinctes ; l'approche analytique permet de différencier les pertes au sein de la pompe centrifuge, ce qui n'est pas le cas pour la CFD. Cette lacune est toutefois compensée par l'analyse entropique, qui permet de localiser les pertes d'énergie. Enfin, la capacité des deux approches CFD considérées à prédire avec précision les performances des pompes véhiculant des émulsions est évaluée en comparant les résultats numériques d'une pompe multicellulaire (ESP) avec les données expérimentales correspondantes.

Abstract

The thesis research work addresses the pumping of fluids with complex rheological behavior. The aim of the thesis is to carry out an exhaustive analysis of the performance and internal flow features of a volute centrifugal pump when handling complex non-Newtonian emulsions. The industrial applications in this field are numerous and can include crude oil emulsion pumping, wastewater pumping, and cosmetic and food emulsions. Two elements combine to explain the complexity of this scientific problem: the first involves the pump and its three-dimensional geometry with a strong coupling with the loop. The second concerns the nonlinear and unstable rheological behavior of the pumped fluid, especially when the pump carries a reduced fraction of the continuous phase. These flows concern fluids with non-Newtonian and particularly unstable behavior. The insights needed to achieve their understanding are sometimes at the limit of chemistry with approaches at the molecular scale. In this work, several approaches were used to study the hydrodynamic behavior of the pump under emulsion flow: an analytical approach, a single-phase CFD simulation, and a two-phase CFD simulation. The analytical approach is based on a mechanistic model for the determination of the emulsion viscosity as a function of the pump operating conditions, which is then coupled to a mechanistic model based on the different losses encountered in volute pumps. The single-phase simulation is based on a CFD study in which the rheological behavior of the emulsions has been considered neglecting the two-phase nature of the fluid, and the two-phase study which considers the two fluids and the different interactions between the phases. The approaches adopted belong to two distinct categories; the analytical approach allows for differentiation of the losses within the centrifugal pump, which is not the case for CFD. However, this shortcoming is compensated for by the entropy analysis, which allows for the localization of energy losses. Finally, the ability of the two CFD approaches considered to accurately predict the performance of pumps handling emulsions is evaluated by comparing the numerical results of a multistage pump (ESP) with the corresponding experimental data.

Contents

List of Tables

List of Figures

Introduction

Turbomachinery, and in particular centrifugal pumps, play a fundamental role in many industrial processes. They are widely used in various engineering sectors, such as the pharmaceutical industry, chemical processes, wastewater treatment, power generation, and the oil industry.

Centrifugal pumps have been studied and perfected to build efficient pumps for specific functions in a wide range of applications. Despite the vast amount of information known about pump design, centrifugal pumps used for unconventional fluids, such as emulsions, have many critical considerations. For instance, significant complications related to the properties of these emulsions, such as their complex, non-Newtonian rheological behavior, remain and are associated with the degradation of pump performance and complications in pump operation. This also implies an increase in the energy required for its operation.

Emulsions and two-phase liquid-liquid flows are present in almost all technical and industrial processes. An example of this type of flow is the liquid-liquid mixture of water and viscous oil commonly found in the oil industry. An important characteristic of these mixtures is their non-Newtonian rheology, in particular, a shear-thinning behavior [1, 2] and an apparent viscosity that is generally higher than the viscosity of the separate liquids [3-5]. The rheology of these fluids varies with the microstructure of the emulsion [4, 9, 10], the chemistry of the coexisting phases, and their stability [11-13]. In addition, the shear stresses and forces acting on the liquid-liquid dispersions define the rheological behavior of these mixtures.

Given the considerable influence of non-Newtonian rheology and emulsion flows on pump performance, research on centrifugal pumps handling non-Newtonian oil-water dispersions has gained importance in recent years. Some studies have been conducted on the influence of viscosity on pump performance by developing mechanistic models and semi-empirical correlations. These studies provide semi-empirical models that depend on the pump geometry and fluid viscosity to calculate the theoretical degradation of the associated head, but these correlations find their limits when the fluid is two-phase and non-Newtonian. Furthermore, the empirical aspect of these models raises questions regarding their universal validity for inferring the pump performance when handling emulsions. On the other hand, this topic has been the subject of many experimental and computational studies. However, these studies have focused on the analysis of the overall performance of a multistage pump carrying emulsions, but no study has focused on a centrifugal volute pump and the effect of the rheological behavior of these fluids on the volute pump. In addition, the manufacturing history of pumps carrying non-Newtonian fluids can also be difficult because the fluid characteristics can change abruptly in a short period of time [24] and these different physical processes can become limiting at different scales of the pump. For centrifugal pumps carrying non-Newtonian fluids, the influence of pump size on the complex rheological behavior of the pumped fluid has not been studied, and the underlying cause and mechanism of hydraulic loss caused by non-Newtonian rheology is not clearly illustrated in the literature. Thus, the lack of knowledge about the effect of pump size on the non-Newtonian behavior of the fluid means that scaling up a centrifugal pump directly from the laboratory to the industrial scale remains an open problem. This hinders the

selection of centrifugal pumps for application to non-Newtonian fluids. Therefore, research is needed to study the energy loss induced by the flow of non-Newtonian fluids in a volute centrifugal pump.

The main objective of this thesis is to investigate the hydrodynamic behavior of a centrifugal volute pump handling emulsions with different dispersed phase volume fractions. In addition, to perform a complete analysis of the overall performance and internal flow characteristics of this volute pump when handling these complex flow systems. The study involves a complementary objective which is the study of the effect of the pump size on the mixture. In this study, several approaches were used to investigate the hydrodynamic behavior of the pump under emulsion flow: an analytical approach, a single-phase CFD simulation, and a two-phase CFD simulation. The analytical approach is based on a mechanistic model for the determination of the emulsion viscosity as a function of the pump operating conditions, which is then coupled to a mechanistic model based on the different losses encountered in volute pumps. The single-phase simulation is based on a CFD study in which the rheological behavior of the emulsions has been considered neglecting the two-phase nature of the fluid, and the two-phase study which considers the two fluids and the different interactions between the phases. The adopted approaches fall under two separate categories; the analytical approach allows for the differentiation of the losses within the centrifugal pump, whereas CFD does not. However, this shortcoming is compensated by the entropy analysis, which allows for the localization of the energy loss.

To this end, we have structured our manuscript as follows:

Chapter 1 presents a state-of-the-art on emulsion pumping and a presentation of the various fundamental concepts related to emulsions and their characterizations within pumps.

Chapter 2 analyzes the influence of the emulsion flow on the characteristic curves of a centrifugal pump by an analytical method. For this purpose, a rheological model of the emulsion in centrifugal pumps proposed in the literature has been adapted to the studied emulsions and has been coupled with a loss model for the prediction of the pump performance.

Chapter 3 analyzes numerically the performance and flow characteristics of a centrifugal volute pump when handling emulsions and oil-water mixtures at different water cuts (WC) considering their experimentally determined non-Newtonian rheological behavior and compares its performance when operating with a Newtonian viscous oil. The effect of the pump size on the rheological behavior of the mixtures is also studied in this chapter.

Chapter 4 aims to investigate the hydraulic losses and performance degradation mechanism of the volute centrifugal pump considered in this study when handling non-Newtonian emulsions using the entropy generation method, focusing on the influence of the emulsion type on the loss mechanism. The influence of pump size on the energy loss in the centrifugal pump is also considered.

Chapter 5 analyzes the hydrodynamic behavior and overall performance of the volute pump conveying emulsions with two-phase modeling. This modeling provides a wider scope of the system allowing the consideration of the two-phase nature of the fluid and the different interactions between the phases.

A general conclusion, synthesizing all the work done, and the results obtained, as well as perspectives for further development, complete this manuscript.

CHAPTER 1

State of the art

Contents

This chapter summarizes the state of the art on emulsion pumping. The first two sections introduce the main concepts related to emulsions and liquid-liquid dispersions with their effect on pump performance. The behavior and characterization of emulsions, particularly within centrifugal pumps, are discussed in section 1.3. Finally, methods for modeling centrifugal pumps under emulsion flow are presented in section 1.4.

1.1 Liquid-liquid dispersions and emulsions

An emulsion is a mixture of two immiscible liquids, where one liquid is dispersed in the form of droplets (dispersed phase) in another liquid (continuous phase). There are two main types of emulsions, namely single and multiple emulsions. The single emulsions are composed of two phases (hydrophilic and lipophilic) that can be a water-in-oil (W/O) emulsion or an oil-in-water (O/W) emulsion. Multiple emulsions consist of two lipophilic phases and a hydrophilic phase or two hydrophilic phases and a lipophilic phase. The structure of multiple emulsions is complicated and consists of tiny droplets within larger droplets, which are dispersed in a continuous phase. These multiple emulsions can be the state of an intermediate emulsion during the inversion of a simple O/W to a W/O emulsion or vice versa. The types of emulsion are shown in Figure 1.1.

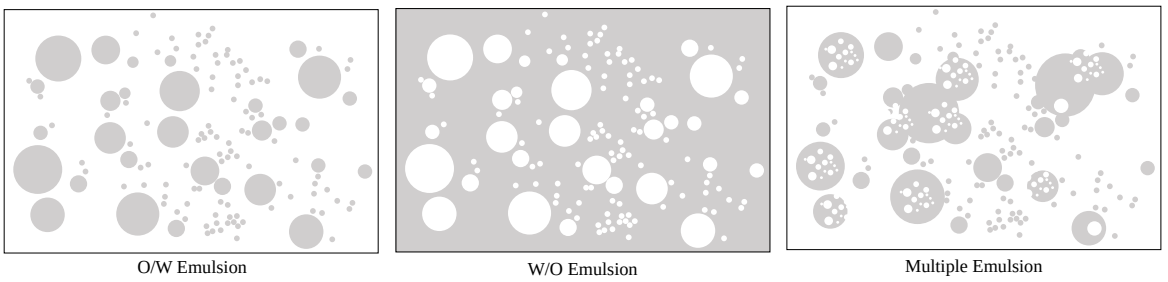

Figure 1.1: Types of emulsions

These emulsions are present in many sectors, including pharmaceutical or chemical processes, wastewater treatment, and petroleum industries. In some industries, these fluids are desirable, but in others, their presence is not desired, as is the case in the petroleum industry. Emulsions are typically formed when the oil and water phases are brought together in a process called emulsification, which is enhanced by proper mixing and/or the presence of a surfactant. High shear promotes emulsification; however, the two coexisting phases tend to separate based on their density differences in the absence of an emulsifier. Thus, this type of emulsion is called unstable due to the unfavorable interface between the two phases.

When the emulsion is formed naturally, the case of oil fields for example, its composition is not only limited to an aqueous and oily phase, but it can also contain surfactants, solid particles, and possibly gas [1]. Surfactants and solid particles are promising emulsification components. Surfactants possess hydrophilic and hydrophobic characteristics, which allows them to interact with the aqueous and oily interface respectively, and to decrease the free energy of these interfaces. This leads to the reduction of the interfacial tension, thus improving the emulsification. Solid particles, on the other hand, generally stabilize the emulsion mechanically, and the effectiveness of stabilization depends on particle interactions, particle size, and material wettability, among other things.

1.2 Performance of centrifugal pumps handling emulsions

Centrifugal pumps, a type of rotary-dynamic pump, are generally designed to convey water or an incompressible fluid of low viscosity. However, they are primarily used in many technical processes where the working fluids are a mixture of two immiscible liquids that form an emulsion. When handling emulsions, which have the characteristic of being highly viscous and exhibiting complex non-Newtonian behavior, it is expected that the centrifugal pumps will experience operating complications and performance degradation. In this regard, several studies have shown that the flow of an oil-in-water emulsion reduces the head and flow rate of centrifugal pumps [2]. In addition, the volume fraction of the dispersed phase of an emulsion can affect the pump performance in terms of pressure drop and flow rate. A higher volume fraction of the dispersed phase results in a higher pressure drop and lower flow rate, where the effect of a progressively-increasing oil concentration, on the pump head, efficiency and power is shown in Figure 1.2.

Pump performance deteriorates when pumping a liquid-liquid dispersion and emulsion because of the complex rheological behavior of these fluids, where it has been reported in the literature that the viscosity of emulsions is higher than that of pure oil and varies with the microstructure of the emulsion [3, 4, 5], the chemistry of the coexisting phases and its stability [6, 7, 8]. Highly viscous fluid results in higher frictional losses in the pump channels, which decreases the head, flow rate, and efficiency of

the pump while increasing energy consumption [9]. Besides, the process of interconversion of the phase configuration (phase inversion phenomenon) causes a dramatic increase in the viscosity of the emulsion, where it has been reported in the literature that the viscosity of the emulsion during the inversion process can be several times the viscosity of the single-phase oil constituting the emulsion [10, 11, 12]. This complex rheological behavior associated with viscosity fluctuations affects as well the flow pattern in the centrifugal pump and thus its performance.

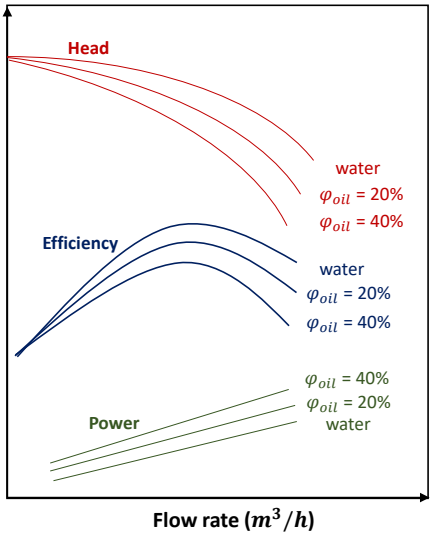

Figure 1.2: Typical illustration of the effect of oil concentration, ϕ_{oil}, on centrifugal pump performance

1.3 Emulsion characterization in pumps

Emulsion characterization can help in understanding the mechanism of pump performance degradation and can provide key information for pump design and operation. The behavior and microstructure of emulsions are highly dependent on the characteristics of the dispersed phase droplets and the production equipment components. In centrifugal pumps, the combined action of shear and centrifugal forces results in both macroscopic and microscopic changes in emulsion characteristics. The high levels of turbulence observed in the impeller promote fragmentation of the dispersed phase droplets, producing smaller droplets and emulsions with different droplet size distributions (DSD). The main parameters that describe the physical behavior of emulsions within pumps are rheology, stability, and phase inversion. Meanwhile, the static parameters intrinsic to its characterization can be described by the size, shape, and droplet size distribution. In the following subsections, an analysis of the emulsion characteristics and its rheological behavior in general and observed in centrifugal pumps is reported. Several typical density functions characterizing the particle size distribution of the emulsion within the pumps are presented along with the definitions of the characteristic diameters.

1.3.1 Stability

Emulsion stability can be characterized through conditions that avoid the coalescence mechanism of dispersed phase droplets. Indeed, a stable emulsion is an emulsion whose dispersed phase is featured by a

very small droplet size. Thus, the coalescence will produce larger dispersed phase droplets and eventually will lead to unstable emulsion [13]. Generally, emulsions are thermodynamically unstable systems owing to the large interfacial area between oil and water molecules [14], and they tend to break over a period of time [15]. However, many factors affect the stability of the emulsions by modifying the interfacial area between the two phases. The stability of the emulsion depends on various processing parameters, including preparation time, temperature, and dispersed phase fraction. For instance, Bellary et al. [11] conducted a study on the effect of water cut and stirring time on the stability of water-in-crude oil emulsion within an electrical submersible pump (ESP). They found that increasing the water content led to a decrease in emulsion stability. Meanwhile, emulsions with a high-water content are very unstable and phase separation begins after 3 minutes. High water droplet motion enhances the destabilization of the W/O emulsion by coalescence and settling [16]. In addition to the above-mentioned parameters, emulsion stability is highly affected by its composition. Several studies have shown that the stability of an emulsion is directly related to the type and amount of surfactants [15] which play an important, if not a decisive role in the rheological behavior of emulsions at any concentration [17]. Surfactants are organic particles comprising of two parts: the polar portion that is attractive to the water phase (hydrophilic) and the nonpolar portion that is attractive to the oil phase (hydrophobic) [18]. These were seen to have two counteracting impacts on the characteristics of the film and the stability of the emulsions. First, it promotes lowering or eliminating the crumpling rate, which is the surface area at which the film crumpled relative to the initial surface area. This process promotes the destabilization of the emulsion. Second, it lowers the interfacial tension which improves emulsion stability [19].

Another important criterion that affects the stability of the emulsion is the mixing speed which counteracts the droplets fragmentation by adding energy to the system, and the emulsion becomes more stable. Shear stresses, for their part, resulting mainly from turbulence, play an opposite role in the stability of emulsions. On the one side, they increase the probability of droplet collision and, consequently, reduce the stability of the interface. On the other side, they can break the emulsion droplets, decreasing their size [20] and thus promoting emulsion stability.

Stable emulsions have been found to have the distinctive feature of being more viscous than unstable emulsions. Khalil et al. [2] showed that the most viscous emulsion was obtained by adding a chemical emulsifier to the emulsion. Additionally, the emulsion viscosity was affected by the emulsifying agent's type. As the operation of centrifugal pumps is very responsive to fluid viscosity variations, thus its performance will be more impacted when the carried emulsion is stable. For instance, Khalil et al. [2] reported that the stable emulsion causes a strong reduction of pump performance while the unstable emulsion affects less pump head and flow rate.

As mentioned above, stability is one of the most important characteristics of an emulsion and is directly related to its rheological properties. The surfactant naturally present in emulsions acts as an emulsifier that promotes the stability of the emulsion, thereby increasing its viscosity. The increase in viscosity leads to an increase in frictional losses. Consequently, a stable emulsion causes significant degradation in pump performance compared to an unstable emulsion. To address this problem, some industries opt for demulsifiers, which are chemical components that destabilize and break the interfacial film of an emulsion [21] to counteract the effects of emulsifying agents and reduce the emulsion viscosity [22]. Accordingly, Barrios et al. [23] reported a 90% reduction in emulsion viscosity by injecting a demulsifier upstream of an ESP handling an O/W emulsion. The pump head obtained after injection of the demulsifier was higher than that obtained without injection, and the power decreased significantly. The authors concluded that the use of a demulsifier substantially improves pump performance by decreasing

the viscosity of the emulsion and thus reducing frictional losses.

1.3.2 Phase inversion phenomenon

Phase inversion phenomenon is the process of inter-conversion between two types of emulsions. This phenomenon is specific to liquid-liquid dispersion and occurs when the emulsion's continuous phase changes to the dispersed phase and vice versa [24]. Two physical mechanisms of the phase inversion process have been distinguished [25], namely [26]:

- The transitional inversion, which proceeds in a certain range of phase fractions (the inversion zone).
- The catastrophic inversion, which occurs at clearly defined phase fractions (the inversion point).

The first mechanism is mainly induced by the interfacial tension force and is considered as an instability between the breaking and coalescing process. Thus, the phenomenon occurs when the fragmentation frequency is relatively low and the frequency of the coalescence process is high [27]. The second mechanism is related to the change of energy in the system, including kinetic and interfacial energy that is related to the mixing conditions.

Phase inversion studies are commonly conducted in pipelines, and mixers, and only a few of them in centrifugal pumps. Among the latter, the studies on phase inversion within centrifugal pumps can be divided into experimental studies and combined theoretical-experimental studies. Table 1.1 and Figure 1.3 summarizes the literature studies on the phase inversion phenomenon in centrifugal pumps. The table is organized by emulsion type, oil properties, pump speed, and water cut results at the inversion point. The experimental studies consider the injection of a specific fraction of both liquids simultaneously at the pump inlet until the phase inversion phenomenon occurs. The flow behavior is then investigated to identify the inversion point, the parameters influencing this point, and its effect on the pump performance. The procedure starts either with pure water, in which oil is added with increasing fractions, such that the emulsion changes from continuous water to continuous oil, or vice versa. In both cases, i.e. from aqueous to oily emulsion or from oily to aqueous emulsion, the inversion point is different.

Emulsion	**Oil properties**					N	WC **at**	μ_e/μ_o	**Ref**
	Name	μ_o (cP)	σ (N/m)	ρ (kg/m^3)	T $(^\circ)$	(rpm)	IP **(%)**	**(%)**	
O/W	Crude oil	6.00	0.027	838	25	2850	20%	-	[28]
W/O	Crude oil	2.47	-	803	-	1340	62%	19	[11]
W/O	Mineral oil	52	-	-	Cts	800	28%	-	[29]
						1200	29%	-	
						2400	33%	-	
W/O	Mineral oil	298	-	-	Cts	800	18%	-	[29]
						1200	21%	-	
						2400	23%	-	

W/O	Crude oil	60					70%	8.5	[23]
W/O	sun flower	58					30%	-	[30]
W/O	ISOPAR-V	15.70	0.027	810	Cts	3500	40%	6.5	[12]
	DN-20	222	0.0275	873			35%	2.5	
W/O	ND-20	97	0.030	867	26.7	3500	19%	1.6	[31]
		67		862	32		21%	1.82	
		46		859	37.7		23%	2.04	
O/W	Mineral oil	13.6	0.027	-	25	280	23%	-	[10]
						400	20%		
						720	13%		
W/O	Mineral oil	13.6	0.027	-	25	280	32%	-	[10]
						400	30%		
						720	21%		

Table 1.1: Summary of studies on the phase inversion phenomenon of emulsions within centrifugal pumps.

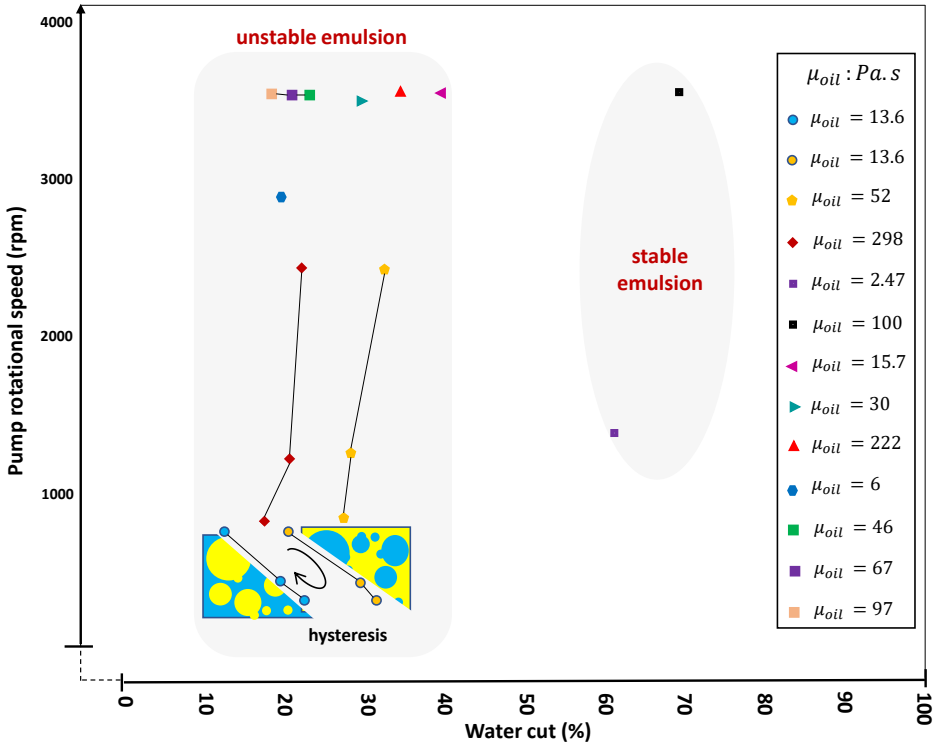

Figure 1.3: Summary of studies on the phase inversion phenomenon of emulsions within centrifugal pumps.

Two main findings are highlighted by the table: (i) phase inversion occurs at low WC for unstable emulsions [29, 12, 31, 30]; and (ii) the viscosity of the emulsion can increase six times more than the viscosity of either the oil or the water. Under the same operating conditions, phase inversion occurs at low water cut (WC) in O/W emulsion compared to W/O [10]. Augusto et al. [29] explained these results by the wettability of the fluid which is evaluated by the contact angle. Water has a greater ability to maintain contact with a solid surface than oils, which reduces the energy of turbulence in the flow. Therefore, water tends to be the continuous phase over a wider range of water volume fractions. However, Bellary et al. [11] and Barrios et al. [23] found a very high water volume fraction at phase inversion compared to other authors. Bellary et al. [11] reported an inversion point of 62% WC and the viscosity of the emulsion at this point is 19 times higher than the viscosity of the oil constituting the emulsion. Barrios et al. [23] on the other hand reported an inversion point of 70% WC and a viscosity 8.5 times the oil viscosity. These large WC may be attributed to the emulsion stability, where the authors who noticed a large WC at inversion tested an emulsion stabilized with a surfactant. As previously mentioned, the more stable an emulsion is, the less coalescence there is, therefore the volume fraction of the dispersed phase must be large enough to ensure the phase inversion phenomenon.

The inversion phenomenon depends on several interacting variables, including the physical and chemical properties of the coexisting phases, the dispersed phase fraction, the intensity of shear, and, in specific cases, the geometry of the vessel [32]. For instance, the viscosity of the coexisting phases has a remarkable effect on the phase inversion process. Bulgarelli et al. [29] studied this phenomenon on a water-in-oil emulsion in an electrical submersible pump using two different oils to investigate this issue. The authors found that the decrease in the viscosity of the oil-continuous phase increases the water cut at which phase inversion occurs. The same observation was reported by Croce et al. [12]. The authors studied the oil/water flow and emulsion formation in a seven-stage electrical submersible pump and evaluated the influence of emulsion effective viscosity on the pump performance. Tap water and two commercial oils with similar densities and surface tensions but different viscosities were used to generate the water in oil dispersions. Based on a qualitative analysis, the authors observed the generation of stable dispersions for each of the two oils. A phase inversion phenomenon was observed at a water cut of 40% for the emulsion having the low-viscous oil continuous phase and at a water cut of 35% for the one having the high-viscous oil continuous phase.

Shear inside the pumps has been reported to enhance the mixing process and have a significant effect on the phase inversion phenomenon. Zhang et al. [10] reported that with increasing shear intensity, an inversion occurs at relatively larger dispersed phase fractions, indicating a more stable emulsion. In addition, phase inversion occurs at higher oil volume fractions for the oil-in-water emulsion as the shear intensity increases compared to the water-in-oil emulsions. This has been attributed to the larger size range of oil droplets compared to water droplets at this point.

In general, phase inversion is not only dependent on the properties of the coexisting phases and the intensity of shear. This phenomenon is caused by the change of thermodynamic state variables such as temperature, surfactant concentration, change of the volume ratio of the phases [33], and the initial conditions, i.e. whether the continuous phase is oily or aqueous. An interesting observation regarding this phenomenon in centrifugal pumps is the hysteresis effect. Bulgarelli et al. [29] observed a hysteresis phenomenon in the phase inversion point within an ESP for a low-viscosity oil at low rotational speed only, changing the phase inversion point. Figure 1.4 illustrates the phase inversion point and hysteresis phenomenon in an ESP by Augusto et al. [34]. The figure shows the dimensionless head as a function of water cut for two opposing experiments, one going from oil to water and the other from water to

oil. The authors pointed out that hysteresis occurred in the phase inversion region, especially with low-viscosity oils, and at a low rotational speed. The authors attributed these results to the same physics that is responsible for the reduction in water content obtained in the phase inversion when the emulsion is O/W, namely the wettability of the fluid.

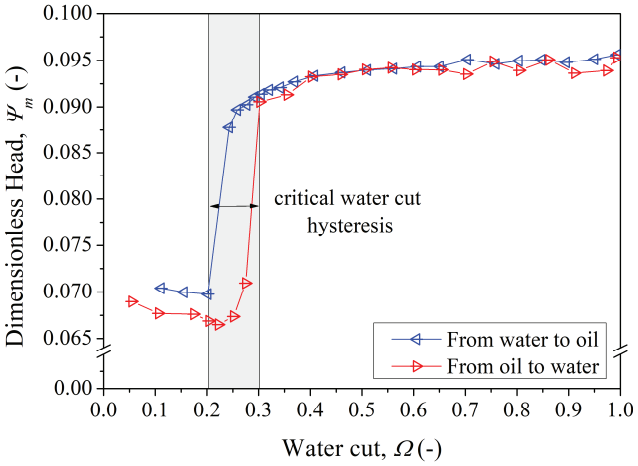

Figure 1.4: Hysteresis in phase inversion [34]

The occurrence of phase inversion and the changes in phase continuity led to substantial changes in the mixture rheology causing large fluctuations in pump operation and performance. Numerous studies have reported that the pump performance undergoes sudden and significant changes at or near the phase inversion point. It has been reported that with increasing water cuts, the viscosity of the emulsion increases to reach its maximum at phase inversion [11, 12, 31, 23] resulting in an important pump performance degradation at this point. This dramatic decrease in pump performance is primarily caused by the frictional shear on the fluid flow within the pump, which leads to an increase in hydraulic losses.

Various models for predicting the phase inversion point have been proposed in the literature [35], based on different physical mechanisms, namely models based on the minimization system and interfacial energy [24], models based on zero shear stress at the interface [36], and models based on drop breakup rate and coalescence [25]. The main correlations are presented in Table 1.2.

Reference	**Phase inversion models**
Yeh et al. (1964)	$\Omega_c = \frac{1}{\left[1+\left(\frac{\mu_o}{\mu_w}\right)^{0.5}\right]}$
Arirachacaran et al. (1989)	$\Omega_c = 0.500 - 0.1108 \log\left(\frac{\mu_o}{\mu_w}\right)$
Nädler and	$\Omega_c = \frac{1}{\left[1+\left(\frac{\mu_o}{\mu_w}\right)^{0.208}\left(\frac{\rho_o}{\rho_w}\right)^{0625}\right]}$

Mewes (1997)	
Brauner and Ullmann (2002)	$\Omega_c = 1 - \frac{\left(\frac{\rho_o}{\rho_w}\right)\left(\frac{\mu_o}{\mu_w}\frac{\rho_w}{\rho_o}\right)^{0.4}}{1+\left(\frac{\rho_o}{\rho_w}\right)\left(\frac{\mu_o}{\mu_w}\frac{\rho_w}{\rho_o}\right)^{0.4}}$

Table 1.2: Proposed models for the volume fraction at phase inversion.

The above models were developed to predict phase inversion in pipelines. Nevertheless, Bulgarelli et al. [34] investigated the adaptability of these models to centrifugal pumps and reported that these correlations are not suitable for predicting phase inversion points in pumps since a disagreement between the experimental results and the correlation's prediction was noticed. Zhang et al. [10] studied a predictive model of the phase inversion region of an oil-water emulsion in a gear pump that combines the interfacial energy balance with the droplet population balance. The authors pointed out that the model proved unsuitable for high-shear devices such as pumps, especially when multiple emulsions begin to form.

In centrifugal pumps, some authors have proposed correlations for estimating emulsion viscosity, in which an inversion point prediction equation has been incorporated. This equation is semi-empirical correlation and is based on the ratio of the viscosity of the two phases $\tilde{\mu}$ and are given by the following equation. ϕ_{WI} is the water cut at inversion and E is an empirical exponent.

$$\phi_{WI} = \frac{1}{1 + \tilde{\mu}^{1/E}} \tag{1.1}$$

In conclusion, the literature on phase inversion within centrifugal pumps is rather limited, especially concerning prediction models. A slight variation in the operating conditions, in the fluid's thermodynamic state, or an increase in the volume fractions of the dispersed phase can trigger the phase inversion phenomenon where the dispersed droplets reorganize and become the continuous phase, while the continuous phase breaks up, generating the new dispersed phase. This phase inversion occurs at a higher volume fraction of the dispersed phase as the shear intensity increases and as the oil viscosity decreases. This process causes a sudden increase in emulsion viscosity, which in turn can cause severe pump operational instabilities.

1.3.3 Rheological behavior

The main rheological characteristic of emulsions is viscosity, defined by the relationship between shear stress and shear rate. The emulsion rheology depends on several parameters, including the microstructure of the mixtures [5, 3], the chemistry of the coexisting phases, and their stability [6, 7, 8]. Emulsion stability, a predominant factor in emulsion rheology, depends primarily on the amount of surfactant added to or present in the emulsion, along with its chemical structure, which changes the interfacial tension between oil and water [37]. Surfactants increase the viscosity of the emulsion by decreasing the interfacial tension between the two phases [8], thus preventing the coalescence of the dispersed phase [15, 37]. On the other hand, the addition of a demulsifier decreases the effective viscosity of the emulsion

by destabilizing the emulsifying film around the droplets of the dispersed phase, thus promoting the coalescence process [1]. Emulsion's viscosity is also affected by drop size and drop size distribution [15] resulting from the competition between droplet breakage and coalescence [38]. Both mechanisms are enhanced by increasing shear stresses, but the properties of the resulting emulsion depend mainly on the volume fraction of the two coexisting phases and the type and concentration of the emulsifier used [39, 38]. Stable emulsions with a small droplet size or stabilized by a surfactant have a higher viscosity than unstable emulsions. Emulsions with low volume fractions of the dispersed phase behave as a quasi-Newtonian fluid where their viscosity is close to that of the continuous phase. Whereas emulsions with high volume fractions of the dispersed phase exhibit non-Newtonian behavior [40]. Typically, at higher water/oil ratios (WC $>$ 30%), the emulsion behaves as a shear-thinning fluid [41, 30]. Another crucial factor that has a noticeable impact on the emulsion viscosity is the phase inversion phenomenon. This process, reinforced by the high shear rate, leads to a dramatic increase in the viscosity of the emulsion, which can reach 19 times the viscosity of the single-phase oil constituting the emulsion [42].

Given the complexity of the rheological behavior of emulsions, few empirical models have been developed to model their viscosity. Table 1.3 gathers some empirical viscosity models of emulsions and liquid-liquid dispersions available in the literature. Einstein [43] proposed a model based on the behavior of very dilute suspensions (X $<$ 2%) and derived from the hydrodynamic theory of rigid spheres. His model applied to emulsions with a volume fraction of the dispersed phase up to 25%. Taylor [44] extended Einstein's model for liquid-liquid dispersion by assuming the effect of internal circulation caused by tangential stresses on the droplet interface. The proposed model was valid providing the surface tension is large enough to keep the droplets nearly spherical. Brinkman [45] presented an expression for the viscosity of solutions and suspensions of finite concentration by considering the effect of the addition of a solute molecule to an existing solution, which is considered a continuous phase. Many other correlations have been developed to estimate the effective viscosity of emulsions [46, 47, 48, 49, 50, 51]; however, these correlations are only suitable for flows in pipes where the shear effect is almost negligible compared to that of a centrifugal pump. Emulsions can exhibit different rheological behavior in a centrifugal pump, although the emulsion has the same oil concentration because of varying operating conditions and mixture properties. Considering these hydraulic parameters of centrifugal pumps, which influences the emulsions behavior, Banjar et al. [31] and Zhu et al. [52] developed a correlation for the estimation of the emulsion's effective viscosity within a multistage pump. The model was derived from Brinkman's model, where the effects of interfacial tension, turbulence, continuous phase viscosity, and shear stress on the rheology of emulsions were considered by Weber number, Reynolds number, and Strouhal number, respectively. The model provides the phase inversion point and can be used for both direct (O/W) and indirect (W/O) emulsions. This correlation, fitted to the experimental results obtained in their studies, provided a reasonable approximation of the viscosity value for emulsions consisting of medium viscosity oils, while a discrepancy was found for emulsions consisting of low viscosity oils. Bulgari [53] developed a model for estimating the relative viscosity of stable emulsions in ESP by adding a term to the Taylor correlation. He assumed a dynamic equilibrium of the droplet breakup and coalescence process and maintained a constant droplet size distribution for each data acquisition of the experimental tests. The model considers the behavior of the emulsion in the impeller through the Ohnesorge number, which relates the viscous force to the inertial and interfacial force. Additionally, it accounts for the shear stresses due to the rotational speed and the flow rate. Furthermore, his model considers the non-Newtonian shear-thinning character of emulsions and contains an index related to the interfacial properties that must be adjusted for each emulsion system. The proposed model gave a

reasonable estimate of the relative viscosity of a stable emulsion with an absolute deviation of 14%. A deviation of 8% was obtained for the emulsion stabilized with an emulsifier.

Model	**Ref**
$\mu_m = (1 + 2.5\phi)\mu_o$	Einstein et al. [43]
$\mu_r = 1 + 2.5\left(\frac{\mu_d + 0.4\mu_c}{\mu_d + \mu_c}\right)\Omega$	Taylor et al. [44]
$\mu_m = (1 - \phi)^{-2.5}\mu_o$	Brinkman et al. [45]
$\mu_m = C\left(\frac{\mu_C}{(1-\phi_D)^E} - \frac{\mu_W}{(1-\phi_O\phi_{OE})^E}\right) + \frac{\mu_W}{(1-\phi_O\phi_{OE})^E}$	Banjar et al. [31, 52]
$\mu_r = 1 + 2.5\left(\frac{\mu_d + 0.4\mu_c}{\mu_d + \mu_c}\right)\Omega$	Bulgarelli et al. [53]

Table 1.3: Viscosity models of emulsions and liquid-liquid dispersions

1.3.4 Dispersed phase morphology

The morphology of the dispersed phase droplets of an emulsion within a pump is determined by the balance between the surface tension and shear stress exerted by the carrier fluid. The emulsion morphology is difficult to define and measure quantitatively [54] and this is usually done by determining the droplet shape factor by identifying two characteristic parameters among the following: volume, V, area, A, projected area, A_p, and projected perimeter P_p [55]. The identification of droplet morphology and the evaluation of their dynamics in centrifugal pumps are studied through flow visualization, where the available methods, their advantages, and limitations, have been reviewed recently by Perissinotto et al. [56]. Droplets adopt regular and irregular geometries, where regular and symmetrical particle shapes facilitate the prediction of flow properties. Within centrifugal pumps, large droplets have an irregular shape while small droplets have a spherical or elliptical geometry [57]. In this alignment, water droplets dispersed in oil have an irregular shape with an easily deformable interface, while oil droplets dispersed in water have an elliptical shape with a well-defined interface [57, 58], as illustrated in Figure 1.5.

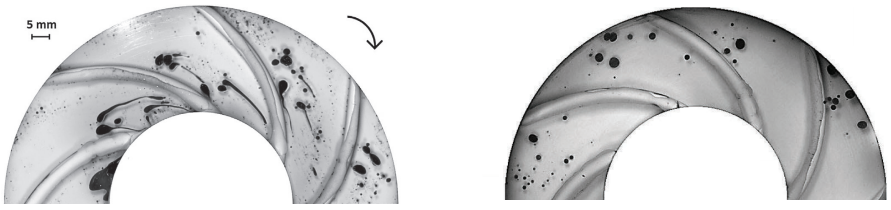

(a) (b)

Figure 1.5: The geometric shape of the water drops dispersed in oil (a) and geometric shape of the oil drops dispersed in water (b) in the impeller of a transparent prototype rotating at 600 rpm. Figure adapted from Perissinotto et al. [57, 59]

The droplets shape results from many contributions, including the size and shape of the flow domain [60] and the physical properties of the two phases, such as surface tension and viscosity [58]. The surface

tension acts on the droplets to give them a spherical shape [61]. While shear stresses due to emulsion motion and centrifugal forces tend to deform the spherical shape of the droplets. Another important aspect to be highlighted is that the shearing process in centrifugal pumps promotes the formation of emulsions by causing the droplets breakage [56]. As revealed by Figure 1.6, Perissinotto et al. [57] showed the droplet break-up process of water in oil dispersion within a centrifugal pump impeller using a high-speed camera and a pump prototype with a transparent shell. The figure shows the fragmentation process, where the water drops present an elongated shape with a nucleus and a tail at the channel entrance resulting from the interaction with the oil continuous phase (a). The tail extends in length and becomes thin forming small nuclei as the fluid moves along the impeller (b). Finally, the water drop is fragmented into several elliptical droplets and keeps the same shape for the rest of the trajectory (c).

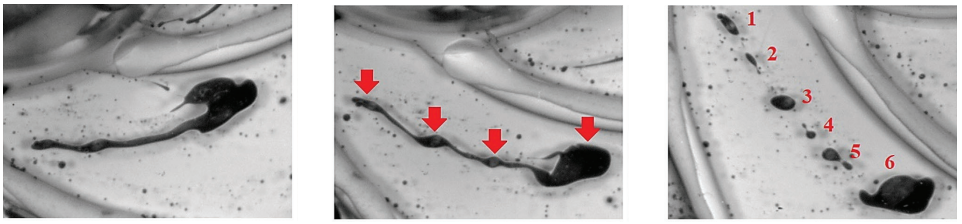

(a) (b) (c)

Figure 1.6: Fragmentation process of a water drop dispersed in the oil inside the pump. Figure adapted from Perissinotto et al. [57]

The behavior of the dispersed phase droplet depends on the flow conditions; thus, the dispersed phase particles undergo deformation and fragmentation as a function of pump speed and flow rate. The pump operating conditions have been shown to impact differently the breakage process of emulsions according to their type, i.e. whether the dispersed phase is water or oil. For instance, the high viscosity of the oil strongly limits the extent of deformation and fragmentation of the oil drops under shear. The fragmentation process is not limited to the regions near the impeller [61] but occurs in various parts of the pump, including the leading edge of the blades [62], in the housing near the discharge nozzle [63, 58], among others. These regions are associated with high shear stress regions caused by the change in flow direction and high turbulence levels. The droplet breakup mechanism is induced by the inertial forces produced by the turbulent velocity fluctuations. It occurs when the droplet size lies between the larger turbulent eddies and the Kolmogorov length scale [64, 61], known as the most minor scale in a turbulent flow where the viscosity dominates and the turbulent kinetic energy is dissipated into heat.

In general, the characterization of liquid-liquid two-phase flows and emulsions within centrifugal pumps is performed by analyzing the size and distribution of dispersed phase droplets in the impeller, since there is a dependency between the average drop diameter and the pump performance. This characterization and its correlation with the pump operation will be discussed in the following subsections.

1.3.5 Drop size distribution and characteristic diameter

The droplet size of the dispersed phase is an important characteristic of emulsions that determines their properties. It influences to some extent the rheological behavior and stability of the emulsion [41] and its measurement is a difficult task given the small diameters of the droplets. The droplet's size in an

emulsion is affected by several factors, including the nature of the emulsifying agents, bulk properties of oil and water, and shear stress [8]. Within centrifugal pumps, it has been reported that the droplet diameter is inversely proportional to the pump speed and flow rate, meaning that the droplet size decreases as the pump speed and flow rate increase. The decrease in droplet size is associated with the breakage mechanism; thus, high turbulence and hydraulic shear lead to droplet fragmentation and the formation of extremely small particles [65]. In a research study, Morales et al. [20] investigated drop breakage in an ESP using a Sympatec OPUS instrument as a particle size analyzer downstream of the pump. The emulsion consisted of a mixture of tap water and mineral oil at water contents of 50% and 75% and was tested at different pump speeds and flow rates. The authors concluded that droplet fragmentation occurred primarily in the pump impeller and that only 0.19% of the pump's hydraulic energy was used for droplet fragmentation. This finding was confirmed by several researchers [66, 67]. Zhang et al. [68, 67] also found a relationship between droplet size and pump operating conditions when studying the pump shear effect on oil-in-water emulsion and water-in-oil emulsion using a high-speed line camera. The authors also report that, not surprisingly, the particle size increases as the volume fraction of the dispersed phase increases. This factor directly affects the droplet coalescence process. It has been stated that significant coalescence rates occur due to the increase in volume fractions of the dispersed phase resulting from a two-step process of droplet collision and collision frequency [69]. Therefore, droplet size will be the balance between the turbulence-promoted fragmentation process and the concentration-promoted coalescence of the dispersed phase, emphasizing that the effects of concentration on the turbulence spectrum are not yet fully comprehended [61]. The effect of shear intensity and volume fraction of the dispersed phase was more pronounced in an oil-in-water emulsion than in a water-in-oil emulsion. Another parameter affecting droplet size and distribution is the emulsification time. Morozova et al. [66] stated that by increasing the emulsion preparation time, the droplet size of the dispersed phase decreases. The emulsion studied was composed of brand fuel oil dispersed in tap water and tested after 15, 30, and 45 minutes of spraying. Figure 1.7 shows the oil-water emulsion samples collected by the authors before and after passing through the pump for different spray times. It is clear that the emulsion preparation time and the particle size of the dispersed phase are inversely proportional. Furthermore, for the same emulsion preparation time, the particle size of the dispersed phase downstream of the pump is much smaller than upstream. The size of the dispersed oil particles is highly variable, and the number of particles less than 10 micrometers in diameter is twice as high after passing the pump.

The emulsion is a dispersion of one liquid in another, and generally, the droplet size of the dispersed phase is not represented by a fixed value but instead presented by a distribution [8]. A convenient mathematical correlation that represents emulsion droplet size distributions in centrifugal pumps is the Rosin-Rammler and lognormal expressions [20, 70]. One of the first research works concerning the distribution of the dispersed phase of an emulsion on a pump is done by Ibrahim et al. [71]. They examined the oil drop size distribution of an O/W emulsion experimentally by fixing a laser particle size analyzer directly on the experimental apparatus. The authors presented a correlation to calculate the average droplet diameter of the dispersed phase as a function of the input distribution. This correlation was extended for different pump speeds using polynomial regression analysis. Zhang et al. [68, 67] reported that the droplet size distribution is no longer affected by the pump speed when it reaches a specific value. The authors attributed this result to the balance between the residence time, which is inversely proportional to the pump speed, and the breakup time, which is proportional to the pump speed. This finding was confirmed by Mohan [70], who presented a detailed study of the droplet size distribution downstream of a centrifugal pump by analyzing the mean Sauter diameter d_{32} and the

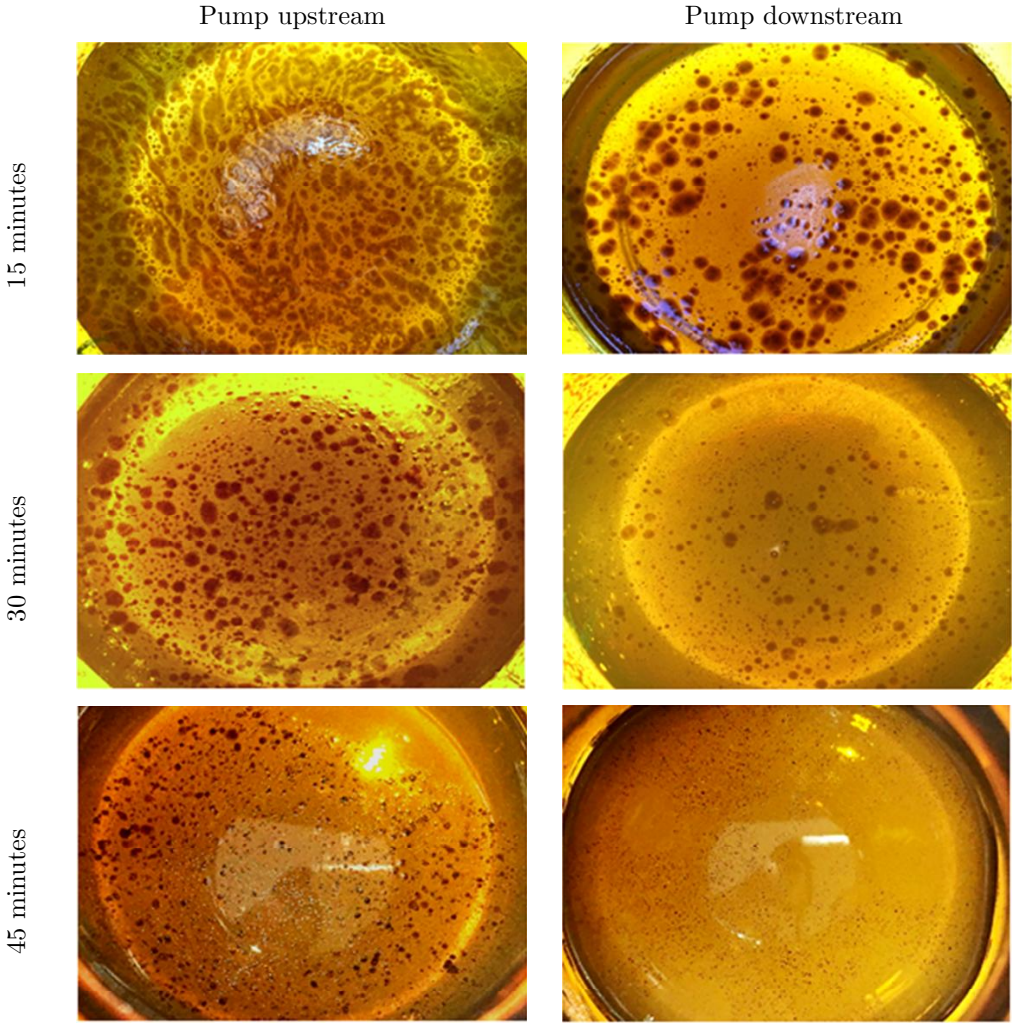

Figure 1.7: Oil-water emulsion samples upstream and downstream of the pump at different preparation times. Figure adapted from [66]

.

droplet diameter at 95% cumulative distribution percentage (d_{95}). Both d_{32} and d_{95} decrease as the shear stress increases until a certain pump speed is reached. The authors also stated that the flow rate and water cut had a negligible effect on the droplet size of the dispersed phase and that the oil droplet size was smaller than the water droplet size under similar conditions. This observation agreed with those of Schmitt et al. [63]. The authors also state that above a specific pump speed, the change in flow rate no longer affects the droplet fragmentation process and that only the pump speed influences the fragmentation process. Figure 1.8 shows the droplet size distribution as a function of rotational frequency for a constant flow rate of 900 L/h and a holdup of 1%. As can be seen, the distribution shifts to the left as the rotation rate increases and become narrower.

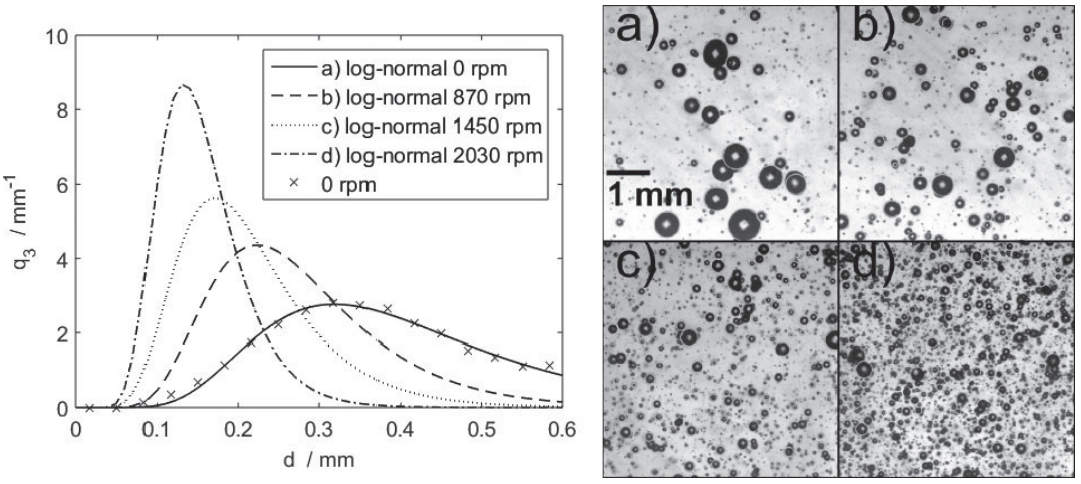

Figure 1.8: Droplet size distributions at different rotational frequencies [63]

In sum, the droplet size of an emulsion is a function of many factors, including the type of surfactant used, the amount of shear applied to the system, and the concentration of the surfactant. Figure 1.9 shows the relation between droplet size of the dispersed phase, shear intensity, surfactant concentration, and emulsion stability.

Increasing shear and surfactant concentration will both result in smaller droplet sizes. The two are also related in that more surfactant increases the effectiveness of shear in decreasing the droplet size. For example, if a surfactant is present, it can lower the surface tension of the droplet and allow the shear forces to break it down more easily, resulting in smaller droplets. The stability of an emulsion is also related to droplet size. Generally, smaller droplets are more stable than larger ones. This is because smaller droplets are less likely to coalesce and form larger droplets, which can destabilize the emulsion. Additionally, smaller droplets have a higher surface area-to-volume ratio, which means that the surfactant can more effectively coat the droplets and stabilize them. Therefore, increasing shear and surfactant concentration can both result in improved emulsion stability.

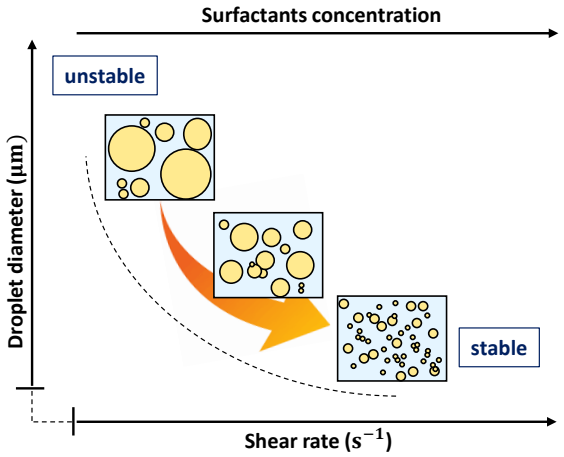

Figure 1.9: Relationship between droplet diameter, surfactant concentration, shear stress, and emulsion stability.

Generally, the droplet size distribution of an emulsion is often used as an average value or represented by different characteristic diameters. These typical diameters are estimated using many formulas, including Sauter's mean diameter d_{32} which is the average diameter of the droplet distribution considering the volume-to-surface ratio [72, 73] and the maximum stable droplet diameter d_{max}. These two characteristic parameters can then be used to approximate a two-parameter droplet size distribution [74]. Several models have been proposed for the prediction of these two characteristic diameters in the literature. This study presents only a review of the diameters commonly used in centrifugal pumps, namely Sauter mean diameter and maximum stable droplet diameter.

Other commonly used diameters to characterize emulsions are d_{10}, d_{50}, d_{90}, d_{95} and d_{min}, which represent the maximum droplet size that 10, 50, 90, 95% of the droplets have [75] and the minimum stable droplet diameter.

Sauter mean diameter and dmax

Determination of particle size is usually complicated owing to the irregular particle shape [54], thus the assumption of a spherical shape is considered in almost all models. Various studies have been conducted to determine the representative size of emulsion droplets in centrifugal pumps. Most of these studies have used Sauter's mean diameter as the representative droplet size [76]. Sauter mean diameter is a valuable parameter for estimating the average diameter of dispersed liquid droplets. It represents the size of identical spherical droplets (mono-dispersed system) whose sum of surface energies is equal to the sum of surface energies of the dispersed droplets. The two dispersions have different numbers of spherical droplets but the same total surface area and total volume [72], as illustrated in Figure 1.10.

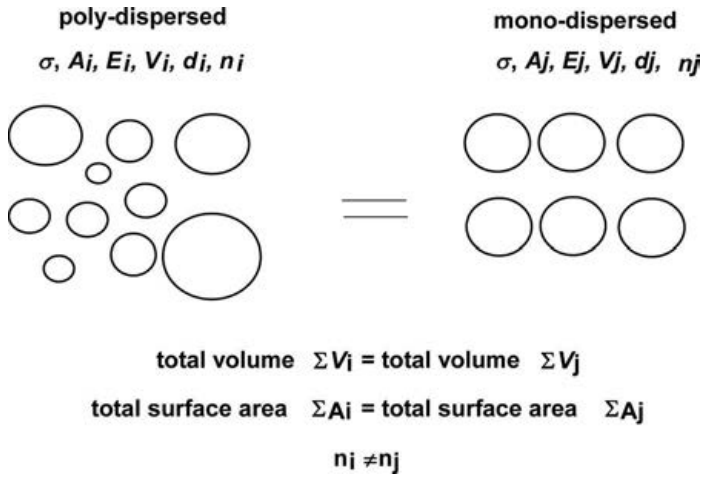

Figure 1.10: Physical meaning of the Sauter mean diameter [72]

The equation below shows how to calculate d_{32}, where n_i is the number of droplets of diameter d_i and N is the total number of droplets [3].

$$d_{32} = \frac{\sum_{i=1}^{N} n_i d_i^3}{\sum_{i=1}^{N} n_i d_i^2} \tag{1.2}$$

Early studies of emulsions flow within centrifugal pumps [58, 63] revealed that the flow conditions change the Sauter mean diameter. It decreases as the pump rotation speed and water flow rate increase. Likewise, Bulgarelli et al. [3] found that the Sauter mean diameter is related to the operational conditions and fluid properties. The authors then proposed a mechanistic model to estimate the value of this characteristic size for different systems of a water-in-oil emulsion.

Another parameter of emulsion droplet size that proves useful in characterizing many dispersed particles in centrifugal pumps is the maximum stable diameter, d_{max}. This parameter is determined by the balance between the turbulent inertial stresses that tend to deform the droplet and the elastic stress generated by the interfacial tension that tends to restore the original droplet shape [77]. In general, the maximum droplet can be a flocculation of droplets [70], and in order not to overestimate its size, some authors represent d_{max} by d_{95} [75, 70]. Similarly to the Sauter mean diameter, the maximum droplet size is affected by the pump operating conditions and decreases with increasing shear intensity. Many empirical correlations have been provided in the literature to estimate the maximum droplet size of liquid-liquid dispersions [64, 78, 79], most of which are based on the concept of turbulent energy cascade [80]. These correlations were developed for the flow of emulsions in pipelines, mixers, or agitated vessels. The application of some of the proposed models to the flow of emulsions in a centrifugal pump was attempted by Mohan et al. [70]. The authors evaluated four models whose mathematical expressions are presented in Table 1.4, namely those proposed by Hinze (1955) [64], Levich (1962) [78], Davis (1985) [79] and Pereyra. The author recommended the use of Peyer's model to predict the maximum droplet diameter of the emulsion in the pump, after providing the most accurate results compared to the other models. According to the authors, Pereyra model introduces the energy dissipation rate in the centrifugal pump, which can be determined by two methods. The first is a function of pressure drop, mixture flow rate, mixture density, and volute volume. The second method is a function of pump speed and impeller diameter. In this context, Pereyra's model considers the effect of specific pump operational parameters

on the droplet size and gives a good estimation of the maximum droplet size of emulsions within pumps.

Few models have been developed specifically to predict the maximum droplet size of emulsions in pumps. Morales et al. [20] derived an equation for the maximum droplet diameter based on the Davis model, which considers the effect of the viscosity of both phases on droplet size. The authors reported in their study that a small influence of flow rate and water cut was observed on droplet size, whereas droplet size is highly dependent on rotational speed. Based on these observations, the authors proposed a model for the calculation of the maximum droplet diameter in pumps in terms of pump speed. The estimate given by this correlation shows reasonable agreement with the experimental results. Zhang et al. [68, 67] reported that with the increase in the volume fraction of the dispersed phase, the droplet size enlarges and the energy dissipation decreases. These results were attributed to the energy dissipation that is transferred in part to the fluid dynamic energy as WC increases. Whereas only a portion of the maximum energy dissipation rate is applied to the droplet breakup process. Based on this analysis, the authors proposed a correlation for the maximum droplet size using a new value for the energy dissipation efficiency as a function of the volume fraction of the dispersed phase in the model proposed by Pereyra [81]. The authors concluded that the proposed d_{max} model gives a good approximation of the experimental data but that the model was only valid for dispersed phase volume fractions up to 15%.

The maximum stable droplet size of an emulsion is directly proportional to d_{32} [82], where a linear relationship is generally observed within a centrifugal pump. Perissinotto et al. [57] calculated d_{32} and d_{95} for both oil-in-water emulsion and water-in-oil emulsion at different rotational speeds and different flow rates. The relationship between the two diameters was found to be d_{32}=0.853d_{95} for O/W emulsion and d_{32}=0.495d_{95} in the case of water in oil emulsion. Zhang et al. [68, 67] obtained a ratio (d_{32}/d_{max}) of 0.55 for the dilute O/W emulsion and 0.48 for the dilute W/O emulsion. These values are close to those obtained by Morales et al. [20] for O/W dispersions, where the authors observed a constant relationship equal to 0.495. On the other hand, Mohan et al. [70] observed an average value of 0.43 for oil continuous emulsion and 0.37 for water continuous emulsion. The authors stated that the water droplet was larger than the oil droplet for the same operating conditions. Furthermore, Bulgarelli et al. [3] observed a linear relationship between the two characteristic diameters for all studied emulsions regardless of the oil composition and the presence of surfactant. The authors obtained a ratio d_{32}/d_{95} = 0.36 and suggested that the proportionality constant may vary only regarding the ESP geometrical characteristics.

Reference	**Maximum droplet diameter models**
Hinze (1955)	$d_{\max}\left(\frac{\rho_C}{\sigma}\right)^{3/5}\varepsilon_0^{2/5} = C$
Sleicher (1962)	$\left(\frac{d_{max}\rho_C u_p^2}{\sigma}\right)\left(\frac{\mu_C u_p}{\sigma}\right)^{1/2} = 38\left(1+0.7\left(\frac{\mu_d u_p}{\sigma}\right)^{0.7}\right)$
Davis (1985)	$d_{max} = \mathrm{We}_{\mathrm{CRI}}^{3/5}\left(\frac{\sigma}{\rho_C}+\frac{\sqrt{2}}{4}\frac{\mu_D(\varepsilon_0 d_{max})^{1/3}}{\rho_C}\right)^{1/5}\varepsilon_0^{-\mathcal{Z}/5}$
Pereyra (2011)	$d_{max} = \mathrm{We}_{\mathrm{CRT}}\left\{\frac{\left[\sigma+2^{-3/2}\mu_D(\varepsilon_0 d_{\max})^{1/3}\right]^{3/5}}{\rho_D^{1/5}\rho_C^{2/5}}\varepsilon_0^{-2/5}\right\}$

Table 1.4: Correlations for the maximum droplet size of liquid-liquid dispersions

1.4 Pump performance modeling under emulsion flow

The pump performance is directly related to the fluid viscosity and is altered when the pumped fluid is highly viscous owing to increased losses. As shown in previous sections, liquid-liquid dispersions and emulsions have complex rheological behavior. The viscosity of these mixtures is higher than the viscosity of the constituent phases and is strongly dependent on several parameters such as operating conditions, temperature, and shear stress. High shear stress promotes the formation of a stable emulsion by decreasing the size of the dispersed phase droplets, thereby increasing their viscosity. A highly viscous fluid leads to higher frictional losses in the pump channels, which decreases the head, flow rate, and efficiency of the pump while increasing energy consumption [9]. Several researchers or research institutions have developed correlations to predict pump performance when operating with non-conventional fluids, which is generally based on the pump head developed for water, multiplied by a correction factor expressed as a function of the fluid viscosity [83, 84, 85]. However, these correlations concern medium to highly viscous Newtonian fluids and find their limits when the fluid follows a complex rheological behavior. Given the complexity of this issue, few studies have attempted to correlate pump performance operating with two-phase liquid/liquid flow and emulsions. The currently available literature on this topic has provided either mechanistic models based on losses encountered in pumps where emulsion rheology has been modeled and incorporated, or numerical models based on CFD. Both approaches are detailed in the following subsections.

1.4.1 Analytical modeling

Analytical models can provide accurate predictions of the effect of fluid viscosity on pump performance (HI/ANSI) [86], and have proven to be an efficient approach for pump design [87, 88]. This method determines the pump's hydraulic performance by calculating the idealized head and various losses based on a one-dimensional analysis [88]. The idealized head based on Euler equation describes the fluid flow in pumps with the assumption of an infinite number of blades and a frictionless fluid. This equation is derived from the Navier-Stokes equations based on the principle of conservation of momentum. Thus, the pump's real discharge pressure is obtained by fixing the finite number of blades and subtracting the various losses encountered within the pumps from the Euler's head.

Several models have been developed in the literature to evaluate the different mechanisms of pressure losses in centrifugal pumps; yet, there is no consensus among the different authors on the classification and behavior of some losses [89].

As an effort to understand oil-water emulsion rheology and its effect on centrifugal pump performance using analytical models, Banjar et al. [31] and Zhu et al. [52, 90] developed a mechanistic model to predict pump performance by considering the effect of emulsion rheology. The authors presented a correlation for predicting the rheology of emulsions in pumps by considering the phase inversion phenomenon which was coupled with a mechanistic model to predict pump performance. The presented correlation for emulsion viscosity is based on the Brinkman equation to determine the fraction of water at which the dispersed phase becomes continuous and includes several parameters affecting the viscosity, namely the effect of the mean droplet diameter, turbulence, and shear rate. To validate the rheology model, Banjar [31] conducted numerous experiments on emulsions composed of tap water and various mineral oils with Newtonian behavior. The results showed that the model predicted the viscosity of the emulsions with medium viscosity oils with a 5% deviation from the experimental data. For low-viscosity oils, a deviation

between the experimental data and the model predictions was perceived. Zhu et al [52, 90] validated the model with experimental data obtained from a water-in-oil emulsion flow where the continuous oil phase covers a wide viscosity range (10-150cp). The proposed rheological model was verified by a qualitative trend analysis, where the authors noted a considerable increase in the effective viscosity of the emulsion when the flow rate increases and a less significant increase when the rotation speed increases. Furthermore, the increase in viscosity of the continuous phase not only decreases the viscosity of the emulsion but also shifts the point of the inversion phase to a lower value. Regarding the mechanistic model to predict pump performance proposed by the authors, it starts from the Euler head (H_E) for a centrifugal pump, from which various losses encountered in the pumps are subtracted. Furthermore, the model introduces a best-match flow rate (Q_{BM}), at which the outflow direction of the impeller matches the designed flow direction. The losses included friction, turn, recirculation, and leakage losses. Hence, the formula for the actual pump head (H) is given by :

$$H = H_E - H_{\text{frition}} - H_{\text{turn}} - H_{\text{leakage}} - H_{\text{recirculation}} \tag{1.3}$$

By subtracting the pressure drops from the Euler's head, and replacing the fluid viscosity with the previously proposed effective viscosity model, a modeled head of a centrifugal pump for two-phase flow can be estimated. As shown by the authors, an appropriate combination of the rheological model and the performance model can produce a good estimate of the pump performance. Zhu et al. [52, 90] reported that the model predicted the performance of the ESP under emulsion flow with an error of about $\mp$ 10% outside the phase inversion region and 50% for the phase inversion region. However, due to the empirical nature of the rheological model, the universal validity of such a combination for inferring emulsion pump performance is questioned. Alternatively, as proposed by Banjar [91], there is a need to further improve the model by fitting the parameters to larger data, and possibly incorporating parameters that have not been considered. Instead, researchers resort to numerical approaches to calculate hydraulic performance and understand the complex flow structures inside pumps.

1.4.2 Numerical modeling

Numerical analysis of the pump performance handling liquid-liquid two-phase flows and emulsions encompasses all the complications of modeling single-phase flows, as well as the inherent complexities of multiphase flows, such as the interaction of small-scale structures, different space-time scales, and the motion and deformation of interfaces. Numerical treatment of multiphase flows is a difficult task due to its complex nature. Given this, multiphase flow encompasses a large spectrum of different length scales, including (1) the microscale that takes into account the interactions between the particles of the two phases, (2) the mesoscale that includes the processes of coalescence and rupture of discrete constituents, and (3) the macroscale which covers the hydrodynamic behavior of the phases at the scale of the device [92, 93].

Computational Fluid Dynamics (CFD) can be used to disclose details of a particular flow physics and clarify mechanisms specific to multiphase flows [92]. Due to the development of parallel computing options and the increase in computing power, its use has proliferated in recent years [94]. The two-phase flow theory is formulated using two techniques. The first is the Eulerian-Eulerian (E-E) approach that treats the existing phases as interpenetrating continua. Conservation equations have a similar structure for all phases and are closed by providing constitutive relations. The second technique is the Eulerian-

Lagrangian (E-L) approach that is a coupling between the Eulerian description for the continuous phase and a Langrangian tracking procedure for the dispersed phase [95, 92, 96]. In the E-E approach, three typical multiphase models exist, namely the fluid volume model (VOF), the Eulerian model (so-called Multiphase Segregated Flow in some literature) and the mixture model [97].

Due to the complexity involved in emulsion modeling, only a few attempts have been made to study the performance of a centrifugal pump under emulsion flow. Table 1.5 lists the summary of numerical studies on pump performance under emulsion flow. The table is organized by the multiphase model used, closure relationships, and results and remarks. All studies on this topic have adopted the E/E approach as shown in the table. The reason is that the E/L approach is inappropriate for liquid-liquid flow modeling where the volume fraction of the dispersed phase is not negligible.

Multiphase model	**Closure Relationships**	**Results and remarks**	**Ref**
VOF	Surface tension force	- The approach correctly models the pump behavior with a root mean square deviation between experimental and CFD results of 5.72% - The model did not capture the phase inversion of the oil-water emulsion	Becerra et al. [98]
	Surface tension force and integration of a slip velocity model to the momentum equation	- Head and efficiency were predicted with 10% and 15% deviation from experimental data respectively	Valdes et al. [99]
Eulerian	Drag and lift forces	- The simulated head obtained for the emulsion is higher than that obtained for single-phase oil and overestimates experimental data by 40%; indicating the inconsistency of the results.	Banjar et al. [91, 100]
	Drag force	- The model predicted head and efficiency with a deviation of 7% and 10% from the experimental results respectively	Valdes et al. [99]

Eulerian-PBE	The Eulerian model considers the drag forces and the PBE the fragmentation and coalescence models.	The model provided reasonable results for the dilute emulsion, with predicted head and efficiency errors of 10% and 15%, respectively. A discrepancy was observed for the concentrated emulsion, with average head and efficiency errors of 14% and 22%, respectively.	Valdes et al. [99]

Table 1.5: Summary of numerical studies on emulsion flow within pumps using the multiphase approach.

Based on the VOF model, Becerra et al. [98] studied the performance of a four-stages ESP under an oil-in-water emulsion flow. The authors opted to use the VOF model because of the weak contact and immiscibility of the oil and water employed in the experiments. The turbulence was modeled using the k-omega model since it has a better performance in low turbulence regions compared to other models. The simulation results showed the effect of increasing the volume fraction of the oil phase on pump performance. As the volume fraction increases, the viscosity of the mixture increased, and pump performance decreased. The ESP operating characteristics predicted by the CFD were compared to the experimental results and found to be in good agreement. This agreement is more pronounced for dispersion with high oil volume fractions than for dispersion with low oil volume fractions, but the phase inversion was not detected by the numerical simulation. Figure 1.11 shows the plot of experimental and CFD viscosity data of oil-water mixture as a function of the oil concentration. The properties of the mixture, such as viscosity, are calculated by volume-averaged relations, i.e. the average of the sum of the viscosity of each phase multiplied by its volume fraction. As a result, the numerical simulation does not reflect the rheology of the emulsion in the phase inversion zone, as shown in the Figure 1.11. By investigating the emulsions flow pattern in one stage of the ESP, the authors highlighted that emulsions with low oil concentration have most of the oil fraction near the pump shaft, indicating a non-uniform distribution of the dispersed phase, whereas for emulsions having high oil volume fraction, a more uniform distribution is observed. The authors highlighted that the non-uniformity observed in the two first cases is contradictory to the phase inversion phenomenon where the droplets of the dispersed phase increase in volume and coalesce. Given the grid requirements for accurate resolution of the interface, the VOF model appears quickly limited when coalesence or breakup phenomena lead to higly polydispersed two-phase flow. Likewise, Valdes et al. [99] attempted to model a wide range of oil-water emulsions (having a multi-scale nature) using the VOF model. The emulsions modeled consist of a dilute W/O emulsion (with oil concentration up to 0-80%), a concentrated W/O emulsion (with the onset of phase inversion at 70% oil) exhibiting pseudo-steady-state behavior, and a multi-regime flow (60-10% oil) exhibiting rapid destabilization as the water fraction increases. The authors modeled the emulsion flow in the pump by solving only the large-scale phase interactions, including a slip velocity model. The latter was coupled to the momentum equation to account for the system inhomogeneity and possible effects that may result from phases moving at varying speeds at the interface. The results showed that the emulsion flow in the

pump is correctly represented by the VOF model, especially for emulsions with multiple regime phase morphology. It was reported that the best predictions were obtained near the BEP, where a deviation of 10% and 15% was noted for head and efficiency, respectively. Besides, the largest deviation was observed for other emulsions types, where the phase morphology is colloidal. The authors explained this discrepancy by the inadequacy of the VOF approach to model turbulence in emulsion flow since not all flow scales are resolved.

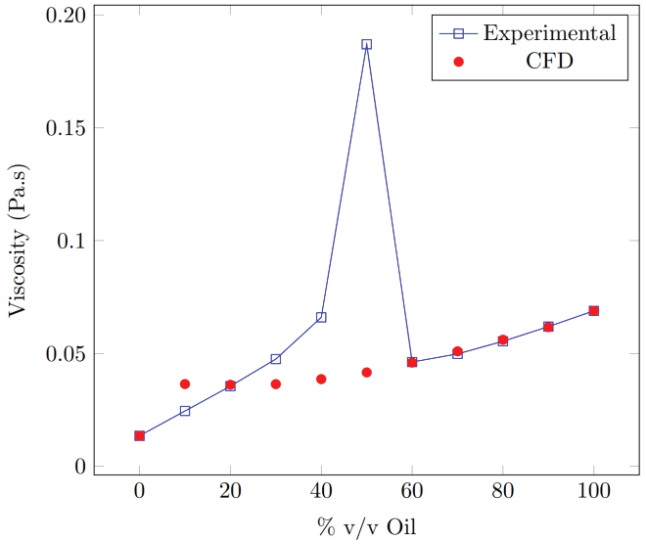

Figure 1.11: Experimental and CFD Viscosity data of oil-water mixture [98]

Unlike the VOF model that establishes a single equation for each transport phenomenon of all phases, the pure Eulerian model uses one equation for each transport phenomenon for each phase [101]. The form of the continuity and momentum equations in the Eulerian model is similar to those that can be used for a single-phase flow, with two main differences. The first difference is the introduction of the volume fractions of the phases i considered. The second is the addition of terms representing the mass, momentum, and heat transfer between the phases. Based on this approach i.e the pure Eulerian, Banjar et al. [91, 100] investigated emulsion flows through a seven-stage electrical submersible pump with different viscosity, temperature, and water fractions. The turbulence was modeled by the standard k- ϵ model and drag and lift forces were integrated into the interfacial momentum transfer terms. The obtained results diverge from the experimental data and the solver could not reflect the rheology of the emulsion. The authors explained this discrepancy by the fact that the emulsion is considered a dispersion where the dispersed phases do not affect the rheology of the mixture. In another study using the same approach, Valdes et al. [99] modeled a multiple-regime liquid-liquid flow within an ESP considering only the drag forces and turbulent dispersion in the interfacial momentum transfer terms. . The numerical simulation results showed that the pure Eulerian model offered a good performance prediction with head increase and efficiency variations under 7% and 10%, respectively.

Generally, the Eulerian model assumes a uniform droplet size of the dispersed phase of the emulsion in the pump and does not account for existing interactions between droplets, such as fragmentation and coalescence, which can have a significant influence on the flow. In reality, a particle size distribution of the dispersed phase of the emulsion in the pump is observed [20, 66, 68]. Besides, this particle size distribution, generally expressed by the semi-empirical (or empirical) formula, is affected by the turbu-

lence and shear rate exerted by the pump [67, 63], which leads to a narrow distribution following the breakage phenomenon. In systems where the particle size distribution changes as a result of dispersed phase droplet behavior such as droplet fragmentation, the Population Balance Equation (PBE) is typically used in conjunction with the pure Eulerian model to account for these changes. The PBE is a set of inter-particle differential equations that define the development of particle populations according to specific properties [102]. They represent a transport equation for the Numerical Density Function (NDF) of particles that depends on time, spatial location and internal coordinates [103]. PBE can determine the particle breakage, coalescence, motion, and particle size distribution in a laminar or turbulent fluid flow [82, 104]. It permits a better synthesis of the behavior and dynamic evolution of the discrete particle population due to its ability to resolve the microphysics that occurs at the mesoscale level [105]. In this regard, Valdes et al. [99] coupled the Eulerian multiphase model with the population balance to model two types of emulsion flow within an ESP, namely a diluted W/O emulsion (80% and 90% oil), and a concentrated O/W emulsion (corresponding to phase inversion). The PBE chosen in their study, which is a simplified version of the general PBE derived by Ramkrishna [102] and Yeoh [105], considers the density flux of the number of particles over a given size range and does not include the particle growth, or the variation in particle velocity as a function of particle size. Two types of methods were used to solve the PBE: the method of moments (S-Gamma), where the breakup and the coalescence models consider both viscous and inertial regimes; and the method of classes (AMuSiG) [99], where the breakup and the coalescence models consider the flow rate and turbulence effect. The results showed that the coupled PBM approach modeled well the diluted emulsion with satisfactory results (deviation $< 7\%$), but larger deviations were observed for the concentrated emulsion, where the mean error obtained was 14%. The authors explained the large discrepancy by the overestimation of viscous friction losses caused by the elevated effective viscosities computed as a consequence of the high concentration of the dispersed phase. Furthermore, both PBM models equally estimated the global pump performance and the average fluid behavior indicating that the AMuSiG method gave a more complete and detailed representation of the system than the S-Gamma method. As pointed out by the authors, the coupled Eulerian simulations with PBE provide a vigorous treatment of phase interactions and the dispersed droplet effect on pump performance but do not consider the fluid rheology given the lack of an emulsion rheology closure model.

Few numerical studies have been carried out on two-phase liquid-liquid flow and emulsions in the pump. Although the multiphase Eulerian approach solves the physics at the macroscale only, it has proven to be relevant to obtain a reasonable estimate of its general performance when the volume fraction of the dispersed phase is not large (less than approximately 20%). Numerical multiphase fluid dynamics coupled with a population balance model is capable of elucidating mesoscale flow parameters, such as droplet size distribution and the fragmentation and coalescence process if the closure relationships are well chosen. On the other hand, a more realistic treatment of emulsion flow within pumps, including the emulsion rheology that incorporates the effect of local droplet size distribution and phase inversion remains a challenge.

Conclusion

This chapter has shown the complexity of analyzing pump performance during emulsion processing due to the large number of parameters related to fluid properties that interact with pump operating parameters. This complexity is also related to the complex flow pattern of the fluid in the pump. Several experimental studies have been conducted on the centrifugal pump's handling emulsion, which allowed

the characterization of this fluid in these machines and the identification of main parameters affecting its proper operation. However, few works have been extended to the pump performance analysis when conveying these complex fluids. The latter concern mainly multistage centrifugal pumps and are based on two-phase approaches where the rheological properties of emulsions are not considered. Moreover, no numerical study has considered the two-phase oil-water flow in a volute centrifugal pump, and no comprehensive analysis has been performed on the effect of the non-Newtonian rheology of emulsions on the internal flow structure and operation of these volute centrifugal pumps. Therefore, this thesis aims to perform a comprehensive analysis of the overall performance and internal flow characteristics of a volute centrifugal pump when processing these complex flow systems. The present work will consider several distinct approaches to address the topics just discussed.

- An analytical approach that considers the emulsion's phase inversion point in the pump performance analysis.
- A numerical approach that will focus on a thorough study of the effects of the rheological behavior of emulsions on the performance of the pump. This approach will consider the non-Newtonian character of the emulsions and will neglect the two-phase character, where the characterization of the losses will be performed by the entropy analysis method.
- A numerical approach that will focus on the two-phase character of the emulsion and will correlate it with the pump operation.

The novelty of this research lies in the following points: (i) the consideration of the non-Newtonian behavior of emulsions in the study of the performance of centrifugal volute pumps, (ii) the modeling of two-phase emulsion with single-phase non-Newtonian model and its comparison with two-phase flow models, (iii) the application of the entropy theory for the determination of the energy loss in the volute pump handling these fluids having complex rheological behavior, and finally (iv) the precise characterization of the different losses in centrifugal pumps with a CFD approach.

CHAPTER 2

Performance analysis of a centrifugal pump under emulsion flow by analytical model

Contents

This chapter analyzes the influence of emulsion flow on the characteristic curves of a centrifugal pump by an analytical method. For this purpose, a rheological model of the emulsion in centrifugal pumps proposed in the literature has been adapted to the studied emulsion and has been coupled with a loss model for the prediction of the pump performance. The coupling considers the rheological model to estimate the effective viscosity of the emulsion as a function of the operating conditions (variable flow rate in this study). The latter is then used in the friction coefficients and closure relationships in the pump performance model. This chapter is organized as follows: first, the emulsion and the centrifugal pump under investigation are described, followed by the presentation of the rheological model and head losses in a pump, and finally, the analysis of the results, including a comparison of pressure drop when handling water and emulsion.

2.1 Studied emulsions

The emulsions studied in the present work corresponded to the emulsions studied experimentally by Valdes et al. [30]. The authors studied two-phase mixtures of sunflower oil and water at 9 different phase compositions, ranging from 90%–10% O-W to 10%–90% O-W, with 10% increments. The rheological properties of these mixtures were measured experimentally under a shear rate ranging from 1 s^{-1} to 3000 s^{-1}, which covers the range of the shear rate of the studied pump. Additional information on the experimental procedure can be found in [30]. Three-phase morphologies were identified (Figure 2.1):

(1) the dilute, pseudo-stable W/O emulsion at high oil fractions (> 80%), exhibiting quasi-Newtonian behavior with a slight tendency to shear thinning at very high shear rates. (2) a concentrated pseudo-stable O/W emulsion where phase inversion occurred at 70% oil volume, characterized by higher viscosity and tendency to shear thinning. (3) Multi-regime emulsion at high water fractions (> 40% water), with a slight tendency to shear thinning (the reader is referred to the article [30] for a better understanding of the fluid characterization performed and the interpretation of the results).

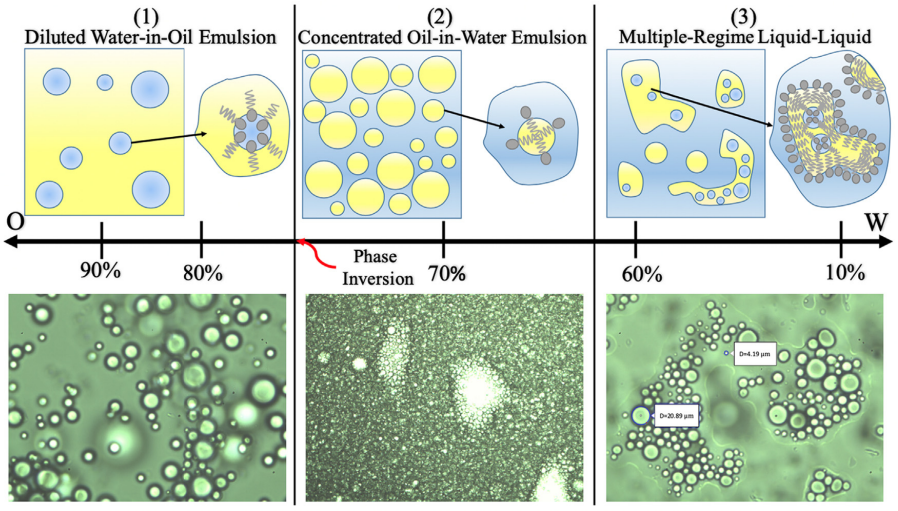

Figure 2.1: Oil–water phase morphology and distribution map for the studied mixtures from Valdes et al. [30]. Phase composition (%v/v) given with respect to the oil phase. The top row gives a schematic representation, while the bottom row provides representative optical microscopic images of each region.

2.2 Description of the studied pump

Centrifugal pumps consist mainly of an impeller, a volute casing, and suction and discharge pipes. They are widely used in many applications due to their advantages in terms of static pressure. The studied pump (NS32) is a volute centrifugal pump with a specific speed of 32. The impeller is semi-open and has five backward-curved blades. The volute, which is the fixed element of the pump, has a circular and symmetrical section. The nominal operating conditions of the pump are a rotational speed of 1470 rpm and a flow rate of 590 m^3/h. The main geometric dimensions of the impeller, volute and pump specifications are summarized in Table 2.1.

	Parameter	**Value**
Impeller		
Inlet diameter (mm)	D_1	150
Outlet Diameter (mm)	D_2	408.4
Inlet blade width (mm)	b_1	85.9
Outlet blade width (mm)	b_2	42
Inlet blade angle (°)	β_1	70
Outlet blade angle (°)	β_2	63

Number of Blades	Z	5
Blade thickness (mm)	e	8
Volute		
Diameter (mm)	D_3	436
Base width of the volute	b_3	50
Nominal Head (m)	H_{bep}	49
Rotational speed (rpm)	N	1470
Nominal Flowrate (m^3/h)	Q_{bep}	590
Specific Speed	N_s	32

Table 2.1: NS32 specifications

2.3 Rheological model

To study the effect of emulsion flow on the performance of the centrifugal pump, the rheological model proposed by Zhu et al. [52] was applied to the emulsion under study. The authors proposed a model for emulsion rheology inspired by the equation proposed by Brinkman (Equation 2.1) for diluted suspension, but with a modified exponent (E) which is a constant obtained experimentally.

$$\mu_E = \frac{\mu_c}{(1-\phi_d)^E} \tag{2.1}$$

μ_c and ϕ_d are respectively the continuous phase viscosity and dispersed phase volume fraction.

The rheological model's first step is to evaluate the volume fraction of the dispersed phase at which phase inversion takes place (the dispersed phase becomes continuous). At this point, the emulsion viscosity is the same whether it was oil-continuous or water-continuous. Thus, the following equivalence is obtained from Equation 2.1

$$\frac{\mu_w}{(1-\phi_o)^E} = \frac{\mu_o}{(1-\phi_w)^E} = \frac{\mu_w}{\phi_w^E} \tag{2.2}$$

$$\frac{\mu_o}{\mu_w} = \left(\frac{1-\phi_w}{\phi_w}\right)^E \tag{2.3}$$

μ_o and μ_w are oil viscosity and water viscosity respectively. ϕ_w and ϕ_o are the volume fraction of water and oil respectively. By rearranging Equation 2.2 and posing $\tilde{\mu}$ (Equation 2.3) as the ratio of oil viscosity to water viscosity, the dispersed phase volume fraction at inversion point is defined as follows [31, 52]:

For water-continuous emulsion:

$$\phi_{oi} = \frac{\tilde{\mu}^{1/E}}{1+\tilde{\mu}^{1/E}} \tag{2.4}$$

For oil-continuous emulsion:

$$\phi_{wi} = \frac{1}{1 + \tilde{\mu}^{1/E}} \tag{2.5}$$

E is an experimentally determined coefficient after fitting the equation to the experimental results.

The following step is the application of the effective viscosity model of the emulsion, given by the relation:

$$\mu_A = C\left(\mu_E - \mu_M\right) + \mu_M \tag{2.6}$$

μ_M is the mixture base viscosity given by:

$$\mu_M = \frac{\mu_w}{\left(1 - \phi_o \phi_{oe}\right)^E} \tag{2.7}$$

Where

$$\phi_{oe} = 1 - \left(\frac{\mu_w}{\mu_o}\right)^{1/E} \tag{2.8}$$

C is a factor that considers the effect of several parameters on the viscosity of the emulsion. It includes the effect of pump rotation speed, surface tension which affects the droplet size of the dispersed phase, and the oil viscosity making up the emulsion. The proposed form of C is as follow:

$$C = \frac{(N_r WeRe)^n}{bSt^m} \tag{2.9}$$

The dimensionless numbers used are Weber Number (We), Reynolds Number (Re) and Strouhal Number (St), which reflect the effect of the mean droplet diameter, turbulence and shear rate on emulsion viscosity respectively. Their respective equations are given in the following chart. N_r is the stage number.

The proposed mechanistic model is a semi-empirical correlation since it's based on experimental data to determine the exponent E figuring in the Brinkman model and to obtain the exponents linking the dimensionless numbers i.e n, m and b of Equation 2.9. The procedure for determining the coefficients together with the calculation of the effective viscosity of the emulsion is summarized in Figure 2.2.

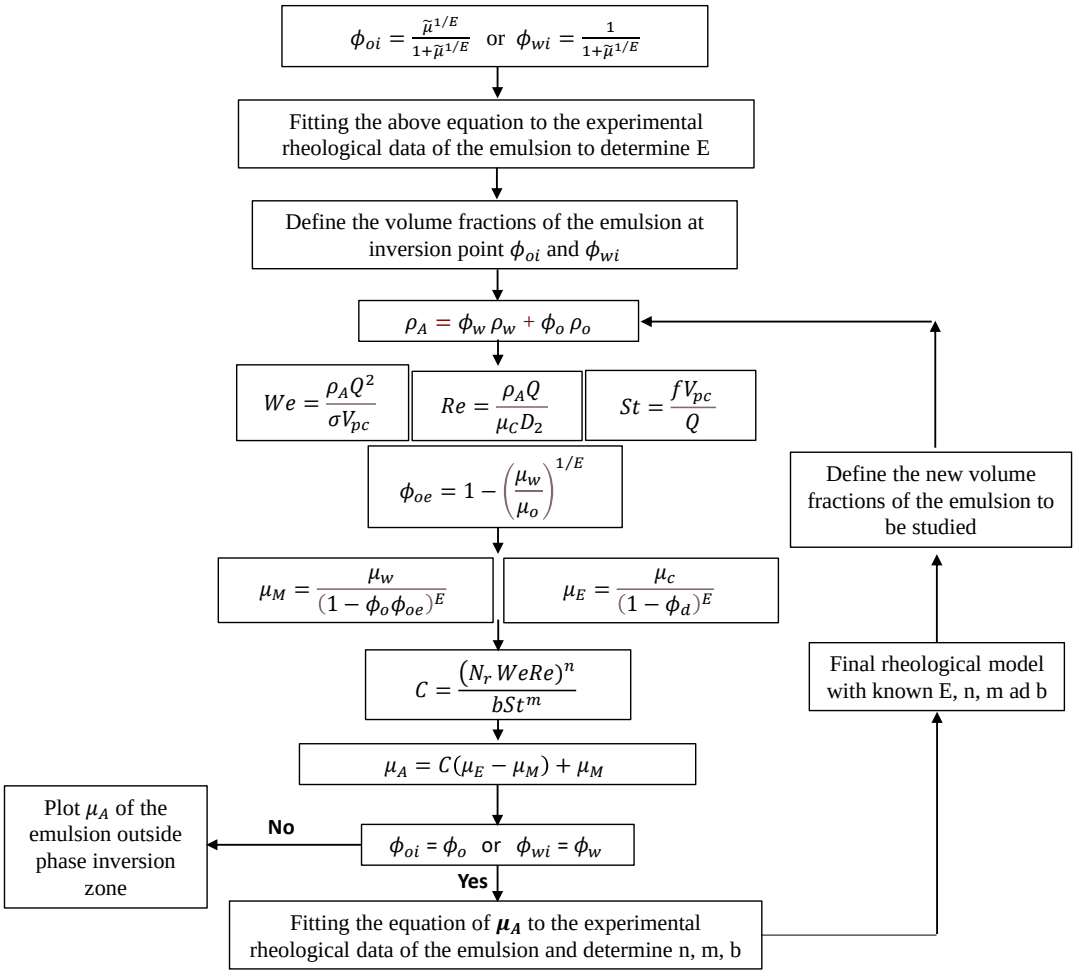

Figure 2.2: Flow chart for the calculation of the effective viscosity of the emulsion

2.4 Analytical model for pump performance

Many theoretical correlations have been proposed to determine pump performance to circumvent experimental testing. Theoretical studies have been of great importance as they provide an overview of the physical nature of the losses and allow their quantification [89] by making noticeable simplifying assumptions. However, these models are based on a set of equations and parameters that describe the pump's operating characteristics and are not versatile. These equations and parameters can be derived from data gathered from experiments or theoretical models. The model can be used to calculate the operating flow rate, pressure, power, and efficiency of a pump for any given combination of operating parameters.

The head characteristic of the pump results from subtracting the different losses from the theoretical head, as shown schematically in Figure 2.3.

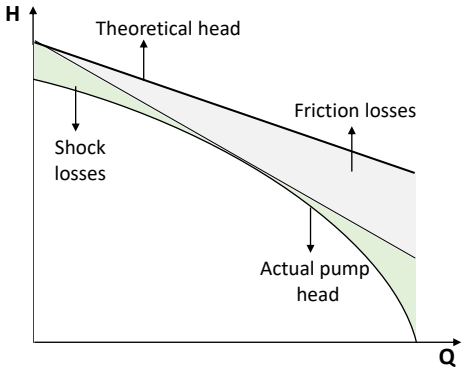

Figure 2.3: Theoretical head curve and hydraulic losses from the ideal head curve. Adapted figure from [106].

The loss mechanism inside a centrifugal pump generally consists of friction, shock, diffusion, recirculation, and wake mixing losses. However, several correlations are available to estimate the different loss mechanisms [89]. Therefore, an appropriate selection of these correlations is necessary to accurately predict the overall pump performance. The different loss mechanisms and models considered in this study are detailed in the following subsections.

2.4.1 Euler's equation

The ideal characteristics refer to the characteristics where the fluid, assumed incompressible and inviscid, is perfectly guided in the blades. This assumption leads to admitting an energy transmission by an infinite number of blades without thickness and losses. Thus, the fluid motion inside the impeller is the resultant of two velocities, the blade linear velocity U, induced by the rotation of the impeller; and the relative velocity W, induced by the displacement of the fluid with respect to the blade. Thus the fundamental equation of turbomachinery for an ideal characteristic is given by Euler [107] by the following equation:

$$\mathrm{H}_E = \frac{\mathrm{U}_2\mathrm{V}_{u2} - \mathrm{U}_1\mathrm{V}_{u1}}{\mathrm{g}} \tag{2.10}$$

U_1 and U_2 are the blade speed at impeller inlet and outlet respectively. V_{u1} and V_{u2} stands for the projection of absolute velocities at the impeller inlet and outlet to the direction of peripheral velocities.

Under the assumption that the fluid enters the impeller without pre-rotation ($V_{u1} = 0$), the analytical expression of the head is given as follow:

$$\mathrm{H}_{th\infty} = \frac{\mathrm{U}_2\mathrm{V}_{u2}}{\mathrm{g}} \tag{2.11}$$

The velocity components of the $\mathrm{H}_{th\infty}$ equation are expressed as follows:

$$\mathrm{U}_2 = \omega \mathrm{R}_2 \tag{2.12}$$

and

$$\mathrm{Vu_2} = \mathrm{U_2} - \mathrm{Vr_2\,tg}\,\beta_{2\infty} \tag{2.13}$$

where

$$\mathrm{Vr_2} = \frac{\mathrm{Qv}}{2\pi \mathrm{R_2\ b_2}} \tag{2.14}$$

Thus the pump theoritical head as a function of the flow rate, the rotation speed, and the geometry of the impeller is given by the following relation:

$$\mathrm{H}_{th\infty} = \frac{\mathrm{U_2}}{\mathrm{g}}\left[\mathrm{U_2} - \frac{\mathrm{Qv}}{2\pi \mathrm{R_2\ b_2}}\,\mathrm{tg}\,\beta_{2\infty}\right] \tag{2.15}$$

Where Q_v is the volumetric flow rate. b_2, R_2 and $\beta_{2\infty}$ are the outlet blade width, impeller outer radius and outlet blade angle respectively. ω is the angular velocity.

The actual pump head is obtained by first correcting the ideal Euler head and then subtracting the various losses generated in the pump. The correction methodology consists of considering the finite number of impeller blades, or in other words, correcting for the non-uniform pre-rotation of the velocity at the inlet and outlet of the impeller. This correction is usually made by multiplying the ideal Euler head by a slip coefficient, to obtain the theoretical pump head. Depending on the type of pump, and the nature of the assumptions considered, several models have been developed to estimate the theoretical head and slip coefficient. In this work, the ideal Euler head (Equation 2.15) is corrected by the slip factor proposed by Wiesner (Equation 2.16) without pre-rotating flow at the impeller inlet. The slip factor presented by the authors is an empirical equation that matches well with the experimental slip factor for a wide range of blade geometries.

$$\sigma = \frac{\sqrt{\sin\beta_{2\infty}}}{Z^{0.7}} \tag{2.16}$$

2.4.2 Head losses

A correct estimation of pump performance requires a careful selection of loss models. Several loss sets have been developed to predict pump energy losses. The classification and description of the loss mechanism differ among authors, whereas an analysis of the different types of losses in centrifugal pumps was reported by Viera et al. [89]. In the present study, the following internal losses are considered: (1) friction loss, (2) shock loss, and (3) diffusion loss. The selected set of losses was found to be sufficiently reliable in a previous study conducted by Kara et al. [108] to predict the performance of two centrifugal volute pumps conveying water and viscous fluids of different viscosities at varying rotational speeds.

2.4.2.1 Friction losses

Friction losses are generated by the shear stresses created by the velocity gradient in the non-separated boundary layers [109]. Within the impeller, the friction losses are modeled using Equation 2.17 (Gülich 2008), where a hydraulic diameter d_h and average relative velocity W_{av} are used.

$$L_{fr,i} = 4C_{fr,i}\frac{l_e}{d_{h,i}}\frac{W_{av}^2}{2g} \tag{2.17}$$

Similarly to the impeller, the friction model in the volute is derived from pipe flow theory and is given by Equation 2.18.

$$L_{fr,v} = 4C_{fr,v}\frac{l_c}{d_{h,v}}\frac{V_{3p}^2}{2g} \tag{2.18}$$

Where V_{3p} is the component parallel to the direction of the volute of the fluid velocity at the volute inlet V_3. The second component of the fluid velocity at the volute inlet is tangential to the impeller and is denoted by $V_{3d'}$. The velocity diagram at the volute inlet is shown in Figure 2.4. The fluid exits the volute with a velocity V_4 which is equal to the velocity component of V_{3p} in the tangential direction denoted by V_{3pu} [110].

The closure relationships of the above equations are grouped in Table 2.2.

Expression	**Complementary expressions and observations**
Impeller	
$d_{h,i} = \frac{2(a_2b_2+A_{q1})}{a_1+b_1+a_2+b_2}$	Impeller hydraulic diameter
$l_e = \frac{r_2-r_1}{\cos\beta_{2B}}$	Blade length
$C_{fr,i} = \frac{2.65}{Re_i^{0.875}} - \frac{2}{8Re_i+\frac{0.016}{Re_i}} + \frac{1.328}{\sqrt{Re_i}}$ $For\ Re_i < 10^5$	$Re_i = \frac{w_{av}l_e}{v}$
$C_{f,i} = \frac{0{,}136}{\left\{-\log\left(0{,}2\frac{\varepsilon_i}{d_{k,i}}+\frac{12{,}5}{Re_i}\right)\right\}^{2{,}15}}$ $For \begin{cases} 10^5 < Re_i < 10^8 \\ 0 < \varepsilon_i/l < 10^{-3} \end{cases}$	Impeller friction loss coefficient
Volute	
$D_{h,v} = \frac{d_2}{\frac{1}{2(b_3/b_2)(b_2/d_2)}+\frac{1}{8(\pi/z_{la})(d_3/d_2)\sin(a_v)}}$	Average volute hydraulic diameter
$Re_v = \frac{c_{3p}D_{h,v}}{v}$	Volute Reynolds number
$C_{fr,v}$	Volute friction loss coefficient, calculated in the same way as the impeller friction coefficient.
$V_{3p} = \frac{V_4}{\cos\alpha_v}$	Component of the fluid velocity at the entrance of the volute
$\tan\alpha_v = \frac{A_c}{\pi d_2 b_2 (d_3/d_2)(b_3/b_2)}$	Volute angle
$V_4 = \frac{Q_v}{A_c}$	Volute outlet velocity
A_c	Volute throat area

Table 2.2: Closure relationships of friction loss correlations

Another friction loss to consider is the disc friction loss that occurs over the impeller shroud and hub. The disc friction losses are expressed according to Gulich [111] as follows:

$$L_{fr,d} = \frac{C_{fr,d}}{\cos\delta}\rho\omega^3 R_2^5 \left\{1 - \left(\frac{R_1}{R_2}\right)^5\right\} \tag{2.19}$$

δ is the deviation angle, given as follows :

$$\delta = \beta_{2b} - \beta_2 \tag{2.20}$$

$$\beta_2 = \tan^{-1} V_{2m}/W_{2u} \tag{2.21}$$

ω is the angular velocity and $C_{fr,d}$ is an empirical friction coefficient calculated from equations within Table 2.3.

$C_{fr,d} = \frac{\pi R_2}{2Res_{ax}}$ for $\mathrm{Re_{lam}} \leq 8.7\left(\frac{s_{ax}}{R_2}\right)^{-1.87}$
$C_{fr,d} = \frac{0.925}{Re^{0.5}}\left(\frac{s_{ax}}{R_2}\right)^{0.1}$ for $\mathrm{Re_{lam}} < \mathrm{Re} < 2\times10^5$
$C_{fr,d} = \frac{0.02}{Re^{0.25}}\left(\frac{R_2}{s_{ax}}\right)^{1/6}$ for $10^5 < \mathrm{Re} < 10^6$
$C_{fr,d} = \frac{0.0255}{Re^{0.2}}\left(\frac{s_{ax}}{R_2}\right)^{0.1}$ for $\mathrm{Re} > 2\times10^5$

Table 2.3: Correlations for the maximum droplet size of liquid-liquid dispersions

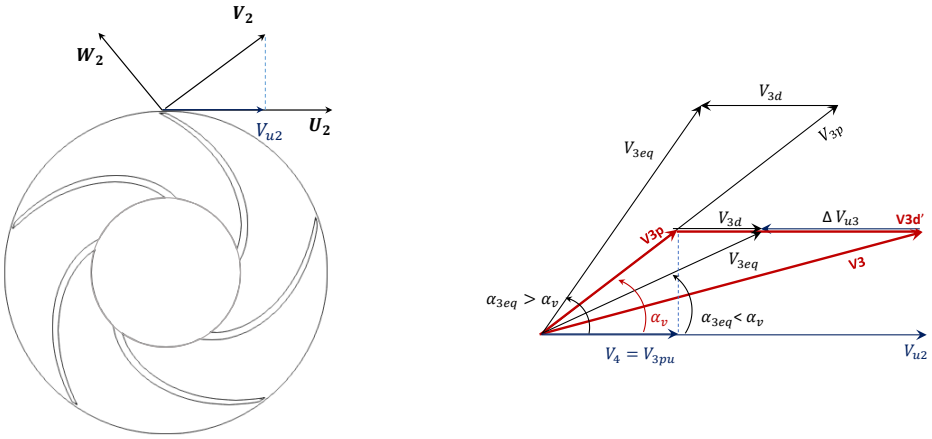

Figure 2.4: Velocity at impeller outlet and volute inlet reproduced from [110]

2.4.2.2 Shock losses

Shock losses are explained by the sudden change in flow direction at the impeller or volute inlet and outlet. These losses change the shape of the streamlines and differentiate them from blade geometry [89]. These losses are generally significant at low and high flow rates, but almost negligible at design point.

The model proposed by Pfleiderer and Petermann [108] was adopted in this work to estimate the shock losses within the impeller. The authors stated that the shock loss depends on the difference between relative velocities before and after the blade leading edge and is given by equation Equation 2.22.

$$L_{sh,i} = C_{sh,i} \frac{(W_1 - W_{1q})^2}{2g} \tag{2.22}$$

$C_{sh,i}$ is the impeller inlet shock loss coefficient, whose empirical value varies from 0.5 to 0.7 depending on the size of the recirculation zone after the blade leading edge [108].

The shock losses inside the volute are described by the difference between the component of the fluid inlet velocity V_3 parralel to the direction of the volute, and the flow velocity through the volute V_{3p}. Referring to Figure 2.4, The flow enters the volute with a through-velocity V_3 at an angel α_3 (α_3 may differ from α_v in Figure 2.4 which is the volute angle) [110]. The velocity component V_{3pu} equals the volute outlet velocity V_4 and the velocity component V'_{3d} is the motive of a second circulatory motion given to the volute flow in the impeller motion direction. Thus, the volute shock losses, according to (Tuzson 2000) [108], are written as:

$$L_{sh,v} = C_{sh,v} \frac{V_3^2 - V_{3p}^2}{2g} \tag{2.23}$$

The closure relationships of the above equations are grouped in Table 2.4.

Expression	**Complementary expressions and observations**
$C_{sh,v}$	Volute shock loss coefficient, whose empirical value varies from 0.5 to 0.7
$V_3 = \sqrt{{V_{3p}}^2 + {V_{3d}}^2}$	Volute inlet velocity
$V_{3d} = V_{2up} - V_4$	Volute circulatory velocity component

Table 2.4: Closure relationships of friction loss correlations

2.4.2.3 Diffusion losses

Diffusion losses are the result of the expansion of the surface of the cross-sectional area of flow channels either within the impeller or within the volute. This expansion takes place simultaneously in the radial and axial directions [112]. This type of loss is denoted in some literature by Wake mixing

loss (Aungier (1995)), explained by the mixing of the blade wake flow and the free steam flow caused by abrupt expansion.

The diffusion loss in the impeller is calculated using the following equation:

$$L_{diff,i} = 0.25\frac{W_1^2}{2g} \tag{2.24}$$

Where W_1 is the impeller inlet relative velocity.

The diffusion loss in the volute is determined by the following equation:

$$L_{diff,v} = C_{diff}\frac{V_{3d}^2}{2g} \tag{2.25}$$

These losses are generated by the volute circulatory velocity V_{3d}. C_{diff} is the volute diffusion loss coefficient, to which a value of 0.8 is assigned [110].

2.5 Results and discussion

2.5.1 Rheological model fitting

As stated previously, the analysis of the effect of emulsions on the performance of the centrifugal pump is based on a rheological model proposed in the literature. Therefore, equation Equation 2.6 is applied to the studied emulsion in order to estimate its effective viscosity.

Figure 2.5 shows the emulsion viscosity predicted by the rheological model using Zhu [52] and Banjar [31] coefficients versus water cut at best efficiency point (BEP) (900 rpm and Q = 300 m^3/h), compared to the experimental data.

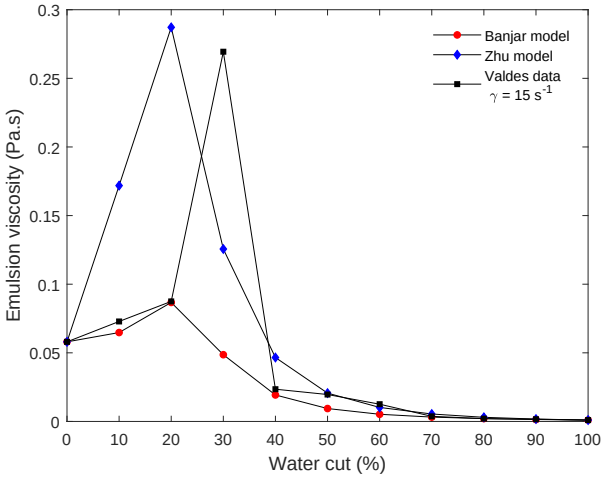

Figure 2.5: Comparison of the emulsion effective viscosity predicted by the rheological model using Zhu [52] and Banjar [31] coefficients with the experimental data [30]

A clear peak in the emulsion viscosity is observed as the water-volume fraction increases, indicating the reversal of the continuous-oil emulsion (water-in-oil) to a continuous-water emulsion (oil-in-water),

resulting in a significant increase in its effective viscosity. From the figure, the phase inversion point predicted by both models is lower than the experimental one (20% WC vs. 30% WC in experimental data), highlighting also that Banjar's model gives a better approximation of the viscosity value at this point. Before the phase inversion, the experimental data are well predicted by Banjar's model with a deviation of 8%. Conversely, after the inversion point, the experimental data are well predicted by Zhu's model with a discrepancy under 14%. The difference between the predicted inversion point and the experimental one is expected since the rheological model is semi-empirical. The proposed equation for inversion point determination (Equation 2.4) depends on the viscosities of the two coexisting phases, linked by an exponent E determined experimentally. The operating conditions of this study and the properties of the oil constituting the emulsion (viscosity and surface tension) differ from those of the two authors, therefore the value of E determined by the authors can not be applied in this case. Besides, exponent E is determined for fixed operating conditions and is applied over the range of flow rates and speeds relative to the studied pump. It has been reported that phase inversion depends on the properties of the emulsion (continuous phase oil viscosity and emulsion stability) as well as the shear rate applied to the emulsion (rotational speed and flow rate). Phase inversion occurs at a higher volume fraction of the dispersed phase as the rotational speed increases and the viscosity of the oil continuous phase decreases [29]. The rheological model proposed by the authors verifies the effect of viscosity on phase inversion but does not reflect the operating conditions or emulsion stability effect. Consequently, the viscosity model (Equation 2.4 and Equation 2.9) should be fitted to the current experimental data to give a better prediction of the inversion point as well as the overall emulsion viscosity.

A model fitting was conducted to find the numerical values of the equation coefficients that best fit the input data. The final C-factor and E-value obtained are compared with those reported in the literature in Table 2.5.

μ (cP)	σ (N/m)	**C**	**E**	**Ref**
100	0.032	$C = \frac{(NWeRe)^{0.1}}{10St^{0.2}}$	3	Banjar [31]
10	0.02	$C = \frac{N^{0.15}(WeRe)^{0.1}}{2.5St^{0.2}}$	3.2	Zhu et al. [52]
58	0.019	$C = \frac{(NWeRe)^{0.05}}{3St^{0.5}}$	4.8	Present work

Table 2.5: Comparison of exponents after model fitting with those in the literature

The difference between the exponents linking the dimensionless numbers and the E value obtained by the two authors is expected since their determination is based on experimental data only, emphasizing that such a close value is explained by the fact that the dimensions of the pumps used by the two authors are similar as well as the operating conditions.

In Figure 2.6, the rheological model with adjusted exponents is plotted against the experimental data as a function of WC. The adjustment consisted of increasing the exponent E (Equation 2.3) (compared to the other models) to account for the difference in operating conditions (lower specific speed and larger pump size compared to the reference papers). The fitted model gives an accurate prediction for the inversion point, however, the viscosity is underestimated with a difference of 20%. Outside the phase inversion zone (a 20% margin before and after the inversion point), the model gives an accurate prediction

of the emulsion viscosity with a difference of less than 9%.

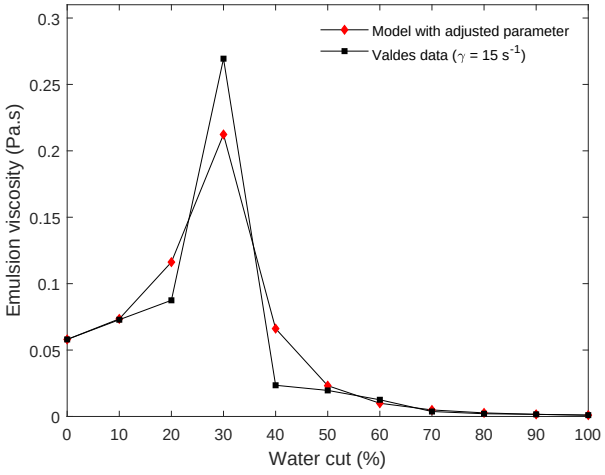

Figure 2.6: Adjusted rheological model versus experimental data

2.5.2 Pump head

To validate the present prediction procedure, the results are compared to the provided catalog performance curve of the centrifugal pump handling water at different rotational speeds. Figure 2.7 shows the comparison of the pump head predicted by the model and the performance curve provided by the manufacturer as a function of flow rate. It should be noted that the studied pump was tested with water at a rotational speed of 900 rpm, and the experimental results corresponded well to the provided curve, with a mean deviation of less than 3% at a low flow rate. Excellent agreement with the catalog head is observed with less than 5% deviation at low and high flow rates for the different rotational speeds considered. This indicates that the hydraulic loss equations used for pump head prediction are correctly evaluated.

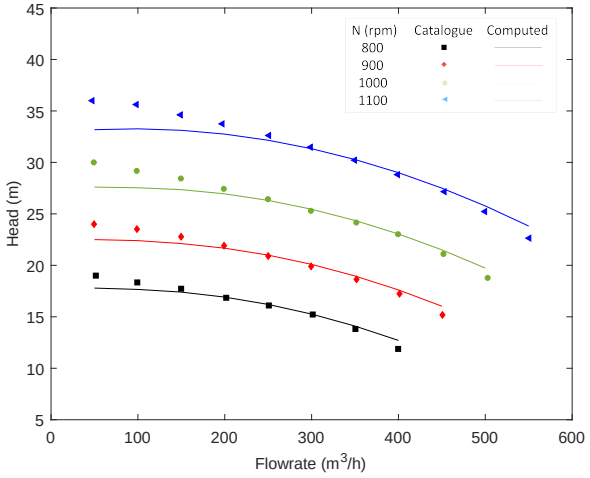

Figure 2.7: Predicted pump head under water flow at 900 rpm versus experimental data

The performance prediction of the centrifugal pump when handling emulsion has been carried out by

incorporating the rheological model in the head losses. The suggested model (Equation 2.6 with fitted parameters (Table 2.5) is used to estimate emulsion rheology first, and the resulting effective viscosity is then used in the pump performance mechanistic model as a single phase oil, i.e in friction loss correlations (in the closure relationship of Equation 2.17 and Equation 2.18).

The emulsions considered in this analytical study correspond to an emulsion of regions 1 and 3 presented previously (Figure 2.1): an oil-in-water emulsion with volume fractions of 40%O-60%W, a water-in-oil emulsion with volume fractions of 20%W-80%O. Since the rheological model is applicable only outside the phase inversion zone and the emulsion has a very high viscosity at this zone, the mechanistic model has not been considered for emulsion in region 2. The predicted head of the pump operating with water and the emulsions considered at different rotational speeds are shown in Figure 2.8.

We observe that as the oil volume fraction increases, the pump head decreases. Since the viscosity of the emulsion is higher than that of water, the pump head decreases, which is caused by an increase in hydraulic losses, mainly frictional losses, as shown in previous studies [113]. For the 40%O-60%W emulsion, the analytical model shows that the pump head degradation caused by the rheological behavior of the emulsion increases with the flow rate. This observation is in agreement with the experimental results of Valdes [30] on an ESP carrying the same emulsion and with the CFD results obtained in this study for the same emulsion which will be seen in the following chapters. Finally, for the oil-continuous emulsion with a water cut of 20%, the model deviates at high flow rates. This is probably due to the high effective viscosity of this emulsion. As stated by Banjar [91], the mechanistic model for pump head prediction gives a good estimate of the pump head for emulsions with relatively low viscosities, and when the viscosity increases beyond 60 cP, the model is not suitable anymore. The authors applied this procedure to estimate the head of a multistage pump handling different emulsions (i.e., coupling their proposed rheological model with a mechanistic model for pump head), where friction, recirculation, shock, and rotation losses were considered in the mechanistic model for pump head prediction (see subsection I.4.1 of the literature review). A similar conclusion can be made in the actual study. The oil constituting the emulsion has a viscosity of 58 cP, and the predicted viscosity of the continuous oil emulsion, i.e., 20%W-80%O, varies from 40 cP to 130 cP as the flow rate increases from 50 m^3/h to 600 m^3/h. Since the predicted viscosity of the latter emulsion is too high, the model is not applicable for estimating the pump head conveying this emulsion.

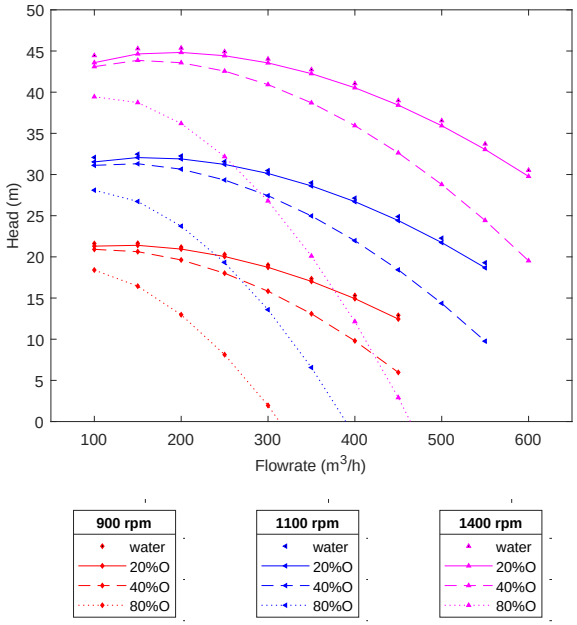

Figure 2.8: Analytical pump head results for water and emulsion at different rotational speeds

To investigate the losses within the centrifugal pump when handling both water and emulsion in detail, the variation characteristics of each loss versus flow rate are shown in the following figures. The 40%O-60%W is selected since its viscosity boundary is included in the model limit. Three categories of pressure losses can be distinguished according to their variation with the flow rate [114]:

- Hydraulic losses which increase with the increase of the flow rate, namely: friction losses in the impeller, diffusion losses in the impeller, and friction losses in the volute. This increase is attributed to the velocity of the fluid increasing with the flow rate. This increased velocity causes more friction between the fluid and the walls of the pump parts, resulting in increased friction losses. It also causes more disturbance of the flow field due to the presence of the blade wake, which can lead to increased turbulence and pressure losses, resulting in increased diffusion losses.

- Hydraulic losses that decrease with increasing flow rate, including friction losses in the disc. As the flow rate increases, fluid velocity increases and the flow that goes between the disc and fluid decreases.

- Hydraulic losses that have a parabolic shape, namely: impact loss in the impeller, impact loss in the volute, and diffusion loss in the volute. This last group is almost negligible at the design flow rate and increases at off-design conditions. These losses occur when the flow rate of a pump is less than or greater than the value resulting from a shock-free approach flow corresponding to the design point. A change in flow rate results in a change in the angle of entry or exit of the fluid in either the impeller or the volute, and thus an increase in these losses as one moves away from the design point.

The skin friction losses in the impeller and volute are shown in Figure 2.9 (a) as a function of flow for both fluids. These losses are dominant in the pump volute when handling water and become of the same

order of magnitude in both parts of the pump when handling emulsion but with a magnitude significantly larger than for water. The disc friction losses (Figure 2.9 (b)) estimated with the empirical correlation decrease with increasing flow rate and their magnitude increases with the viscosity of the emulsion. At low flow rates, the disc friction loss has a significant impact on the pump head loss, along with shock and diffusion loss in the volute.

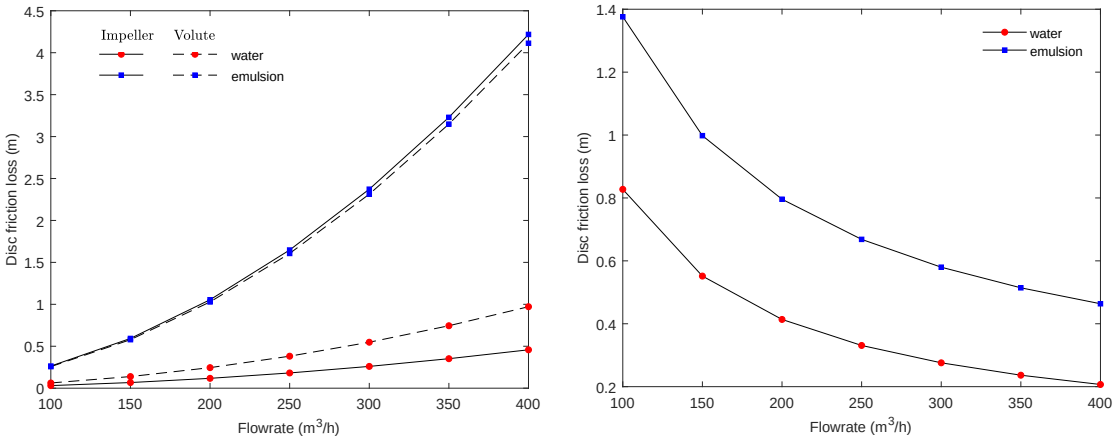

Figure 2.9: Surface friction loss in (a) impeller and volute, (b) disc

The diffusion losses in the impeller and volute are shown in Figure 2.10 for the two fluids. The diffusion loss is viscosity independent and is significantly large in the volute. Previous studies have shown that the diffusion losses are viscosity independent in turbulent flow when the Reynolds number is between $3 \cdot 10^4$ and $6 \cdot 10^4$ [112], which is the case in our study as well. Furthermore, no clear evidence has been found in the literature regarding the effect of Reynolds number on diffusion losses [112] and no analytical model accounting for this effect has been proposed. Compared to frictional losses when handling water, the diffusion loss within volute is quite large, so the divergent part of the volute should be thoroughly designed so that the diffusion loss is as minor as possible. The magnitude of this loss within impeller i.e diffusion loss is comparable to the skin friction loss in the impeller but much smaller than that in the volute. When handling emulsion, friction losses within the impeller and volute increase significantly, which is caused by the increase of the fluid viscosity. This is what explains the degradation of the performances obtained previously. However, the other losses estimated with the analytical models, namely shock loss (Figure 2.11), and diffusion loss remain invariant when the viscosity of the fluid changes. The impact loss in the impeller is insignificant compared to the impact loss in the volute, and both become almost negligible at design point. The two previous losses are viscosity independent since the proposed models do not consider the effect of viscosity on the velocity triangle and thus these loss models are functions of the flow rate and the pump geometry only.

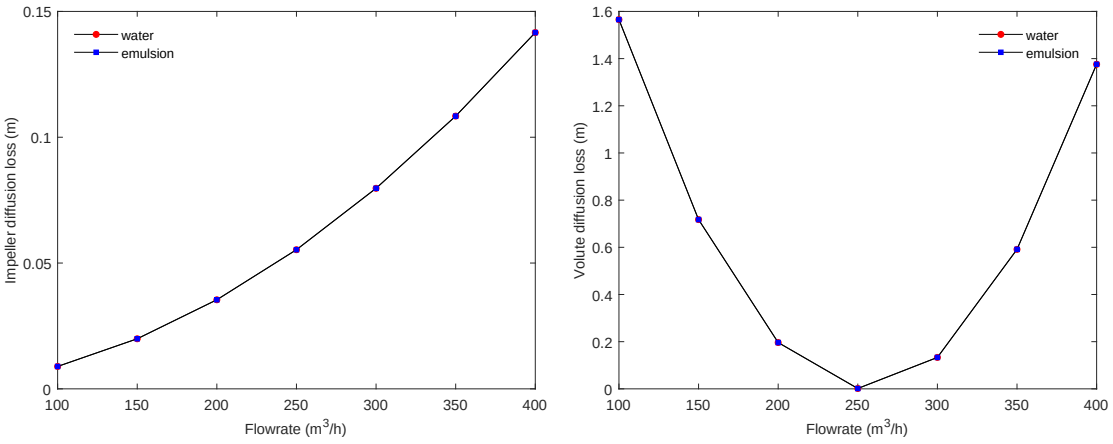

Figure 2.10: Diffusion loss in (a)impeller, (b) volute

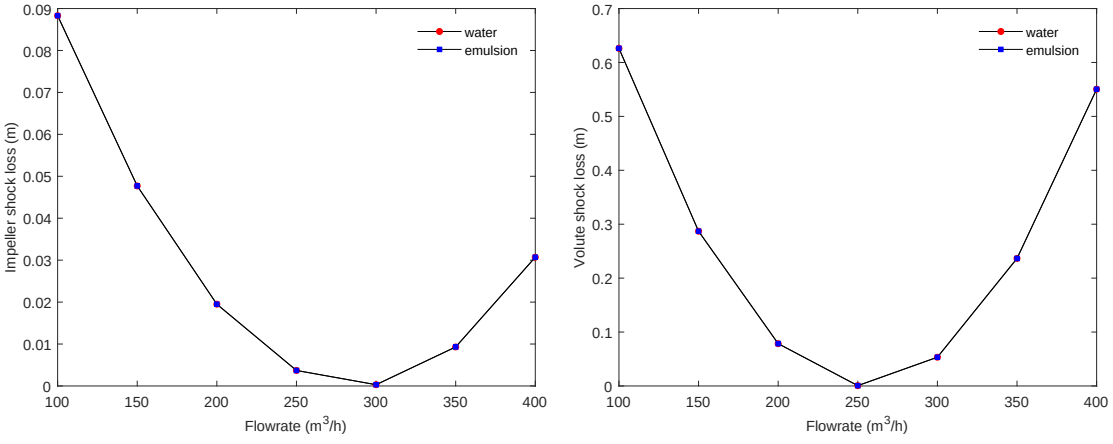

Figure 2.11: Shock loss in (a)impeller, (b) volute

2.5.3 Model limitation and conclusion

The analytical model shows that pump performance degrades when the fluid is an emulsion due to its high viscosity. The friction losses in the impeller, volute and disc depend on the fluid viscosity, and the associated correlations for their estimation consider the effect of the viscosity. The correlations proposed to estimate the other losses are viscosity independent. These models depend however on empirical coefficients and may thus overestimate or underestimate the effect of viscosity on the associated losses. These losses are generally based on the velocity triangle which is based on a theory that neglects fluid viscosity and assumes an idealized two-dimensional flow through the impeller. The fluid viscosity affects recirculation phenomena, changes the shape of the streamlines, and differentiates them from the blade geometry. In addition, there are several parameterizations in the correlations of these losses that depend on the adjustment factors and experimental data which are generally obtained with water.

No conclusion can be made regarding the accuracy of the analytical correlation for pump head estimation under emulsion flow given the lack of experimental results. The analytical model is semi-

empirical and finds its limits when the fluid is very viscous. The viscosity of the fluid is considered only in the friction loss equations which neglects thus the other effect that the viscosity may have on the losses. Moreover, the rheological model for the estimation of the emulsion viscosity is not universal. Figure 2.12 (a) shows that the emulsion viscosity obtained with the proposed model decreases with increasing pump rotational speed which is consistent with the experimental data. However, the effect of the flow rate on the rheological behavior of the emulsion is not considered correctly, as we see in the Figure 2.12 (b) and Figure 2.13 that the estimated emulsion viscosity increases with increasing flow rate. Figure 2.12 (b) shows the viscosity of the emulsion obtained from Equation 2.6 by varying the volume fraction of water in Equation 2.1 and Equation 2.7, as well as the flow rate in Equation 2.9. While Figure 2.13 shows the effect of flow rate on an emulsion with fixed volume fractions (40%O-60%W), obtained from Equation 2.6 by varying the flow rate in Equation 2.9. This last remark is indeed contradictory to the shear-thinning behavior of emulsions previously observed from experimental data. The analytical model of viscosity gives an approximate estimation of the emulsion impact on the pump's performance but does not describe the fluid behavior within the pump. This is an important limitation for analytical approaches.

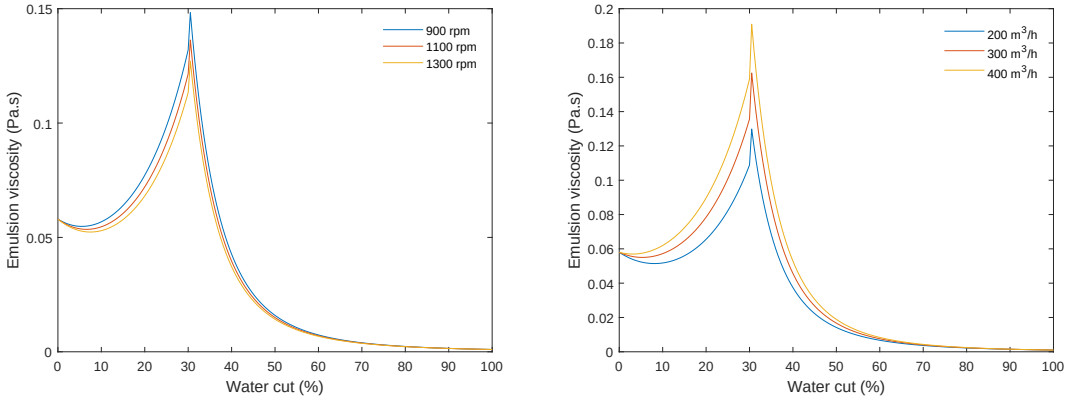

Figure 2.12: Emulsion rheological behavior predicted by the model at (a) different rotation speeds and (b) different flow rates

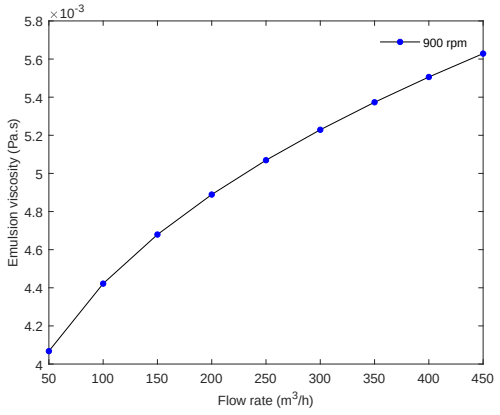

Figure 2.13: Variation of the emulsion viscosity as a function of the flow rate

CHAPTER 3

Hydrodynamic behavior of a centrifugal pump handling emulsions modeled as a non-Newtonian fluid by CFD

Contents

Introduction and motivation

As stated in the state-of-the-art, many researchers have investigated the viscosity of emulsions at different water cuts (WC) and found that in most cases, the emulsion exhibits a shear-thinning behavior. On the other side, the work in the literature on the operation and performance of centrifugal pumps handling emulsions and oil-water mixtures is few and has mainly focused on experimental investigations, which confirmed the non-Newtonian behavior of emulsions in pumps. Few numerical analyses have been performed on this topic given the complexity involved in emulsion modeling. These numerical studies have focused on the analysis of the overall performance of a multistage pump handling emulsions, but no studies have focused on a volute centrifugal pump while considering the rheological behavior of these fluids. Therefore, a thorough study of the hydrodynamic behavior of volute centrifugal pumps when handling emulsion, considering their non-Newtonian rheology, remains to be done.

The main objective of this chapter is the analysis of the performance and flow characteristics of a volute centrifugal pump numerically when handling emulsions of oil–water mixtures at different water cuts (WC) by considering their non-Newtonian rheological behavior, as well as to compare its performance when operating with Newtonian viscous oil. The mixtures' rheological properties were investigated experimentally, and the results were fed into the transport properties section of the open-source library

OpenFOAM v1906 which is the library used for the simulation. Therefore, the mixtures have been modeled and simulated as a single-phase fluid following non-Newtonian rheology. In addition, a more in-depth analysis of the internal flow is performed in this chapter, relating the hydrodynamic performance of the pump to the rheological properties of the emulsion.

3.1 Numerical set-up

The first step in CFD is the modelization of the geometry and the flow domain as well as the generation of the three-dimensional mesh for the chosen domain. The following step consists in establishing the initial and boundary conditions as well as a simulation strategy. This last point involves the determination of elements such as the choice of the turbulence model and the solution algorithms.

3.1.1 Geometry and mesh

The initial steps of the numerical simulation are the determination of the computational domain (volume of fluid) and the generation of a three-dimensional mesh for the selected volume. Due to the complex geometry of the centrifugal pump, the geometric model was generated using CATIA software. As mentioned earlier, the studied pump consists of a five-bladed backward-curved impeller and a volute and is designed in four parts, as shown in Figure 3.1.

- Inlet pipe
- Impeller
- Volute
- Outlet pipe

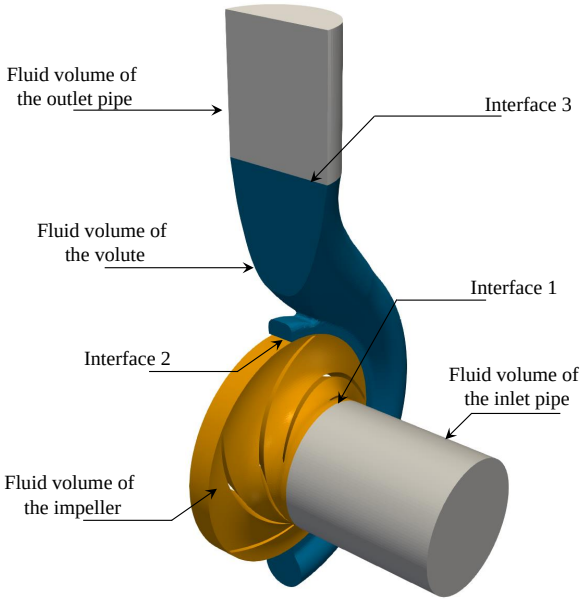

Figure 3.1: Fluid volume

Following this configuration, three interfaces are considered:

- Interface 1: an interface between the inlet pipe and the impeller inlet,
- Interface 2: an interface between the impeller and the volute,
- Interface 3: an interface between the volute and the outlet pipe.

The quality of the mesh used to solve a fluid mechanics problem is critical to the solution outcome. Structured meshes are the most efficient in terms of computation time and accuracy and are often preferable. However, it is very cumbersome to generate structured meshes for many complex geometries, as is the case for a centrifugal pump. Thus, it becomes necessary to use an unstructured mesh type for some parts of the computational domain.

For mesh generation, an unstructured mesh was generated due to the complex geometry of the centrifugal pump as stated above. Two types of mesh elements were considered: polyhedrons and prisms. The hexahedral elements were employed in the inlet and outlet sections, while the polyhedron elements were employed in the impeller and volute. To capture the flow details near the flow domain boundaries, a structured mesh was used for the boundary layer of the near-wall regions. This led to an average $y+ < 5$ and direct resolution of the viscous sublayer of the inner region as shown in Figure 3.2. This ensures a good evaluation of the wall shear stress for highly viscous fluids like oil and emulsion having 70% oil volume fraction (inversion zone). For water and other fluids (see Table 3.3), wall functions are selected to deal with the near-wall region. This approach guarantees more precise calculations in cases where the mesh has a medium resolution and is located in the buffer sublayer ($5 < y+ < 30$). These $y+$ values are guaranteed for the large pump (NS32) and its reduced model which will be studied later. In OpenFOAM, the existing wall functions have been modified to ensure that they can provide accurate results wherever the position of the first cell center [115]. Figure 3.3 gives an overview of the generated mesh.

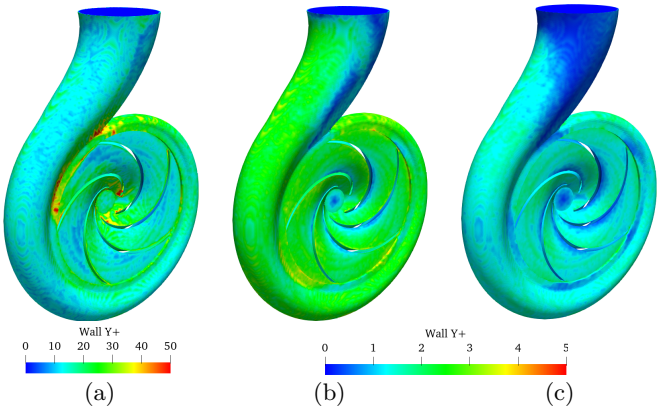

Figure 3.2: Distribution of Y+ value at BEP for (a) water, (b) 70%O-30%W, (c) oil.

The information between the different pump regions is transferred through an arbitrary mesh interface (AMI). At these interfaces, a steady-state flow velocity condition is applied, which assumes the same absolute velocity on both sides of the interface and thus for each reference frame. To implement the motion of the rotation domain in the stationary case, the multiple reference frame (MRF) models is used. In contrast, for the transient case, the motion is implemented using a dynamic mesh. The challenge of

the MRF method is the correct positioning of the interfaces in the geometry and the generation of a consistent mesh for both sides of the interface. Although the meshes at the interfaces do not have to match perfectly due to the AMI approach, a similar and uniform cell size on both sides can significantly increase the accuracy of the results.

To determine the most favorable number of cells to use for the simulations, a mesh independence test was performed. The centrifugal pump head considering the water was taken as a reference parameter to determine the influence of mesh size on the convergence to the exact solution. Four different mesh sizes were evaluated; M1: coarse, M2: basic, M3: fine, and M4: ultrafine (Table 3.1. The convergence criterion chosen was a relative head difference with a maximum value of 1 %. Figure 3.4 shows the convergence of the calculated discharge pressure to an asymptotic value as the number of grids increases. The M3 grid ($4 \cdot 10^6$ grids) was found to be sufficiently reliable to ensure non-dependence of the grids and was used for the rest of the study. The quality of the mesh used to solve a problem is critical to the quality of the solution. Some essential parameters for mesh quality were evaluated, including Skewness, Orthogonal Quality, and Aspect Ratio, the values of which are given in Table 3.2 for the selected mesh.

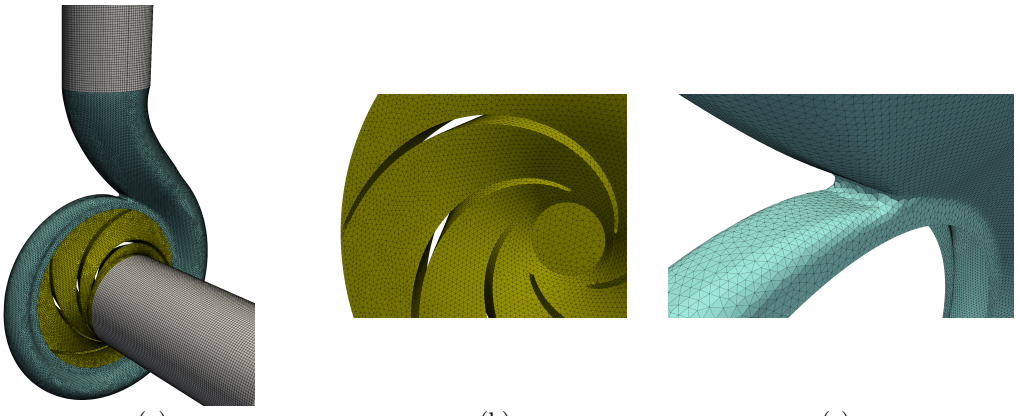

(a) Computation domain (b) Impeller mesh (c) Volute tongue mesh

Figure 3.3: Fluid volume mesh

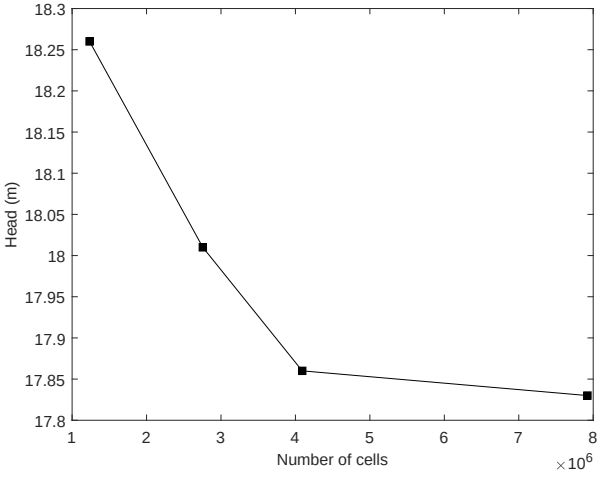

Figure 3.4: Grid sensitivity study

Characteristics	Number of Cells
M1	1,230,000
M2	2,750,000
M3	4,091,000
M4	7,900,000

Table 3.1: Mesh size used

Parameter	Value
Max cell openness	9.173e-15 OK
Max aspect ratio	3.496e+2 OK
Non-orthogonality check	OK
Face pyramids	OK
Max skewness	3.139 OK

Table 3.2: Parameters evaluated for the quality of the mesh

3.1.2 Emulsion Rheology

The non-Newtonian behavior of the emulsion can be presented as the shear thinning effect. In shear-thinning non-Newtonian emulsion models, the viscosity becomes a nonlinear function of the shear rate. In this study, the emulsions under consideration exhibit shear-thinning behavior, as stated previously in Chapter 2. They were tested under a shear rate ranging from 1 s^{-1} to 3000 s^{-1}, and the rheological characterization results were fitted to the conventional effective viscosity models of Cross and Carreau. The following correlations correspond to the Cross and Carreau models, respectively.

$$\frac{\mu_{eff} - \mu_\infty}{\mu_0 - \mu_\infty} = [1 + (k_c\dot{\gamma})^{n_c}]^{-1} \tag{3.1}$$

$$\frac{\mu_{\text{eff}} - \mu_\infty}{\mu_0 - \mu_\infty} = \left[1 + (\lambda_t\dot{\gamma})^2\right]^{\frac{n_{car}-1}{2}} \tag{3.2}$$

Where k_c and n_c are the Cross time and Cross rate constant, respectively. λ_t and n_{car} are the relaxation time and power index, respectively. ν_0 and ν_∞ are the viscosity for zero shear rates and very high shear rates. Table 3.3 summarizes the emulsions studied and the associated non-Newtonian model parameters.

$(\%v/voil)$	Viscosity Model	$\rho\ (kg/m^3)$	n_c/n_{car}	$k_c(s^n)/\lambda_t(s)$	$\nu_0(m^2/s)$	$\nu_{\text{inf}}(m^2/s)$
100	Newtonian	922.8	–	–	–	$6.29\ 10^{-5}$
90	Carreau	947.8	0.471	$2.03\ 10^{-4}$	$7.59\ 10^{-5}$	$2.40\ 10^{-5}$

80	Carreau	952.2	0.421	$5.30\ 10^{-3}$	$9.01\ 10^{-5}$	$6.82\ 10^{-5}$
70	Carreau	953.0	0.339	45.88	$1.57\ 10^{-2}$	$3.14\ 10^{-5}$
50	Cross	966.9	0.339	1.94	$4.44\ 10^{-5}$	$1.03\ 10^{-5}$
40	Cross	978.3	0.416	21.06	$3.27\ 10^{-5}$	$1.02\ 10^{-5}$
0	Newtonian	1000	–	–	–	$1.00\ 10^{-6}$

Table 3.3: Measured density, Cross/Carreau fitting parameters for each composition studied, data from [30]

3.1.3 Numerical model

The numerical simulation consists of solving the averaged 3D Navier Stokes equations with a RANS approach for turbulence modeling. The simulations were performed with the open-source library OpenFOAM v1906 which uses a finite volume method (FVM) to discretize the fluid equations.

In this study, the flow field within the centrifugal pump was assumed to be incompressible, single-phase, isothermal, viscous, and turbulent. The mass and momentum equations (Equation 3.3 and Equation 3.4 respectively) are solved using the SIMPLE algorithm (Semi-Implicit Method for Pressure-Linked Equations).

$$\frac{\partial}{\partial t}(\rho) + \nabla \cdot (\rho \overline{\mathrm{u}}) = 0 \tag{3.3}$$

$$\frac{\partial}{\partial t}(\rho \overline{\mathrm{u}}) + \nabla \cdot (\rho \overline{\mathrm{u}} \otimes \overline{\mathrm{u}}) = g + \nabla \cdot \overline{(\tau)} - \nabla \cdot (\rho \mathrm{R}) \tag{3.4}$$

$\overline{(\tau)}$ is the averaged stress tensor and R is the Reynolds stress tensor. The Reynolds stress is the component of the total stress tensor in a fluid obtained from the averaging operation over the Navier–Stokes equations to account for turbulent fluctuations in fluid momentum.

Turbulence is based on the concept of "energy cascade" developed by Kolmogorov [116, 117], which states that turbulence is composed of vortices of different sizes, each possessing a certain amount of energy that depends on its size. Three approaches exist to solve the turbulent flow. The first one is based on the direct resolution of the full spectrum of time and space scales of the turbulent terms of the Navier Stokes equations, known as DNS (direct numerical solution). This method is extremely expensive regarding the computation time and requires a small time step and a very fine mesh (For example, the number of meshes required for a direct numerical simulation of the studied pump (NS32) is approximately 687 trillion cells ($687 \cdot 10^{12}$)). The second method is the Large Eddy Simulation (LES), which is a method developed to simplify the solution of turbulent flows. The concept of this method is that large-scale turbulent structures are directly simulated, while small-scale turbulence is modeled using subgrid-scale models. The third approach is solving the Reynolds averaged Navier Stokes (RANS) equations, which are based on the concept of modeling all scales of turbulent flow. This approach is the most popular one for solving industrial problems and proceeds directly to the averaging of the Navier-Stokes equations by redefining the variables as the sum of two values: an average value and a fluctuating value. During the averaging process, the nonlinearity of the Navier-Stokes equations gives place to Reynolds stresses that

must be modeled.

Models for direct calculation of Reynolds stresses are based on the Boussinesq assumption [116] which postulates that the Reynolds stress tensor is proportional to the average strain rate tensor. Boussinesq's hypothesis introduces the concept of turbulent eddy viscosity which calculates the large-scale eddies in the flow and characterizes the transport and dissipation of turbulence. The models can be grouped into four categories:

- algebraic (zero equation) models,
- one equation models,
- two-equation models,
- second-order closure models.

The choice of a turbulence model depends on the physical nature of the problem and the computational power. Nevertheless, traditional RANS models, such as $k-\epsilon$ or $k-\omega$ (which are part of the two-equation models), are widely used and produce satisfactory results [87], and are known to be the most appropriate for the internal flow of rotating machines [118, 119].

Given the nature and geometry of the flow under study, the two-equation k-epsilon model is used to model the turbulence, as it satisfies the mathematical constraints on Reynolds stresses, which are consistent with the physics of turbulent flows [120]. The solved turbulent kinetic energy equation k and dissipation rate equation ϵ are given by Equation 3.5 and Equation 3.6, respectively. The basic assumption of this model is that the turbulent viscosity, modeled by Equation 3.7, is isotropic, meaning that the ratio of the Reynolds stress to the mean strain rate is the same in all directions. Turbulent viscosity can hide the non-Newtonian shear-thinning character of emulsions subjected to high shear rates. Emulsions are highly viscous non-Newtonian fluids with apparent molecular viscosities thousands of times greater than the viscosity of water at low shear rates (as shown in Table 3.3 when comparing $\nu_0(70\%O-30\%W)$ and the viscosity of water). However, the shear-thinning behavior causes the bonds between the molecules of the coexisting phases to be broken as the shear rate increases, and the apparent molecular viscosity of the emulsion decreases. Thus, the inertial forces of the flow field override the viscous forces.

$$\frac{D}{Dt}(\rho k) = \nabla \cdot (\rho D_k \nabla k) + P - \rho\epsilon \tag{3.5}$$

$$\frac{D}{Dt}(\rho \epsilon) = \nabla \cdot (\rho D_c \nabla \epsilon) + \frac{C_1 \epsilon}{k}\left(P + C_3 \frac{2}{3} k \nabla \cdot \mathbf{u}\right) - C_2 \rho \frac{\epsilon^2}{k} \tag{3.6}$$

$$v_t = C_\mu \frac{k^2}{\epsilon} \tag{3.7}$$

Figure 3.5 shows the inverse of the eddy viscosity ratio, $\frac{1}{\frac{\mu_t}{\mu}}$, of 70%O-30%W emulsion flow within the NS32 pump at best effeciency point (BEP). It shows the importance of molecular viscosity governed by non-Newtonian behavior compared to turbulent viscosity. The figure shows that the magnitude of molecular stresses exceeds five times the Reynolds stresses in some regions. Thus, the damping effect of the emulsion viscosity outweighs the kinetic energy, requiring additional energy for the flow.

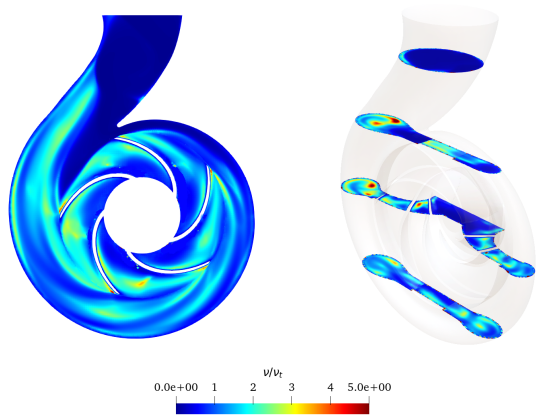

Figure 3.5: Eddy viscosity ratio of 70%O-30%W emulsion flow within the NS32 pump at BEP

The motion of the rotational domain was modeled using the multiple reference frame (MRF) technique, in which the impeller is in the rotating frame, and the volute and the rest of the pump geometry in the stationary frame. This technique is a steady-state approximation where the effects of rotational motion are reproduced via source terms in the fluid equations. The information between the different regions is transferred by an arbitrary mesh interface (AMI), where the flow variables are assumed steady. This allows the flow field within the centrifugal pump to be predicted by steady-state calculations and saves simulation time.

The inlet and outlet boundary conditions were set to a fixed volumetric flow rate and static pressure of 0 Pa, respectively, and a no-slip velocity condition was imposed on all pump walls. By changing the volumetric flow rate, the performance curves of the centrifugal pump were acquired.

3.1.4 Validation of the model

In the interest of assessing the accuracy of the CFD model, a standard case with water only was first considered. The numerical simulations were performed at a rotational speed of 900 rpm, as the experiment was realized under these conditions. The head developed by the pump was estimated as the difference between the surface averaged pressure at the outlet and the inlet. The head and efficiency were calculated following Equation 3.8 and Equation 3.9, respectively.

$$H = \frac{\Delta P}{\rho g} + \frac{v_2^2 - v_1^2}{2g} + \Delta z \tag{3.8}$$

$$\eta = \frac{\rho g Q H}{\tau N} \tag{3.9}$$

Figure 3.6 shows the comparison between the simulated pump head and the experimental data as a function of flow rate. Although the trend is well reproduced by the steady-state numerical model, the model underestimates the head values compared to the experimental data. Nearly all data points are within a 10% discrepancy. The differences are related to the assumption of a steady-state simulation to model the flow field inside the centrifugal pump. Therefore, only one impeller position is considered and the interaction between the impeller blades and the volute tongue is not taken into account.

In a previous study, Asuaje et al. [87] verified the effects of the interaction between the impeller and the volute for the same pump, by performing steady-state computations of several impeller positions. The author found that impeller position influences the head obtained and that the amplitudes of the pressure fluctuations reached 27% of the average pressure generated by the impeller.

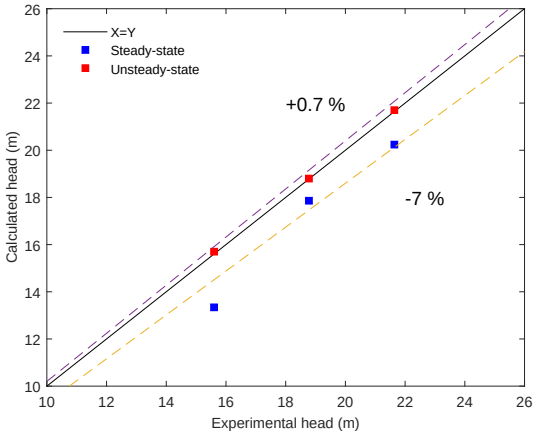

Figure 3.6: Comparison of pump head predicted by the CFD model with experimental data for water

To further investigate this point and to account for the different positions of the impeller, a simulation of the flow field in the pump in an unsteady regime was considered with the same mesh. The PIMPLE algorithm (merged PISO-SIMPLE) was used to solve the continuity and momentum equation. The stator–rotor interaction was modeled using a sliding grid approach. This transient method rotates the rotor part of the mesh relative to the stator part at each time step and the local flows were transferred using the AMI interface. Thus, the interaction between the impeller and the volute was fully resolved. The results of the unsteady simulation of the water flow field within the pump are shown in Figure 3.6. The comparison with the experimental data shows that the unsteady numerical results overestimated the head by about 0.7%. The numerical model did not consider the effect of the tip clearances of the pump, which accounts for a maximum of 2.5% of the head losses. Therefore the quasi-perfect agreement found here could be due to the compensation of small errors. Based on these results, the current numerical model can be considered satisfactory in terms of accuracy, thus validating the numerical model. For the sake of computational resources, simulations of the flow fields inside the studied centrifugal pump handling emulsions of different concentrations are performed at steady-state conditions. The objective is to investigate the internal flow within the pump handling emulsions, modeled as non-Newtonian fluids, along with the performance degradation of the pump carrying this type of fluid. The influence of unsteady phenomena is not included in this study.

3.2 Results and discussion

3.2.1 Overall performance

Figure 3.7 shows the head developed by the pump and the performance obtained for the selected compositions of each region. Simulations were performed on a flow rate ranging from 100 m^3/h to 400 m^3/h, with a step of 50 m^3/h. Since the degradation varied only slightly with the flow rates, in this

study, only the nominal flow rate and the lower and upper limits of the flow range were considered. In this context, the analysis considered the entire operating range of the centrifugal pump. The regions shown previously in Figure 2.1 (chapter 2) are highlighted to relate the composition and rheological properties of the emulsion to the pump operation. First, a clear transition is observed in the head and performance curves before and after the phase inversion point (region 2). The pump performance developed for indirect emulsions (region 1) and oil is significantly close. However, the head obtained for the oil is higher than the one obtained for the 80%O-20%W emulsion. The head difference between the two fluids decreases as the flow rate increases to approximately the same head value at high flow rates. On average, the 80%O-20%W emulsion obtained a head degradation of 10% in underflow, which increased to 26% in overflow. On the other hand, the oil led to a head degradation of 9% in underflow, which increases to 25% in the overflow. This difference in performance is related to the composition of the emulsion and its viscosity. The 80%O-20%W emulsion is close to the phase inversion point, where high viscosity is observed compared to other emulsions outside the phase inversion zone so that losses increase, and pump performance deteriorates. On the other hand, the 80%O-20%W emulsion follows a shear-thinning behavior, so its viscosity decreases as the shear rate increases to reach a lower viscosity limit which is close to the oil viscosity (Table 3.3). This explains the decrease in the head difference at high flow rates.

Comparing the performance of the pump when handling 90%O-10%W emulsion with the performance of the pump when handling oil, it can be seen that at low flow rates, the head developed for oil is higher than the head developed for emulsion. At nominal flow and overflow, the opposite occurs. Given the shear-thinning behavior of the emulsion, its viscosity will tend to decrease at high shear rates. This implies that the effective viscosity of this emulsion is lower than the viscosity of the oil ($\nu_{oil} > \nu_{\infty(90O10W)}$), thus decreasing the hydraulic losses encountered in the pump and resulting in higher head values. As for region 2, a viscosity peak of the emulsion was observed at phase inversion as shown in Figure 3.8, but the performance of the pump carrying this emulsion is better than that of the pump handling region 1 emulsions and oil (Figure 3.7). This is attributed to the strong shear thinning behavior of the emulsion and the lower limit of its effective viscosity range. The 70%O-30%W emulsion will undergo a significant viscosity drop until viscosity values lower than those of the Region 1 emulsions are reached at the same shear rates. As a result, losses will be lower and pump performance will be improved.

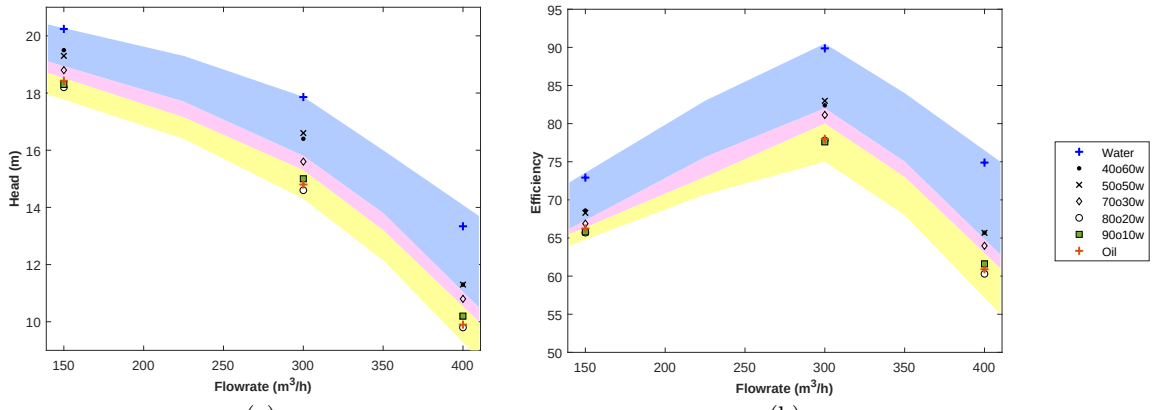

(a) (b)

Figure 3.7: CFD head (a) and efficiency (b) curves of the studied emulsions. Yellow, pink, and blue shaded areas correspond qualitatively to regions 1, 2, and 3, respectively, as classified in Figure 2.1

The pump performance degradation observed when pumping the emulsions in region 3 is noticeably close, especially at the nominal flow rate. This is attributed to the close viscosity range of the two emulsions and their sensitivity to shear rate governed by the coefficients k and n (Table 3.3). Emulsion 50%O-50%W has a higher viscosity at low shear rates than emulsion 40%O-60%W, and at high shear rates, their viscosities were almost equal. In addition, 40%O-60%W emulsion had a more pronounced shear-thinning behavior ($k > k$, $n \approx n$), so that over the entire shear rate range, the viscosity of emulsion 40%O-60%W will be lower than that of emulsion 50%O-50%W. This explains the slightly better performance obtained for emulsion 40%O-60%W at underflow and nominal flow rates. Nevertheless, both emulsions will see their effective viscosities decrease sufficiently to reach the lower bounds (ν_∞) at very high shear rates. Therefore, both emulsions developed the same performance at overflow.

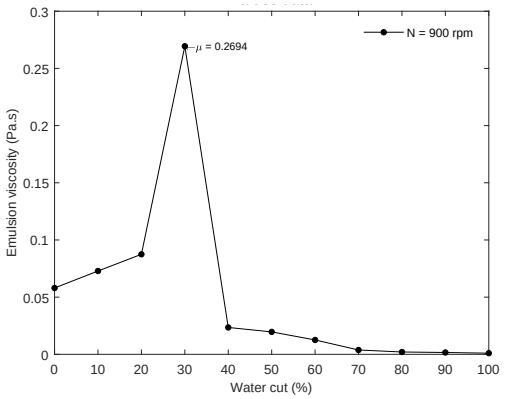

Figure 3.8: Viscosity curve as a function of the water cut and the inversion point (graph based on experimental data from Valdes et al. [30] by selecting the shear rate corresponding to the studied pump)

Another interesting point to discuss is the rate of head decline. A larger drop in the head curve at higher flow rates is observed in region 1 (degradation rates between 24% and 26%, corresponding to the 90%O-10%W and 80%O-20%W emulsions, respectively) when the oil fraction is large (> 70%) (see Figure 3.9 (a)). This suggests that systems with higher oil fractions generate higher frictional losses, which is consistent with the increase in the effective viscosity range shown in Table 3.3 and especially the lower bound of the viscosity range. The centrifugal pump generated high shear rates so that the fluids reached the lower Newtonian plateau. Thus, the increase in frictional losses is directly related to the lower bound of the viscosity range of each emulsion. This explains the minimal change in head obtained by increasing the oil fraction by 10% in region 3 ($\nu_{\infty(40O60W)}/\nu_{\infty(50O50W)} \approx 1$), compared to the sharp drop observed by increasing the oil fraction by 10% in region 1 ($\nu_{\infty(80O20W)}/\nu_{\infty(90O10W)} \approx 2.8$). This also explains the more pronounced degradation in performance of the 80%O-20%W emulsion compared to oil ($\nu_{oil} < \nu_{\infty(80O20W)}$), as shown in Figure 3.9 (a). A similar analysis could be made from the pump efficiency results, where the pump efficiency decreased as the volume fraction of the oil phase increased, which can be explained by the increase in the effective viscosity range of the different emulsions.

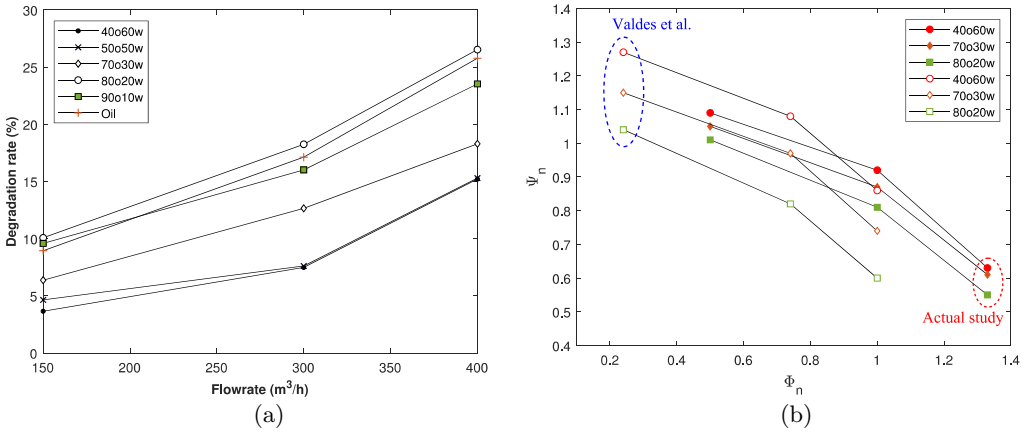

Figure 3.9: (a) Degradation rate of the pump head of the studied compositions and (b) Curves of normalized head coefficient as a function of the normalized flow coefficient for CFD results and Valdes [30] experimental data

A comparison between the CFD results and the experimental data from the reference paper is presented in Figure 3.9 (b). This figure shows the normalized head versus normalized flow rate for the CFD results and Valdes's experimental data based on a multistage pump with a specific speed twenty times the specific speed of the studied pump. As can be noticed, the graph trend is similar for both results. Another interesting observation is the rate of head deterioration rate. The head curve for emulsion shown in Figure 3.9 (b) showed a more pronounced drop at higher flow rates. This observation is in accordance with the experimental results of Valdes et al. [30], where, for example, a 4 % performance degradation was noted before BEP for 40%O-60%W emulsion, increasing up to 14% at this point. In this study, the degradation rate was 9 % before BEP and increased up to 17 % after this point. First, this difference in deterioration is mainly attributed to the difference in pump geometry and operating conditions that affect the hydraulic losses in terms of quantity. Second, despite the shear-thinning behavior of the emulsion, its high effective viscosity led to degradation of pump performance, primarily through increased frictional losses at high flow rates.

3.2.2 Internal Flow Analysis

In this section, the effect of the non-Newtonian behavior of the studied emulsions on the internal flow structure within the centrifugal pump is put into perspective. For this purpose, the relative velocity fields, streamlines, and velocity vectors in the impeller (Figure 3.10, Figure 3.11) as well as the absolute velocity fields in the volute (Figure 3.12) is analyzed for each emulsion and compared to the velocity profiles of water and oil. Emulsions from the same region show very similar behavior, so the streamlines and velocity vectors of a single emulsion from each region are selected to show the flow through the pump. First, all recirculation zones appear at underflow for all fluids and the inter-blade spaces in contact with the volute nozzle (Figure 3.10), and they highlight the asymmetric operation of the pump. As the impeller periodically swept the volute nozzle, the fluid discharged by the impeller interacts with the volute nozzle, producing a large amount of energy dissipation, resulting primarily from impact and recirculation losses.

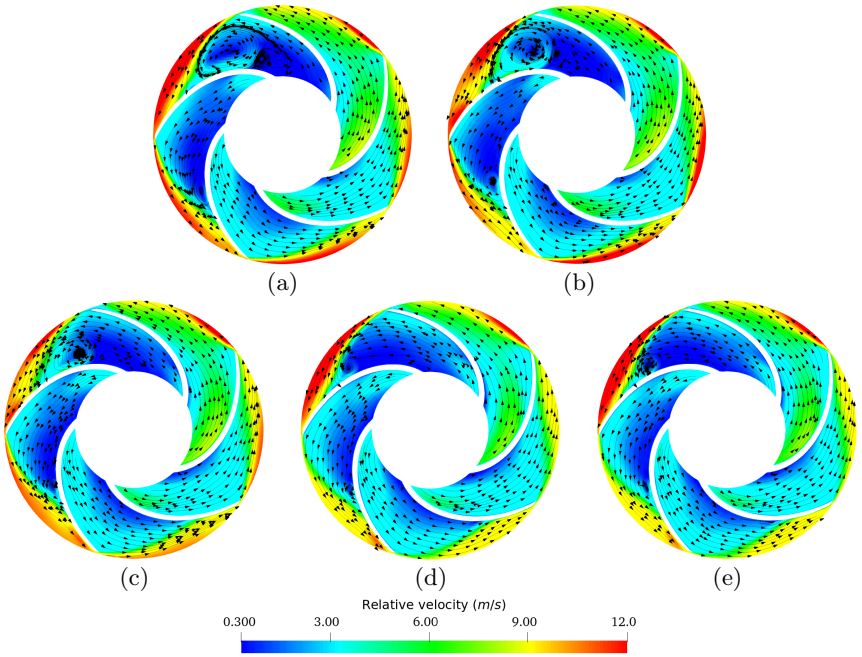

Figure 3.10: Relative velocity profiles and streamlines on the impeller at 0.5 Q_{bep} for oil fraction (%v/v): (a) 0%, (b) 50%, (c) 70%, (d) 80%, (e) 100%.

According to Figure 3.10, significant areas of recirculation are observed in the impeller when handling emulsions in region 3 (50%O). This is attributed to the low viscosity range of these two emulsions, where the high shear rate generated by the impeller drops the viscosity of these fluids to the lower Newtonian plateau, thus exhibiting similar behavior to water. For the 70%O-30%W emulsion (Figure 3.10 (c)), smaller areas of recirculation than those generated by the region 3 emulsions (Figure 3.10 (b)) appear but larger than those of the region 1 emulsion (Figure 3.10 (d)). This is due to the strong shear-thinning behavior of the emulsion (high k, high n) despite the very high viscosity range at low shear rates. As mentioned earlier, the studied centrifugal pump generates high shear rates that lead to a sharp decrease in the effective viscosity of this emulsion until it reaches the lower Newtonian plateau. Further, if we compare the lower limit of the viscosity ranges of the different emulsions (Table 3.3), we observe that the viscosity of the emulsion 70%O-30%W at high shear rates is between the values of the viscosities of the emulsions in regions 1 and 3. Region 1 emulsions have a higher effective viscosity range caused by the higher oil phase concentrations, thus influencing the velocity field and vortex formation. For emulsions in this region, a behavior similar to that of oil is observed. This indicates that recirculation loss with this type of centrifugal pump decreases with increasing fluid viscosity and that the most influential factors on recirculation loss when dealing with non-Newtonian fluids is the lower limit of the effective viscosity range, as well as the strong tendency to shear thinning of the fluid to reach this limit. This is especially true when comparing the flow field of oil and water, where smaller recirculation zones are observed for oil. Similar conclusions could be drawn when looking at the magnitude of the relative velocities (especially at the blade passage inlet). From the results obtained at underflow, it can be seen that the relative velocities increase with the volume fraction of the oil phase. This occurs at the suction blade passages and the impeller inlet. Another observation concerns the direction of the velocity vectors at the impeller exit. For the emulsions of region 3 and water, we notice a deviation of the vectors from the direction of the blade profile, for all the blades of the impeller. For emulsions with a high volume fraction of oil

($> 70\%$) and pure oil, we observe an accentuated deviation of the velocity vectors with respect to the direction of the blade profile in contact with the tip of the volute and much less accentuated in the other blades of the impeller. This is caused by the high viscosity of the oil and emulsions in region 1, and the non-symmetrical geometry of the pump (presence of the volute). For all fluids, as the flow rate increases, the relative velocity values increase, and the streamlines tend to better follow the blade profile. One can note that the relative velocities at the impeller inlet are almost identical for all fluids and the velocity distribution in the impeller is almost similar (Figure 3.11). As a result, recirculation and impact losses became significantly lower and friction losses became more influential than other losses as the flow rate increased for all fluids.

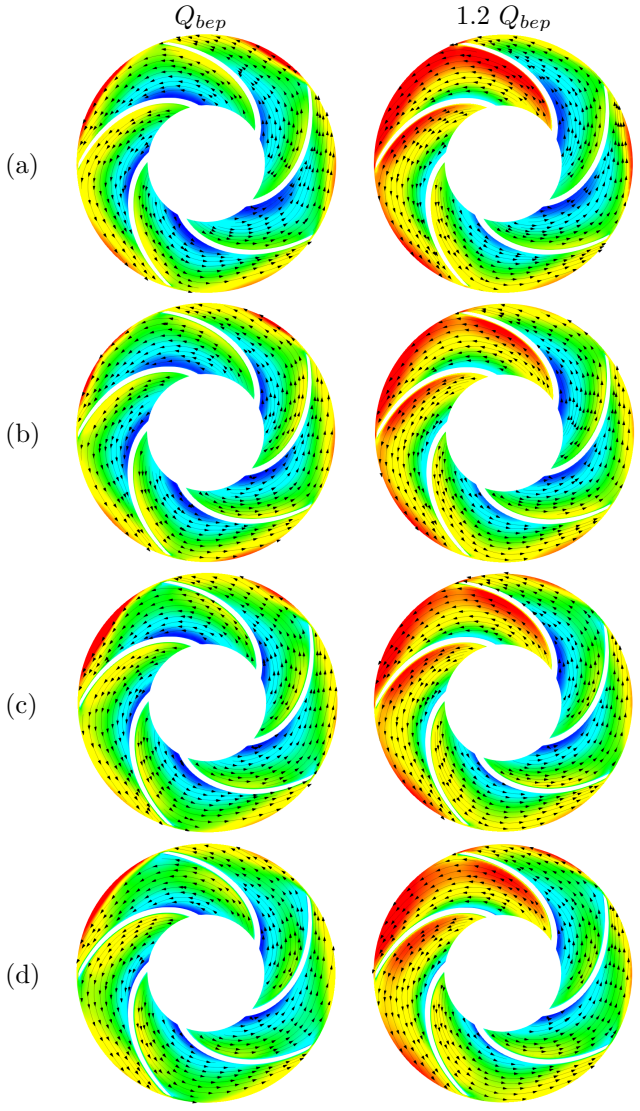

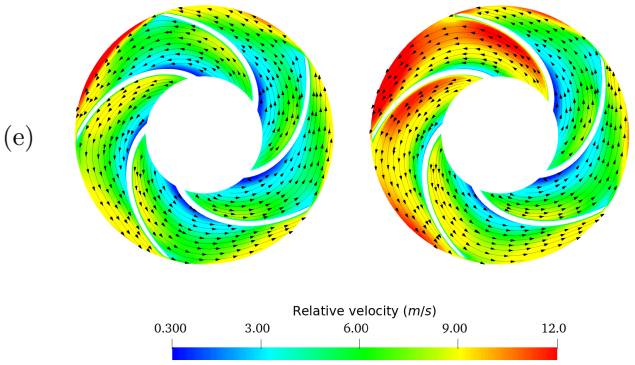

Figure 3.11: Relative velocity fields and streamlines on the impeller at Q_{bep} and 1.2 Q_{bep} for oil fraction (%v/v): (a) 0%, (b) 50%, (c) 70%, (d) 80%, (e) 100%.

For the flow field in the volute, Figure 3.12 represents the absolute velocity fields and streamlines in the volute for different fluid handled versus flow rate. At the nominal flow rate, the oil and emulsions in region 1 are properly channeled Figure 3.12(d-e)). The water and other emulsions exhibit vortices at the volute neck and outlet Figure 3.12(a-c). These vortex areas are more prominent in the case of water. We observe that as the oil fraction increases, both vortex zones increase and coalesce. These figures show a transition from chaotic to uniform flow at the volute neck as the fluid viscosity increases (see fluid viscosity range limits in Table 3.3). This is especially true when comparing the flow profile of the 90%O-10%W emulsion to that of the 80%O-20%W emulsion. A chaotic flow in the neck of the volute is observed for the 90%O-10%W emulsion, whereas the 80%O-20%W emulsion exhibits a uniform flow given its high effective viscosity range. The same observation could be made for the underflow. However, at the overflow, the flow profiles in the volute are almost similar for all fluids. We note a zone of acceleration at the neck of the volute (Figure 3.12 (1.2 Q_{bep})), which is damped as the fluid viscosity increases. Therefore, the flow structure in the vicinity of the volute is strongly influenced by the fluid viscosity and flow variation. These vortices and dead zones contribute to hydraulic losses by causing the fluid to lose kinetic energy.

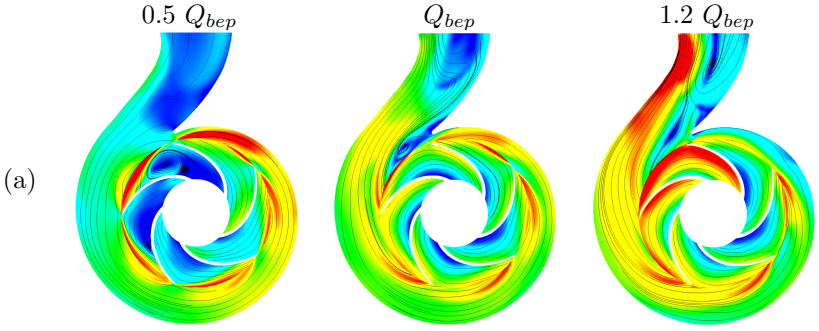

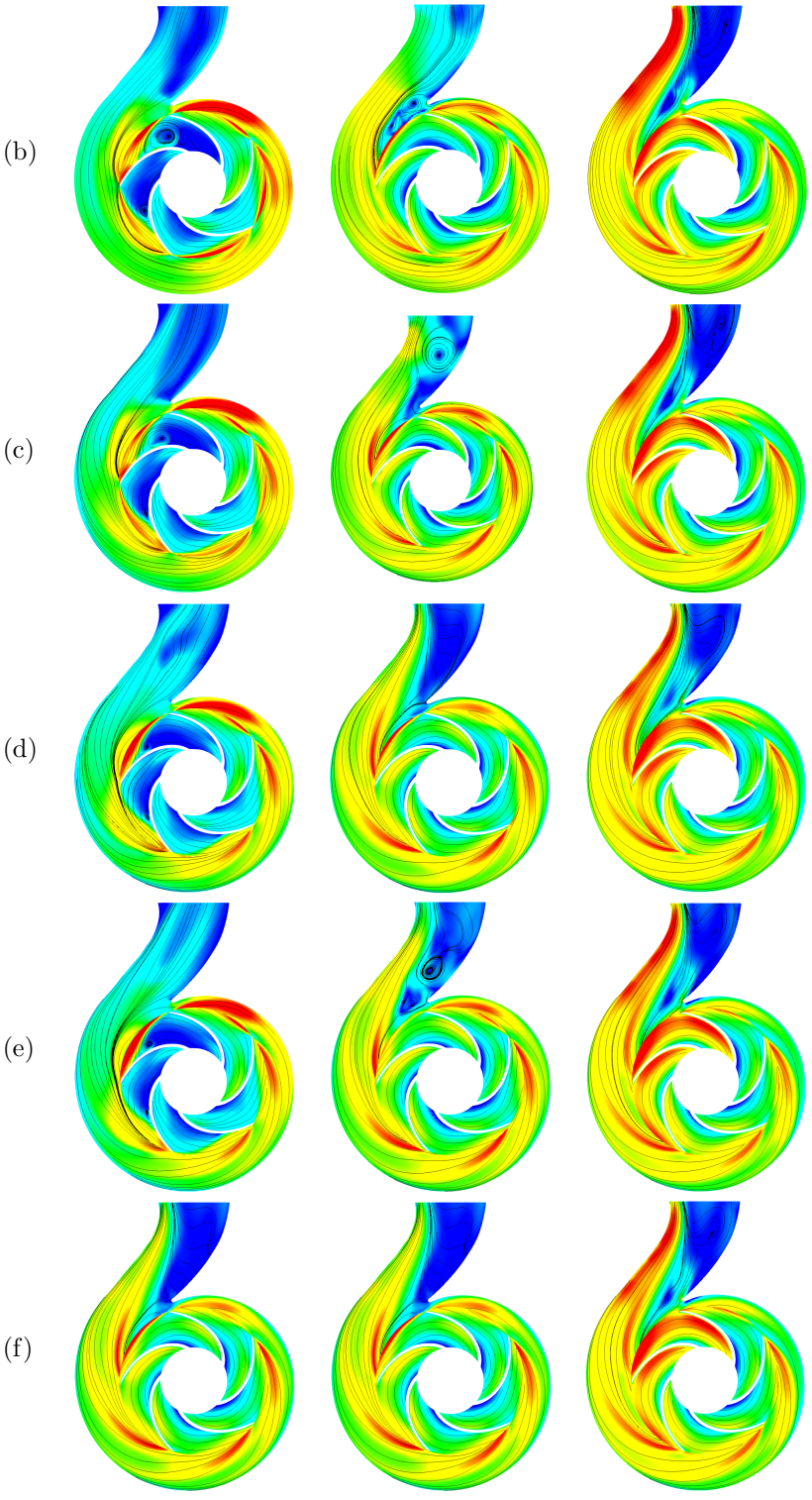
(b)
(c)
(d)
(e)
(f)

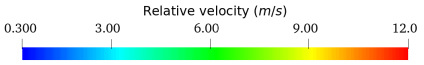

Figure 3.12: Absolute velocity fields and streamlines on the volute at 0.5 Q_{bep}, Q_{bep}, and 1.2 Q_{bep} for oil fractions (%v/v): (a) 0%, (b) 50%, (c) 70%, (d) 80%, (e) 90%, and (f) 100%.

3.2.3 Effective viscosity variation and shear stress profiles

Figure 3.13 shows the effective viscosity distribution for emulsions having 50% and 80% oil volume fractions. From the figure, the effective viscosity of emulsions decreases with increasing operating flow rates, consistent with their shear thinning behavior. This shear thinning behavior, which is observed for all studied emulsions, is highlighted in Figure 3.14 which shows the effective viscosity distribution compared to the shear rate distribution for a typical emulsion operating at BEP. As can be seen, the regions of high shear stress in Figure 3.14 (b) (volute neck, blade surfaces, and at the impeller-volute contact interface) correspond to the low viscosity region in Figure 3.14 (a).

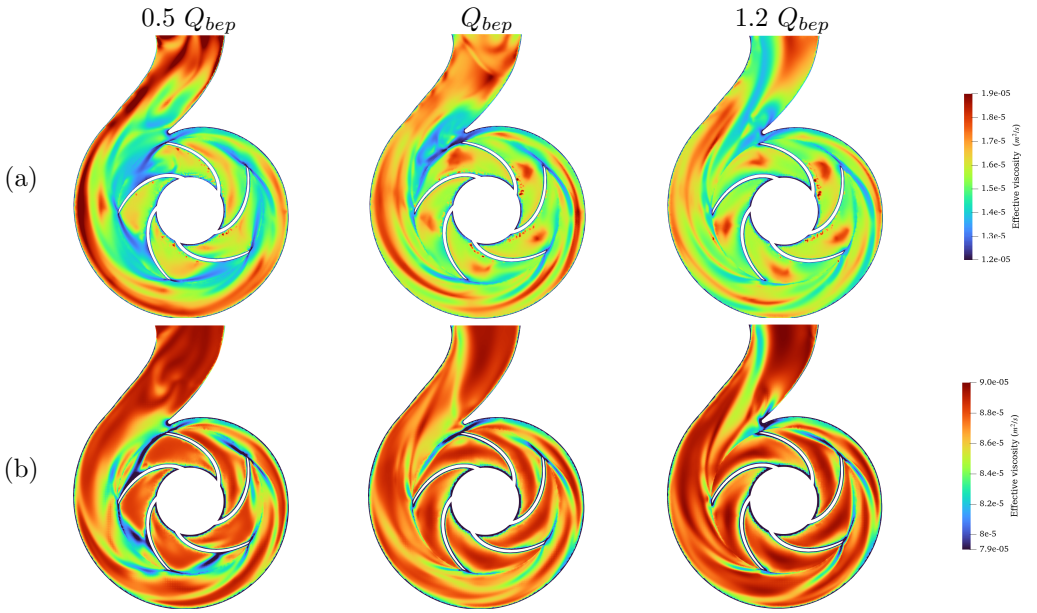

Figure 3.13: Effective viscosity distribution for oil fractions (%v/v): (a) 50% and (b) 80% operating at 0.5 Q_{bep}, Q_{bep}, and 1.2 Q_{bep}.

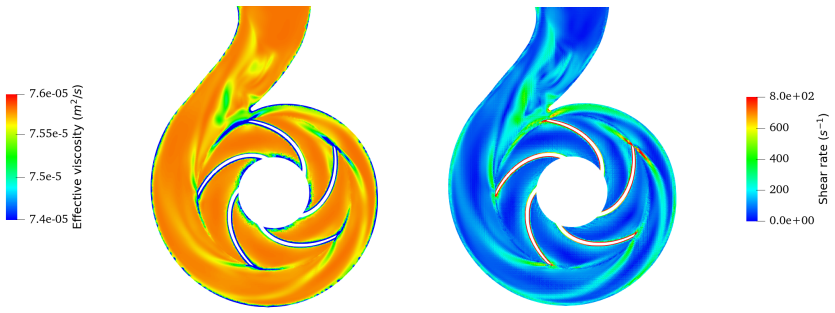

(a) (b)

Figure 3.14: Effective viscosity distribution (a) compared with shear rate profile (b) for 90%O-10%W emulsion operating at Q_{bep}.

The second crucial result is that the effective viscosities observed at the outlet section and the volute are significantly higher than those observed at the rotating zone for the region 1 emulsion fitted to the Cross model, for all flow rates considered, as shown in Figure 3.13 (a). In sum, higher viscosities are observed away from the impeller due to the lower shears exerted on the fluid in this region [121]. In this figure, it can be seen, for example, that the maximum viscosity of emulsion 50%O-50%W at the impeller is about $1.24 \cdot 10^{-5} m^2/s^2$, while its upper limit in the volute reaches $1.91 \cdot 10^{-5} m^2/s^2$. It is also observed for emulsions of this region, that the lower limit of the expected viscosity range at the impeller and volute is the same, and the flow rate doesn't affect this value. On the other hand, the upper limit of the viscosity range varies with the flow rate and differs between the rotating and static parts (Figure 3.15 (a,b)).

The region 1 emulsion modeled by Carreau shows a different behavior, their viscosity drops at the walls to very low values, but small viscosity variations are observed away from the walls throughout the pump Figure 3.13 (b). The lower limit of the viscosity range at the impeller and volute varies with the flow rate and differ between the rotating and static parts. However, the upper limit of the viscosity range is the same, and the flow rate doesn't affect this value (Figure 3.15 (d,e)). If we examine the influence of the flow rate on the viscosity profile in the rotating part and the static part for all emulsions, we observe that the rate of change in viscosity in the rotating part is lower than the rate of change in viscosity in the static part. This suggests that the shear rate in the rotating region is dominated by rotational speed and is less sensitive to flow variations. In contrast, in the other regions of the pump, the shear rate is very sensitive to flow variations.

Figure 3.15 shows the viscosity variations of the different emulsions in the pump at different flow rates. The effective viscosity range of emulsion 70%O-30%W (region 2), bounded by ν_∞ at high shear rates, is significantly larger than that of emulsions of region 3, despite its greater tendency to shear thinning. This implies that emulsion 70%O-30%W will exhibit greater viscosity decreases. The effective viscosities will yet still be higher than those of the two emulsions in region 3 but lower than those of emulsions in region 1. This explains the lower pumping performance obtained when handling emulsion 70%O-30%W relative to the other emulsion, as presented previously in subsection 3.3.1. On average, the effective viscosity of the 90%O-10%W emulsion is $4.06 \cdot 10^{-5} m^2/s^2$ on the impeller wall and $5.47 \cdot 10^{-5} m^2/s^2$ on the volute wall. The average viscosities of this emulsion in the walls of the rotating and stationary regions are lower than the viscosity values of the oil. This means that the oil will generate greater frictional losses than this emulsion.

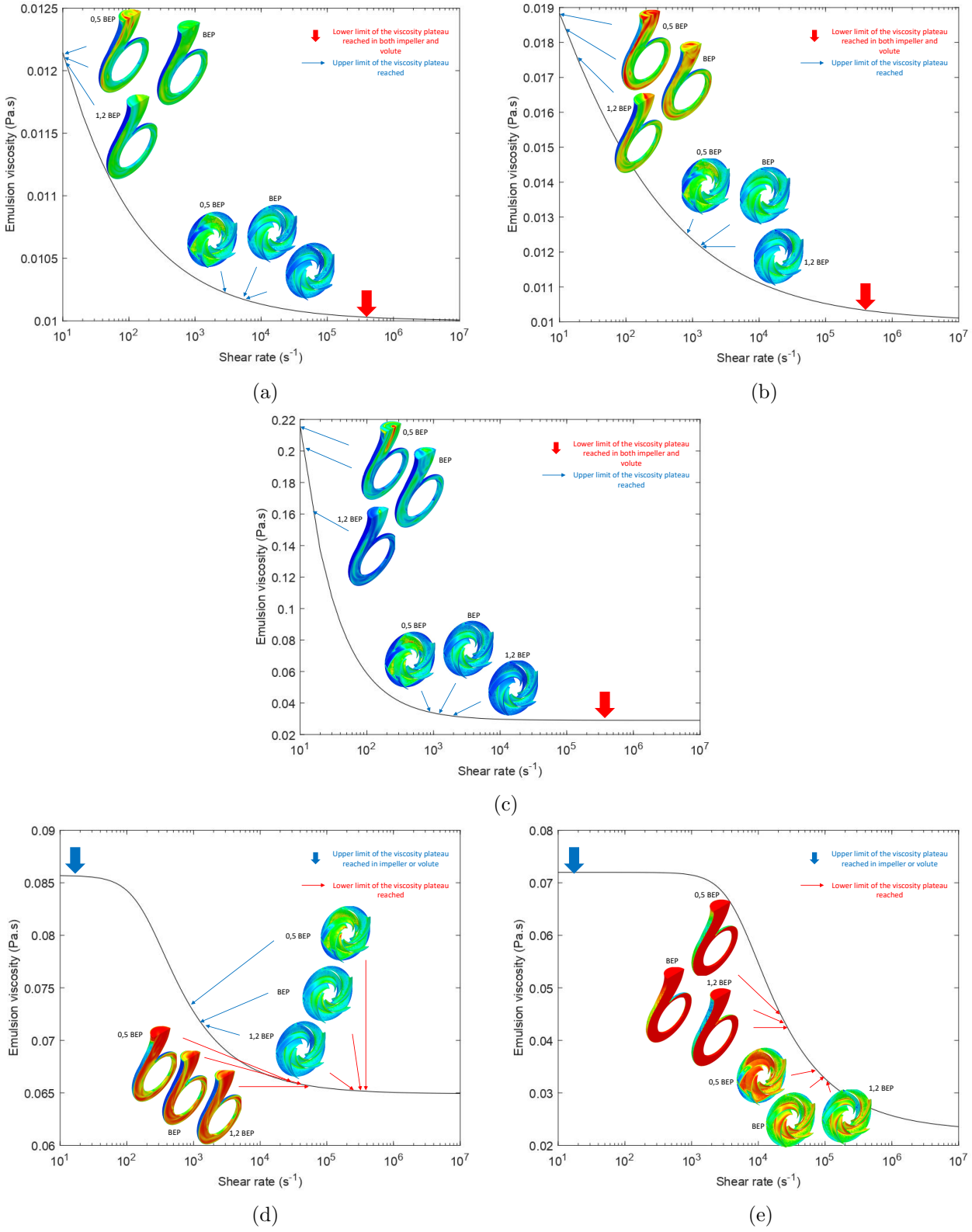

Figure 3.15: Viscosity range in the impeller and volute at operating conditions 0.5 Q_{bep}, Q_{bep}, and 1.2 Q_{bep} for oil fractions (%v/v): (a) 40%, (b) 50%, (c) 70%, (d) 80%, (e) 90%.

On the other hand, moving away from the walls, the effective viscosity slightly increased to $7.53 \cdot 10^{-5} m^2/s^2$ and $7.59 \cdot 10^{-5} m^2/s^2$ in the impeller and volute, respectively, which are values higher than the viscosity value of the oil. This led to smaller recirculation zones for the emulsion than for the oil. This may explains the higher performance obtained by the pump when handling emulsion 90%O-10%W compared to oil. In contrast, emulsion 80%O-20%W shows average values of $6.82 \cdot 10^{-5} m^2/s^2$ at the impeller and $8.89 \cdot 10^{-5} m^2/s^2$ at the volute. These viscosity values are higher than the viscosity value of the oil, which explains the more pronounced performance degradation when handling this emulsion.

For the emulsions in region 3, the effective viscosity of the two emulsions is remarkably close at high flow rates, noting an average effective viscosity over the whole domain of $1.06 \cdot 10^{-5} m^2/s^2$ and $1.11 \cdot 10^{-5} m^2/m^2$ for the 40%O-60%W and 50%O-50%W emulsions, respectively. A slight difference in viscosity values at low flow rates is noted, given the upper limit of their viscosity range. This explains the very close pump performance observed previously when handling these two emulsions.

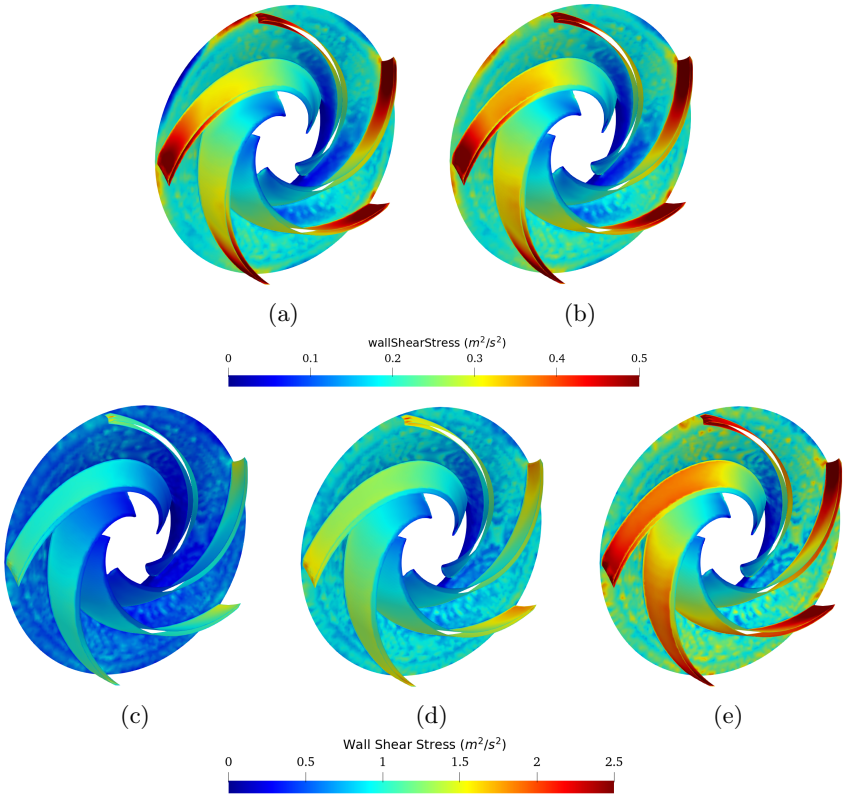

Figure 3.16: Q_{bep} Wallshear Stress (divided by density) distribution on the impeller for oil fractions (%v/v): (a) 0%, (b) 50%, (c) 70%, (d) 80%, (e) 100%.

From Figure 3.16, it can be seen that the shear stresses generated on the impeller are significantly higher for oil and emulsion 80%O-20%W compared to other emulsions and water. The average shear stresses of emulsion 80%O-20%W oscillate between 800 and 2800 Pa, that of oil oscillate between 700 and 2300 Pa, that of emulsion 70%O-30%W oscillate between 476 and 1200 Pa, while the two emulsions of region 1 and water show a maximum of $700 - 850$ Pa. Furthermore, the shear-thinning behavior of all fluids is again highlighted in this figure; the shear stresses generated at the impeller for oil and emulsion 80%O-20%W are almost the same ($\nu_{\infty(80O20W)}/\nu_{oil} \approx 1$), and so for the shear stresses generated for the

two emulsions of region 3. This suggests that non-Newtonian fluids behave like viscous Newtonian fluids in the rotating part independently of their sensitivity to shear-thinning, with viscosities near the lower Newtonian plateau, given the high shear rates generated by rotational speed. The studied centrifugal pump generates high shear rates in the rotating part so that the non-Newtonian fluid behaves like viscous Newtonian fluids whose viscosity is near the lower Newtonian plateau.

3.2.4 Influence of pump size

The results obtained in subsection 3.2.3 showed that shear-thinning emulsions exhibit quasi-Newtonian behavior in a large-size pump, which depends on the local shear rate. However, the shear rate changes with the size and geometry of the pump. So how will a non-Newtonian fluid behave in a small-size pump and what will be the effect of this non-Newtonian rheology on the hydrodynamic behavior of the pump.

Before manufacturing and operating a pump, generally, small-scale model tests are used to estimate its actual performance. However, the actual operating conditions are not similar to those in the laboratory. Many on-site experiments discovered some phenomena that were never observed in model tests [122]. Because of the pump size, each pump can respond differently to viscous dissipation or other losses that affect its performance. Similar performance degradation is not expected since the fluid rheology depends on the geometry and the local shear stress. Also, the structure of the non-Newtonian flow can differ according to the pump's dimensions even if the geometry remains the same.

This subsection aims to numerically investigate the scaling phenomenon in a centrifugal volute pump and its influence on the non-Newtonian behavior of emulsions. The main objective is to analyze whether the performance degradation when handling non-Newtonian fluids is size dependent and give an in-depth analysis of the internal flow behavior in a real and scaled-down pump. The same numerical study (same settings presented in subsection 3.1.1) is conducted on a geometrically similar pump, but with smaller dimensions. A scaling factor of $\mu = 1/5$ is applied to all parts of the pump. This scaling factor was chosen to obtain a laboratory design scale dimension while maintaining the same flow regime (similar Reynolds range and close specific speeds). The characteristics of the scaled-down pump are listed in table Table 3.7 and compared to the large-size pump (NS32). The study was performed considering an emulsion from each region having an oil volume fraction of 40%, 70%, and 80%, and the results will be presented by analyzing the slip factor, secondary losses, and skin friction coefficient in both pumps.

Characteristic	NS32	SM
Nominal Head (m)	49	10.63
Rotational speed (rpm)	1470	3450
Nominal Flowrate (m^3/h)	590	7.5
Specific Speed	32	26
$Re{=}R_2^2\omega/\nu$	3.93 10^6	6.02 10^5

Table 3.7: Scaled model nominal operating conditions

3.2.4.1 Overall performance comparison

Figure 3.17 shows the performance of the two pumps, described by the normalized head relative to the best efficiency point Figure 3.17 (a-b) and the efficiency Figure 3.17 (c-d) as a function of the flow rate.

First, it is important to point out the progressive deterioration of the performance of both pumps when the oil volume fraction increases. The performance degradation is governed by the lower Newtonian plateau because centrifugal pumps generate high shear rates so that the viscosity of emulsions approaches this plateau. As a result, degradation increases with oil concentration. These results have already been observed and explained in subsection 3.2.1 for the large-size pump. Regarding the performance degradation of the small-size pump, the same behavior is observed.

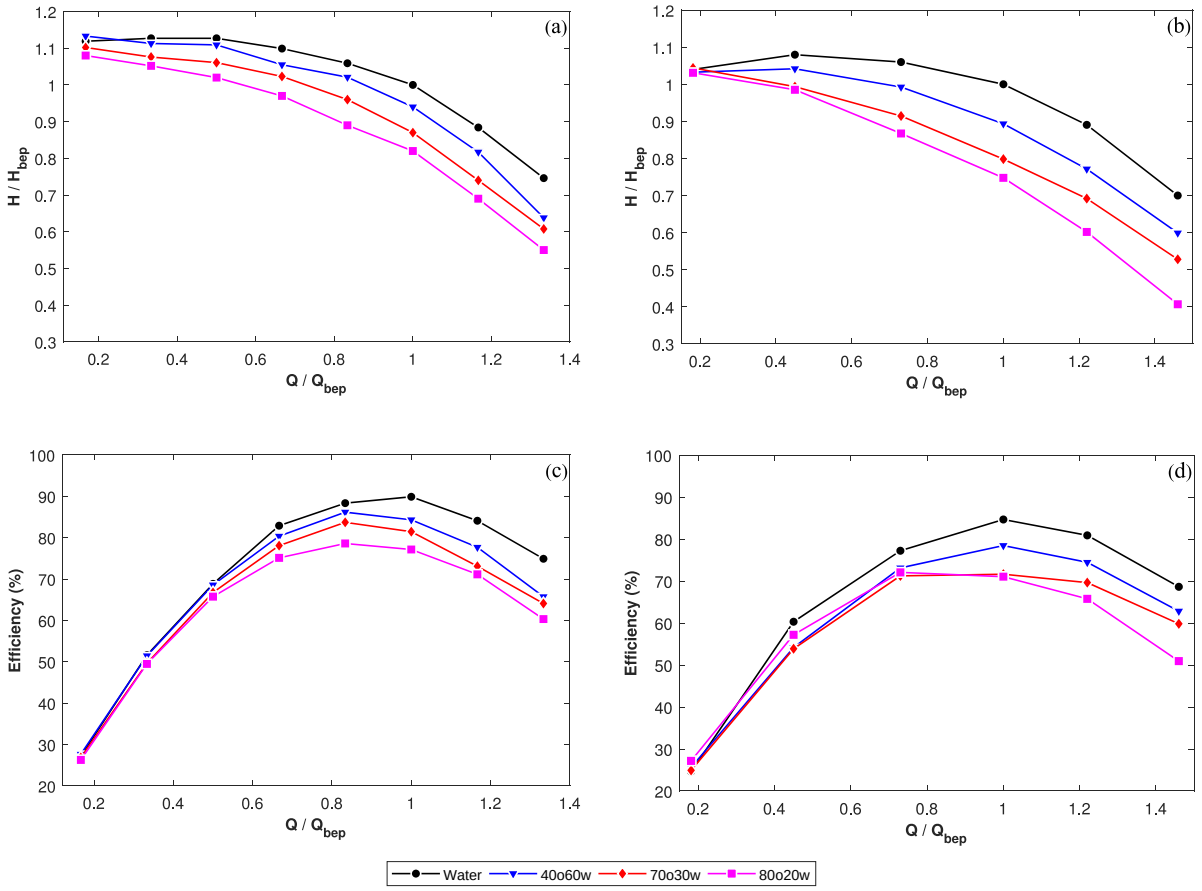

Figure 3.17: CFD head of NS32 (a) and scaled-down pump (b), efficiency of NS32 (c) and scaled-down pump (d)

Another interesting point to discuss is the head degradation observed at low flow ($Q = 0.15Q_{bep}$) (almost the shut-off point). Theoretically, at zero flow rate, the pump develops the same head regardless of the fluid according to the Euler equation. From the results obtained, we observe that the head of the small-size pump is identical for all the fluids, but the large-size pump develops different heads for each fluid. This phenomenon is already observed by Valdes et al [113] in an ESP when the pumped fluid has

a non-Newtonian rheology. The author explained these results by phenomena such as secondary flow regions, a decrease in the relative outlet flow angle or incidence losses related to the fluid rheology. In this study, we can attribute these results to the different phenomena cited previously. This suggests, therefore, that hydraulic losses related to various phenomena such as secondary flow regions, decreasing relative outlet flow angle, or incidence losses will be greater in the large-size pump since friction losses are not accounted for at the shut-off point.

The comparison between the head degradation of both pumps handling the same emulsion clearly shows the effect of pump size on the emulsion behavior and performance degradation (Figure 3.18). The scaled-down model shows a higher performance degradation than the large-size model, and this is for all emulsions. There is also an increase of degradation with the increase of flow rate in both pumps. The effect of pump size on the head and efficiency curves are dependent on the type of emulsion and thus on the viscosity of the working fluid. As the lower viscosity limit increases, the degradation in the small-size pump becomes more significant. This can be attributed to the reciprocal effect of different pump losses and changes in emulsion viscosity which will be discussed in the next paragraphs.

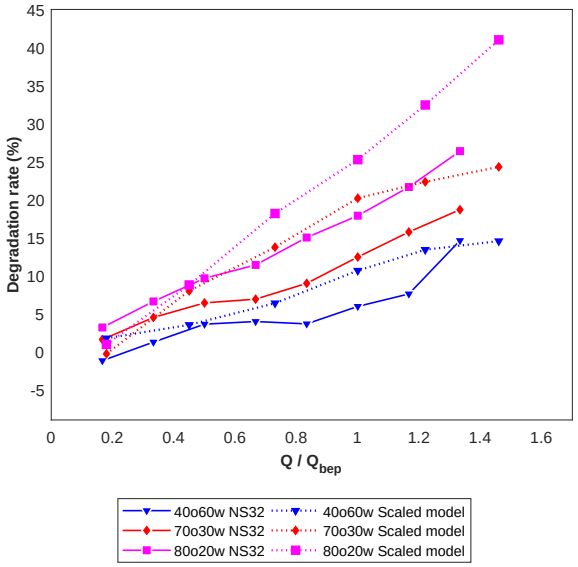

Figure 3.18: Comparison of head degradation rate in both pumps

3.2.4.2 Slip factor

The slip factor reflects the mismatch between the angle at which the fluid leaves the impeller and the angle of the blade. Slip is a very important phenomenon that occurs especially in radial impellers and is valuable in determining the accurate estimation of impeller-fluid energy transfer, head rise, and velocity triangles at the impeller exit. Because the flow does not precisely follow the blade curve, the angle of the fluid streamline is slightly smaller than the blade angle, as shown in Figure 3.19.

The figure shows the velocity triangle at the impeller exit, where absolute velocity is denoted by V, tip velocity by U, and relative velocity by W. The subscript u and r are the projections of the velocities on the tangential and radial planes respectively. β_2 and $\beta_{2\,\mathrm{inf}}$ are the impeller blade discharge angle and the impeller blade angle respectively.

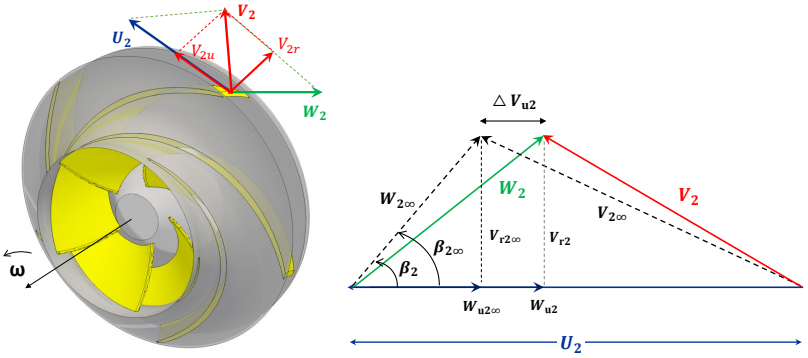

Figure 3.19: Velocity triangle at the impeller exit

Many correlations have been proposed to estimate this factor, but in most cases the proposed formula does not take into account the effect of flow rate, viscosity, and impeller geometry. In this study, the slip coefficient based on the velocity triangles given by Equation 3.10 is used.

$$\sigma_{\Delta} = \frac{\Delta V_{u2}}{U_2} = \frac{W_{u2} - W_{u2\infty}}{U_2} \tag{3.10}$$

where ΔV_{u2} is the slip fluid velocity at impeller outlet in circumferential direction and $U_2 = \omega D_2/2$ the impeller tip speed. Based on the correlation proposed by Li [123], the tangential component of the relative velocity in infinite number of blade $W_{u2\infty}$ is determined from the 1D uniform ideal flow, and given by Equation 3.11 while W_{u2} which is the tangential component of the relative velocity is determined from CFD.

$$W_{u2\infty} = \frac{V_{r2\infty}}{\tan\beta_{2b}} = \frac{Q}{\eta_V A_2 \psi_2 \tan\beta_{2b}} \tag{3.11}$$

η_V is the volumetric efficiency determined using Equation 3.12, where N_s is the specific speed of the pump in US Units.

$$\eta_v = \frac{1}{1 + 0.68 N_s^{-2/3}} - 0.07 \tag{3.12}$$

$A_2 = \pi D_2 b_2$ and $\psi_2 = 1 - Z S_{u2}/\pi D_2$ stands for the impeller exit area and the blade blockage coefficient respectively. S_{u2} is the tangential exit blade thickness. Thus the final expression of the slip factor is given by Equation 3.13.

$$\sigma_{\Delta} = \frac{W_{u2}}{U_2} - \frac{Q}{\eta_V A_2 \psi_2 \tan\beta_{2b} U_2} \tag{3.13}$$

The slip factor extracted for the two pumps using the previous method (Equation 3.13) is shown in Figure 3.20 versus flow rate. The different parameters appearing in this equation are extracted from the CFD results, at the impeller exit i.e. by taking the average of the parameters on the periphery of the impeller exit. The slip factor proposed by Wiesner [124], based on the blade number Z and given by the Equation 3.14 is drawn on the graph for comparison.

$$\sigma = \frac{\sqrt{\sin \beta_{2\infty}}}{Z^{0.7}} \tag{3.14}$$

The slip factor of a conventional closed impeller corresponds well to the value of the Wiesner formula [125], which is constant in the same pump for all fluids and flow rates. Furthermore, the Wiesner slip factor is constant for all geometrically similar centrifugal pumps since the relative design exit angle is the same. However, Figure 3.20 shows that the slip factor is highly dependent on pump size and fluid viscosity, along with flow rate for the specific pump considered in this study. Both centrifugal pumps have a larger slip factor than the Wiesner formula and decreases with increasing fluid viscosity and flow rate. Furthermore, by comparing the slip factor of the small-size pump and large-size pump, we notice that the slip factor of water is higher for the scaled-down pump, but the value decreases when handling a non-Newtonian fluid. In addition, the slip factors for the smaller pump size are more dependent on viscosity variation. The shape of the graphs is almost similar for both pumps and the slope of the slip factor becomes flat at high flow rates. As the fluid viscosity increases, the slip factor approaches the Wiesner slip factor. Another point to highlight is that the slip coefficient obtained for the 40%O-60%W emulsion is higher than that of water between the 0.4 Q_{bep} and 0.9 Q_{bep} flow rates in the large size pump. The high slip factor values obtained at low flow rates may be attributed to vortex and recirculation zones in the inter-blade space of the impeller. A vortex increases the curvature of the flow streamlines, producing a strong slip effect at the impeller discharge and an increased slip factor as noticed in previous studies ([126]).

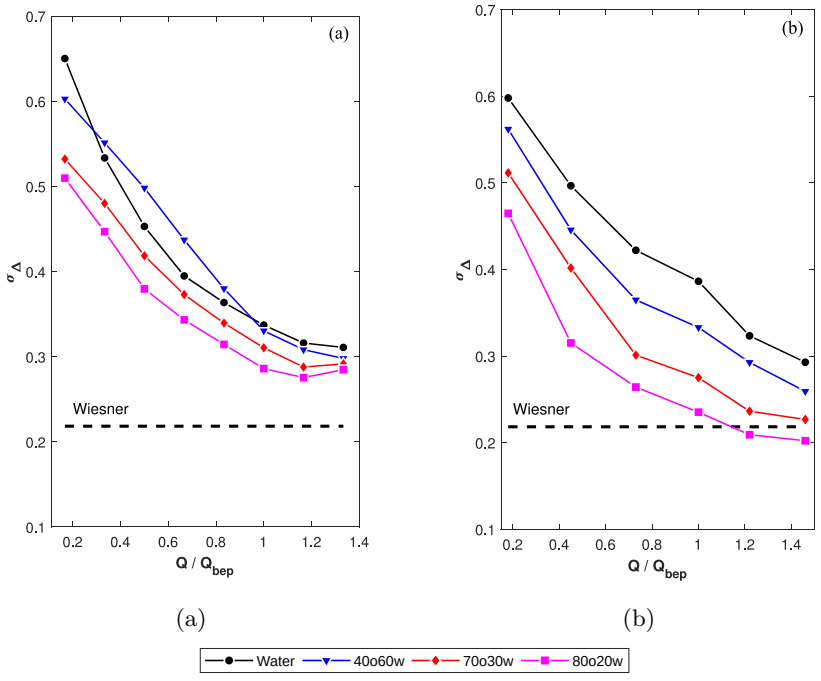

Figure 3.20: Slip factor of the large-size (a) and the scaled-down pump (b)

From the values of the obtained slip factor, which depends on the pump size and fluid viscosity, it is evident that the relative tangential velocity is strongly influenced by the pump size and the viscosity of the fluid. Figure 3.21 shows the variations of the absolute relative velocity calculated at the impeller

outlet $R/R_2 = 1$ for both pumps. The effect of fluid rheology and flow rate is more pronounced for the small size pump (SM). It can be seen from the figure that the predicted emulsion velocity appears to have a slight difference with water under the same operating conditions for the large pump. This difference decreases as the flow rate increases. On the other hand, the difference between emulsion velocity and water velocity is more significant in the small-size pump. It is important to note that the simulated flow fields are more sensitive to the change in fluid viscosity in the small pump than in the large-size pump.

In the light of these results, we can conclude that slippage is greater in large pumps when handling a non-Newtonian fluid than in small pumps, i.e., the difference between the theoretical head (H_{th}) and the theoretical head for an infinite blade number ($H_{th\infty}$) is lower in the small pump than in the large pump. However, the performance curves observed in section 3.3.4.1 show that the degradation is larger in the scaled-down model than in the large-size pump. Given that the slip factor calculated in this study takes into account secondary losses and mismatch losses, this leads to the conclusion that the performance degradation is more dominated by the remaining losses, such as the friction losses, which will be relatively more significant in the small-size pump.

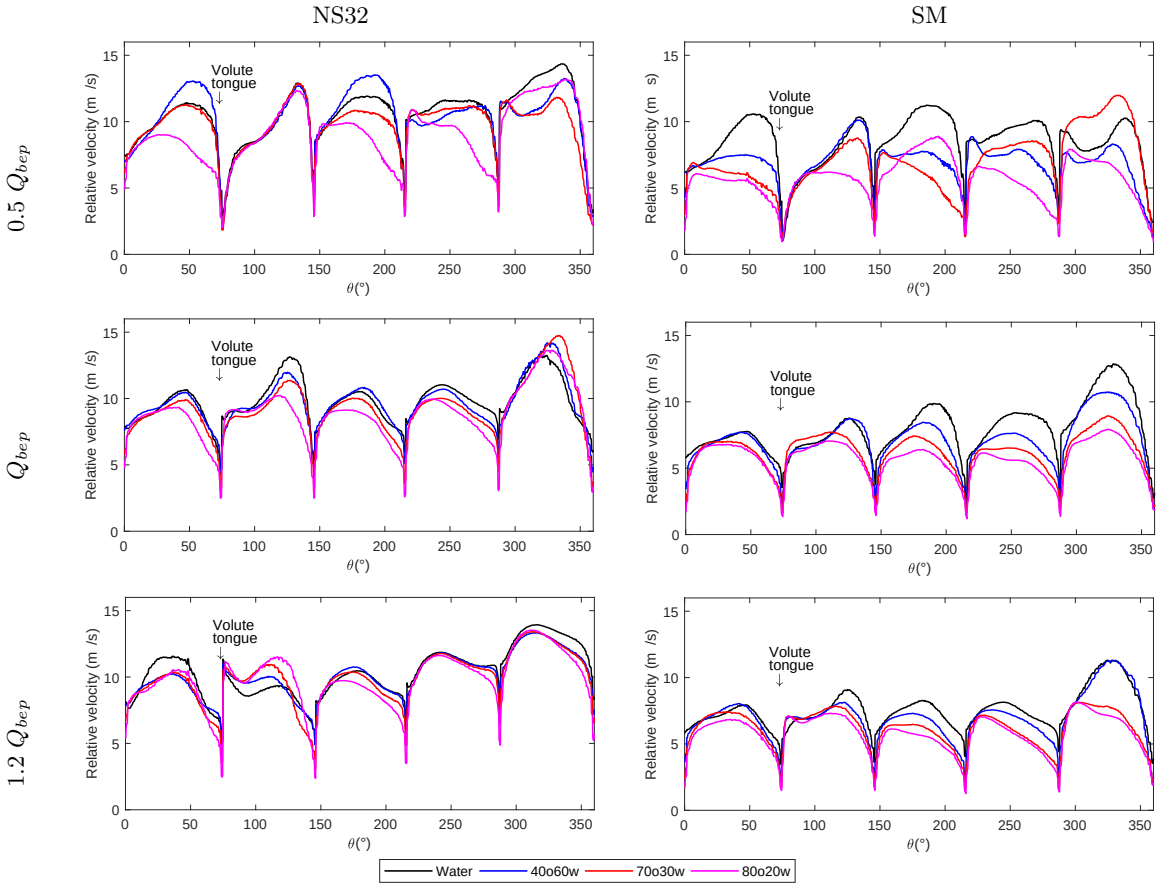

Figure 3.21: Absolute relative velocity at impeller exit

3.2.4.3 Secondary losses

In order to investigate the effect of pump size on the internal flow structure of non-Newtonian fluids, the relative velocity distribution and streamlines in the mid-span surface of the impeller and volute of

both pumps and for all fluids are presented in the following figures. The impeller passage flow is expressed by relative velocity fields and the volute passage flow is expressed by absolute velocity fields.

Figure 3.22 shows the relative velocity and streamlines in the large pump and the small size pump at partial flow ($Q/Q_{bep} = 0.5$). A vortex area appears near the pressure side of the impeller blades in contact with the volute tongue in both pumps. The size of this vortex decreases as the volume fraction of the oil phase of the emulsions increases, as stated previously in subsection 3.2.2. Nevertheless, a uniform flow is observed in the inter-blade passages away from the volute tongue. In addition, this vortex is larger in the scaled-down model than in the large-size pump when handling water and is smaller when handling emulsions, and develops in the opposite direction to the impeller rotation. These vortex areas in the impeller cause a sharp decrease in the relative velocity at the impeller outlet. As a result, the theoretical head decreases significantly due to the decrease in absolute tangential velocity at the impeller outlet. This suggests that the secondary losses will be smaller in a small-size pump than in a large pump when handling non-Newtonian fluid. This observation supports the results obtained previously, where higher slippage is observed in the large pump when handling non-Newtonian fluid.

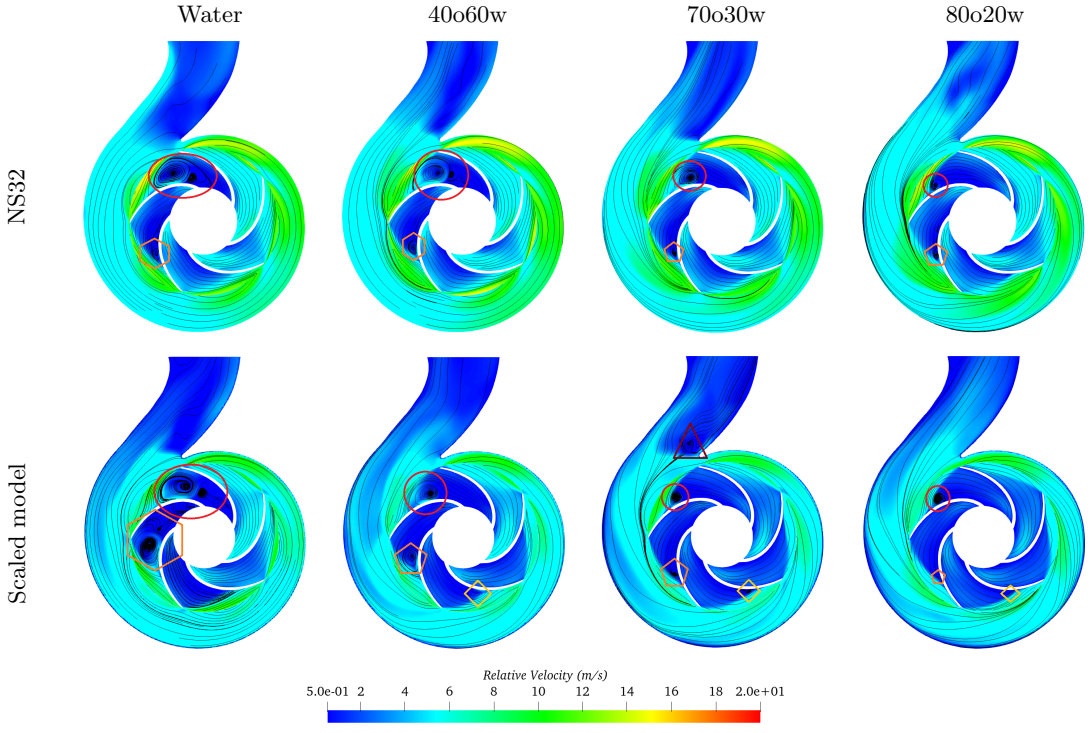

Figure 3.22: Velocity distribution and streamlines on the impeller at 0.5 BEP

At the design flow rate (Figure 3.23), the entire flow direction in the impeller passageway deflects toward the pressure side of the blades relative to the suction side of the blades. The velocity distribution shows a low velocity near the pressure side of the blades and a high velocity near the suction side at the impeller inlet. However, moving toward the exit of the impeller, the velocity profile has a high velocity near the pressure side and a low velocity near the suction side. The overall flow field in the scaled-down pump is asymmetrical to the impeller axis for water and 40%O-60%W emulsion and becomes symmetrical as the volume fraction of oil increases (increasing viscosity as well), while the flow field within the large

pump is relatively symmetrical to the impeller axis for all fluids. A notable feature recognized in these figures is the presence of vortex zones near the volute tongue of the large pump that develops and moves toward the volute divergent as the fluid viscosity increases. For the scaled-down model, a small vortex zone appears in the volute divergent for 70%O-30%W emulsion only.

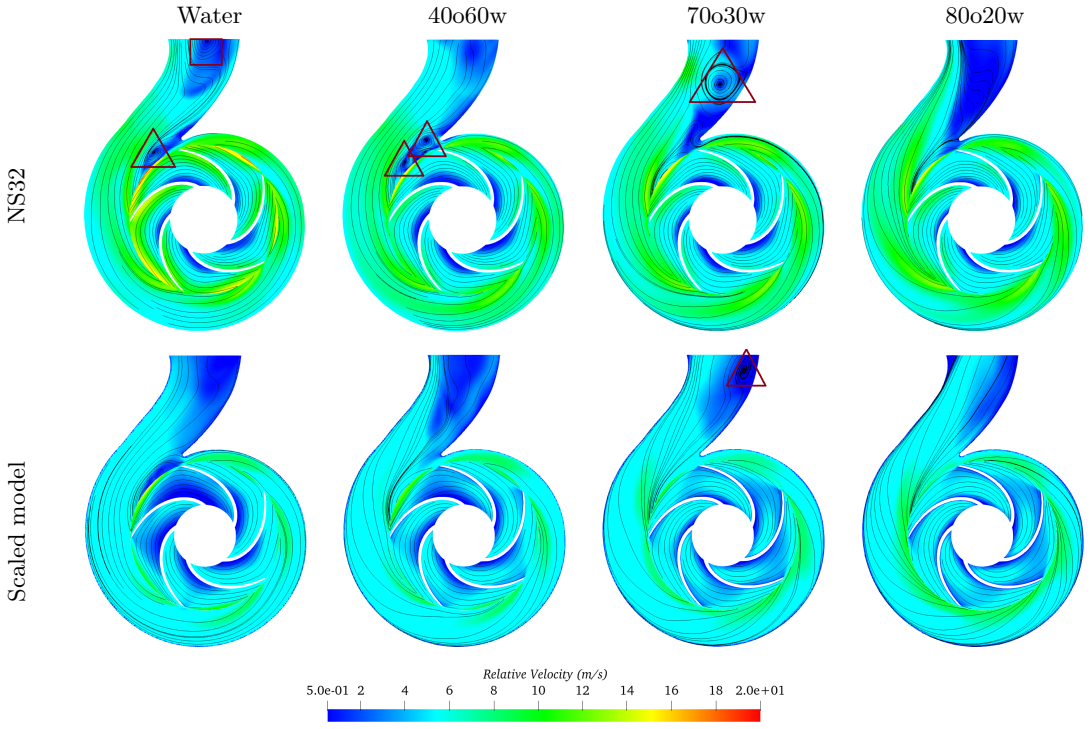

Figure 3.23: Velocity profiles and streamlines on the impeller at BEP

In Figure 3.24, the flow profile becomes asymmetric to the axis of rotation of the impeller for all fluids. A large recirculation zone appears in the divergent part of the volute and decreases as the oil volume fraction increases. In comparison to the real pump, the scaled-down model shows uniform flow in the impeller for all fluids, but the relative velocity increases with increasing oil volume fraction. Vortex and recirculation zone appears at the volute tongue for water and 40%O-60%W emulsion only. These vortex and dead zones contribute to hydraulic losses by causing the fluid to lose kinetic energy. It can be noted that the relative velocities at the impeller inlet are almost identical for all fluids in the same pump, and increase with increasing flow. As a result, impact losses become smaller and friction losses more influential as the flow rate increases.

Figure 3.26 shows the radial component of the relative velocity profile along an inter-blade line in contact with the volute nozzle (as shown in Figure 3.25), for different flow rates. It can be seen that the shape of the graphs under the same operating conditions is generally the same in both pumps. However, the velocity distributions at the impeller outlet are different in the two pumps for different fluids as the flow rate increases. At partial flow, an unstable distribution of relative velocity toward the impeller outlet is observed, which decreases for both pumps, resulting in the recirculation observed in Figure 3.22.

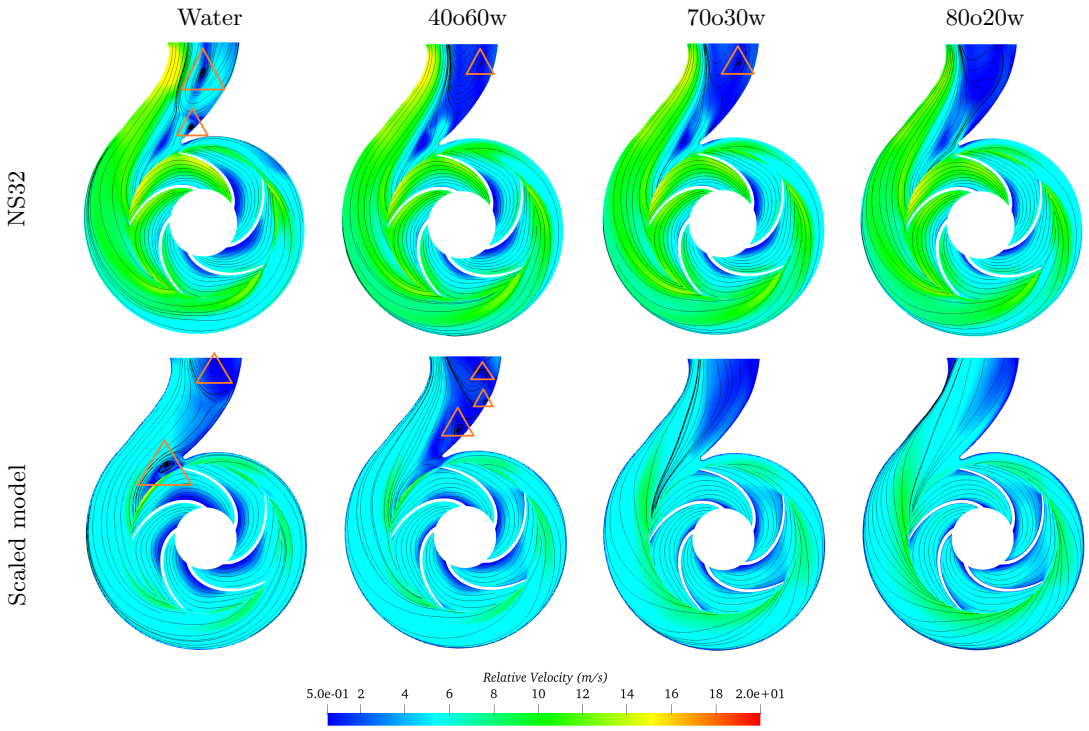

Figure 3.24: Velocity profiles and streamlines on the impeller at 1.2 *BEP*

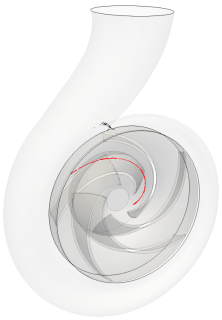

Figure 3.25: Relative velocity plot line

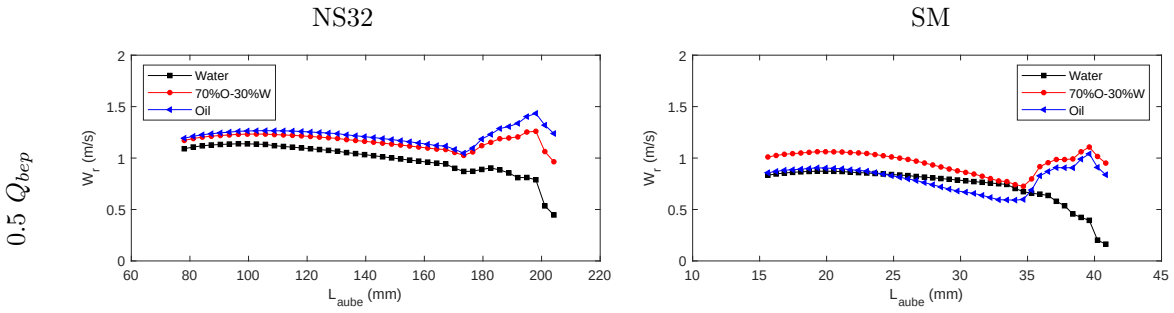

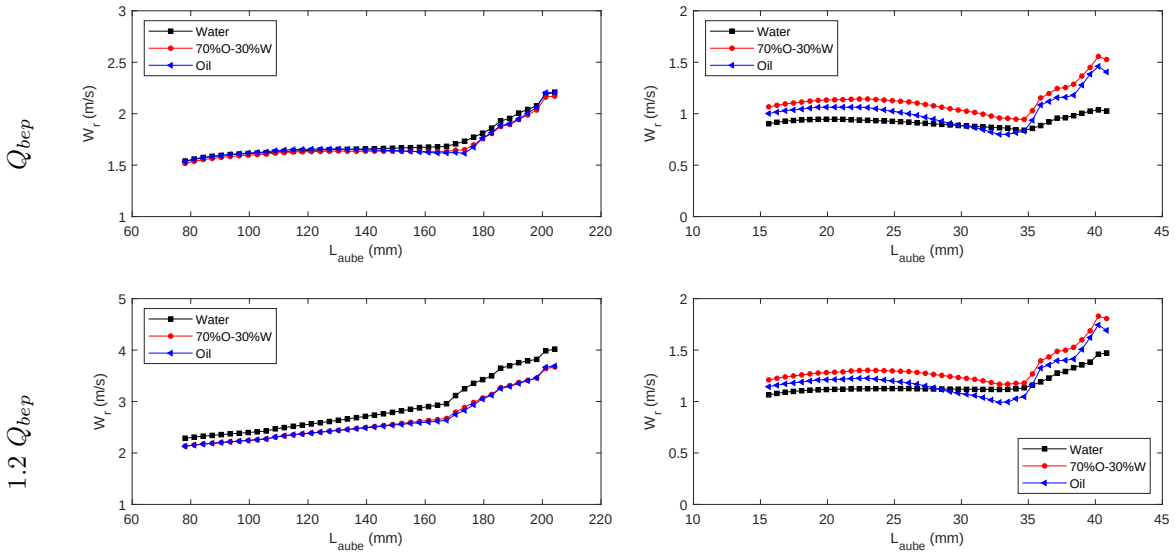

Figure 3.26: Radial component relative velocity profiles for the different fluid versus flow rate

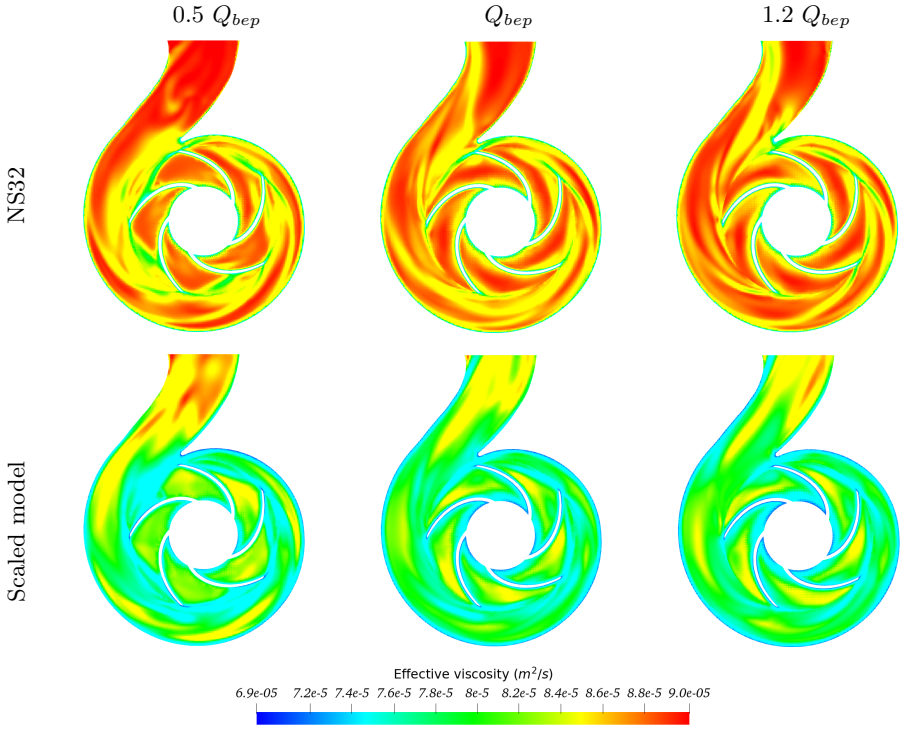

Figure 3.27: Effective viscosity profiles for 80%O-20%W emulsion versus flow rate

As mentioned earlier, the small-size pump generates higher shear rates than the large-size pump. This means that the viscosity of the emulsions will be lower in the scaled-down model than in the large pump, depending on their shear thinning behavior. Effectively, this expectation is observed in Figure 3.27,

which shows the distribution of the effective viscosity of the 80%O-20%W emulsion in the two pumps for different flow rate. All the emulsions studied have a lower viscosity in the scaled-down model due to the high shear rate generated by the pump. Another result to note is that in both pumps, the increase of the flow rate does not induce significant variations of emulsions viscosity in the impeller. However, it involves viscosity variations in the volute, as already highlighted in subsection 3.2.3 for the large-size pump.

3.2.4.4 Non-Newtonian global importance factor I_G

The importance of the non-Newtonian character of the studied emulsions in the two pumps is measured by the global non-Newtonian importance factor given by [127]:

$$I_\Omega = \frac{\sqrt{\Delta^2 \mu_\Omega}}{\mu_\infty} \tag{3.15}$$

$$\Delta^2 \mu_\Omega = \frac{\int_\Omega (\mu - \mu_\infty)^2 \, \mathrm{d}\Omega}{\Omega} \approx \frac{\sum_{i=1}^{N_\Omega} (\mu_i - \mu_\infty)^2 \, \delta\Omega_i}{\sum_{i=1}^{N_\Omega} \delta\Omega_i} \tag{3.16}$$

The quantity $\Delta^2 \mu_\Omega$ is the volume-averaged squared discrepancy of viscosity from the lower Newtonian limit value μ_∞.

Table 3.9 shows the non-Newtonian importance factor calculated for both pumps when handling the different emulsions.

Emulsion composition		**Flow rate**		
		0.5 Q_{bep}	Q_{bep}	**1.2** Q_{bep}
40%O-60%W	NS32	0.185	0.183	0.172
	SM	0.106	0.0964	0.0963
70%O-30%W	NS32	2.519	2.279	2.125
	SM	0.849	0.645	0.611
80%O-20%W	NS32	0.512	0.515	0.515
	SM	0.333	0.300	0.292

Table 3.9: Non-Newtonian importance factors

Figure 3.28 shows that the non-Newtonian character is more significant in the large pump than in the small pump. This factor is very low for the emulsions in regions 1 and 2 with oil volume fractions of 40% and 80% respectively and varies slightly with flow rate. On the other hand, this factor is very important for the emulsion of region 2 (70% oil) corresponding to the phase inversion in both pumps and decreases significantly with the increase of the flow rate. Note that for the latter, the volumetric factor is higher in NS32 by a ratio greater than two over the entire flow range.

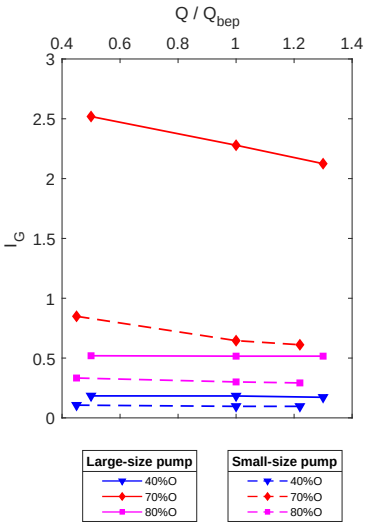

Figure 3.28: Comparison of I_Ω within the two pumps versus flow rate

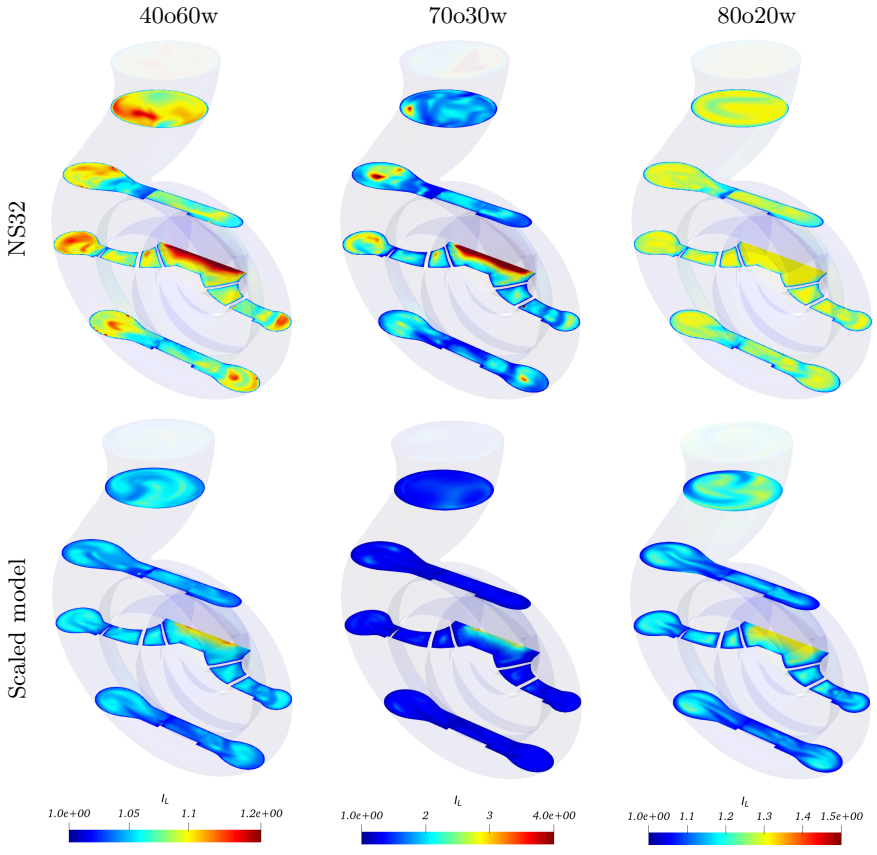

Figure 3.29: Distribution of I_L at several cross-section planes of the two pumps at different flow rates

The extent of the non-Newtonian effect given by the relationship $I_L = \frac{\mu}{\mu_\infty}$ is shown in Figure 3.29

in both pumps as a function of the emulsion processed. The concept is that the ratio indicates the significance of non-Newtonian effects in the flow in general. Since near the pump walls, the shear stresses are relatively very large, lower viscosity levels are observed near the wall ($I_L \approx 1$). In the local distributions of I_L, shown in Figure 3.29 for different longitudinal section planes, we see that non-Newtonian effects are strong only in certain regions of the flow away from the walls. I_L is high in the core of the central region of the volute and the inter-blade space of the impeller, where the shear reaches its minimum. In addition, the distribution of this factor is much flatter in the small pump. This indicates that the small-size pimp exerts more shear than the large-size pump. In addition, low values of I_L indicate that the emulsion behaves like a quasi-Newtonian fluid.

3.2.4.5 Skin friction factor

Since the viscosity in the scaled-down pump is lower than in the large pump, we can expect that the frictional losses are less significant in this small pump. Nevertheless, we have seen in section 3.2.4.1 that regardless of the flow rate, the performance of the reduced model degrades more than the real model for the same fluid. Moreover, the slippage becomes less significant in the small pump when handling emulsions. Therefore, an analysis of viscosity variation in the pump's wall and friction coefficient values is necessary to further investigate the results.

For both pumps, the 40%O-60%W emulsion shows a very well-defined shear-thinning tendency, and at high shear rates, its viscosity change is minimal. Since both pumps generate high shear rates, this emulsion will have almost similar viscosity values at the walls of both pumps. On average, the effective viscosity of the 40%O-60%W emulsion is 1.08 10^{-5} m^2/s^2 at the walls of the reduced model and $1.11 \cdot 10^{-5}$ m^2/s^2 at the walls of the large model. The same observation for the 70%O-30%W emulsion, the viscosity drops sharply to values of the Newtonian lower plateau at medium shear rates. The average viscosities values of this emulsion reach $3.16 \cdot 10^{-5}$ m^2/s^2 in the walls of the reduced model and $3.17 \cdot 10^{-5}$ m^2/s^2 in the walls of the large-size pump. In contrast, the 80%O-20%W emulsion exhibits minimal viscosity variations at low shear rates, with a slight tendency toward shear thinning at very high shear rates. The effective viscosity averages $3.45 \cdot 10^{-5}$ m^2/s^2 and $4.29 \cdot 10^{-5}$ m^2/s^2 in the walls of the reduced model and the large model, respectively.

The averaged skin friction factors applied to the different emulsions by the wet surfaces of the impeller and volute are shown in Figure 3.30 versus flow rate. These skin factors are extracted from CFD results and defined by Equation 3.17 and Equation 3.18 for impeller and volute respectively:

$$f_i = \frac{\bar{\tau}_{wi}}{0.5\rho u_2^2} \tag{3.17}$$

$$f_v = \frac{\bar{\tau}_{wv}}{0.5\rho u_2^2} \tag{3.18}$$

where $\bar{\tau}_{wi}$ and $\bar{\tau}_{wv}$ are the averaged shear stress on wet surface of the impeller and volute respectively. ρ is the fluid density and u_2 the impeller tip speed.

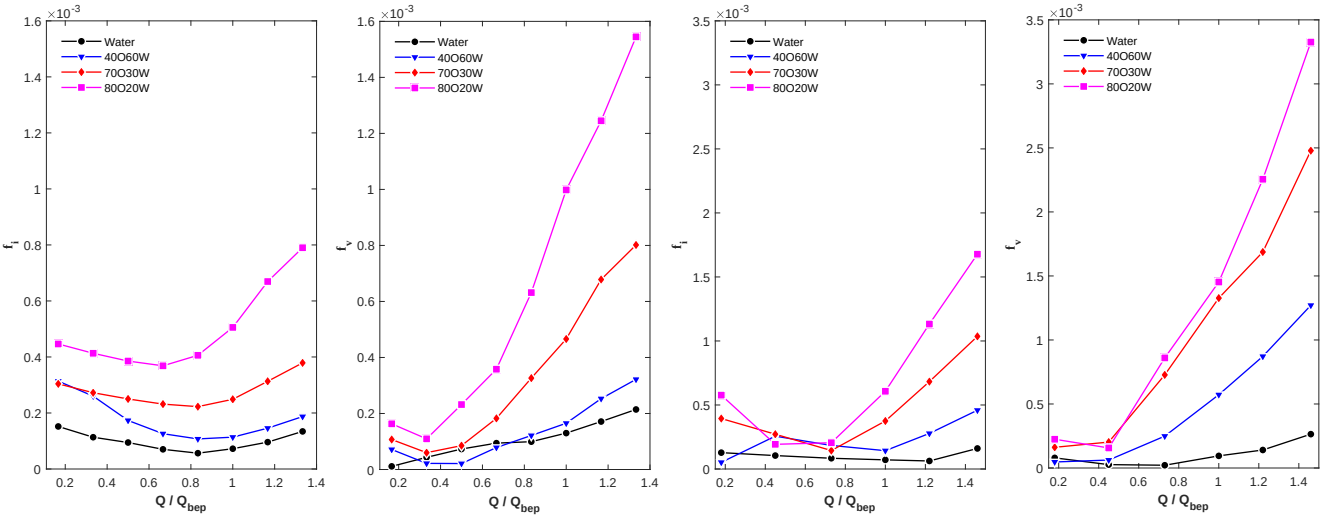

Figure 3.30: Averaged skin friction coefficient of the impeller (a-c) and the volute (b-d) in the large size pump (a-b) and scaled-down pump (c-d) versus flow rate

Regardless of pump size, the influence of flow rate on the skin friction coefficient differs between the impeller and the volute. In both pumps, friction losses in the impeller are higher prior to design flow and become more influential in the volute at higher flow rates. The skin friction factors increase with increasing oil phase volume fraction, which is consistent with increasing fluid viscosity. Comparing the skin friction for the two pumps, the magnitudes of f_i and f_v are almost twice as high in the small-size pump than in the large pump. However, the skin friction coefficient of water in both parts (impeller and volute) is almost similar in both pumps over the entire flow range.

Generally a higher viscosity in the impeller and volute results in a higher skin friction factor. In centrifugal pumps, the shear rate generated at the walls is very high so that the emulsion viscosity approaches the Newtonian lower plateau. Thus, the fluid viscosity will have almost the same impact on the skin friction coefficient in both pumps. The friction losses caused by the shear force on the wall surfaces are proportional to the skin friction coefficient which depends on the Reynolds number (i.e flow regime). However, the flow in the impeller is not fully developed in most of the regimes inside the impeller [128]. So that the impeller rotational speed and passage curvature affect the value of the skin friction coefficient. Although the CFD losses are not exact predictions since the skin friction coefficient (cf) was assumed to be constant and equal to its average along all impeller and volute walls, it was shown that friction losses are higher in a small-size pump than in a large one, which explains the increased head degradation obtained previously despite the lower slippage.

Conclusions

In this Chapter, CFD analysis was performed to investigate the performance and flow characteristics of a centrifugal pump handling emulsions and oil–water mixtures at different water cuts. The mixtures were modeled and simulated as a single-phase fluid following shear-thinning non-Newtonian rheology.

In addition, the effect of pump size on pump performance degradation when handling non-Newtonian emulsions was investigated. The internal flow was then analyzed in order to compare qualitatively the different losses within a large-size pump (NS32), and a 1/5 reduced model of the same pump. The numerical results have shown a progressive deterioration in pump performance as the oil fraction increased in the emulsion, except for the composition at the inversion zone. Despite the high effective viscosity of this composition, the strong tendency of the fluid to shear-thinning and the high shear rates of the pump caused the viscosity to decrease sharply. Pointing out that the head developed by the pump at a low volume fraction of the dispersed phase (up to 20% WC) is almost identical to that developed by the continuous phase. The model prediction for the pump performance is based on the shear rate values. CFD analysis has shown that the Non-Newtonian behavior of the emulsions was observed with a wide range of effective viscosity in the volute. In contrast, the emulsions exhibited minor non-Newtonian characteristics and/or a small effective viscosity range in the impeller due to the high shear rate generated by rotation in this region. In addition, the mechanical shearing in small-scale pumps is higher than that of large-scale pumps. Even though the emulsions are subjected to a high shear rate and have a lower viscosity due to their shear-thinning behavior in the small pump, the skin friction coefficient is more significant in the small-size pump.

CHAPTER 4

Application of entropy production theory to the evaluation of energy losses of centrifugal pumps

Contents

Introduction and motivation

Thorough investigations have been conducted in the literature on the influence of emulsion flow on pump performance by developing theoretical and semi-empirical correlations to estimate hydraulic losses. As seen in Chapter 2, these studies provide models that depend on pump geometry and fluid viscosity to calculate the associated theoretical head degradation, but these correlations find their limits when the fluid is non-Newtonian. Furthermore, the empirical aspect of the proposed rheological model raises questions regarding the universal validity of using this correlation in conjunction with the head loss models originally developed for water for inferring the pump performance when handling emulsions. Traditional methods are thus very limited in determining energy losses due to the complex rheological behavior of such fluids. Therefore, other loss assessment methods should be explored and used to determine the losses in centrifugal pumps handling non-conventional fluids.

With the development of CFD, the numerical resolution of mathematical models of turbulence are developed more and more perfectly. As a result, the internal flow and energy characteristics can be predicted with accuracy by simulation, which allows us to evaluate the energy losses of the fluid in turbomachinery. The energy performance of hydraulic machines can be quickly evaluated using the energy loss by entropy generation approach. Recently, this method is increasingly adopted in the evaluation of energy losses in turbomachinery, especially due to advances in theoretical and computer developments and the evolution of technology [129]. Many researchers have used the entropy production theory to investigate the effects of some parameters like impeller tip clearance [130, 131, 132], clocking position [133, 134], impeller trimming [135], and blade thickness [136, 137] on the internal flow field and the hydraulic losses of pumps. Also, for identifying the process mechanism of hydraulic losses and the fluid flow state in the different components of specific types of hydraulic machinery, including centrifugal pumps

[138, 139, 140, 141], mixed and axial flow pumps [130], and hydro-turbine [142, 143, 144, 145, 146]. Most of these studies were collected in the review article [129], where the authors emphasized the importance of entropy production theory in the study of the internal flow mechanism of turbomachinery, the evaluation of their hydraulic performance, and the optimization of pump design.

This chapter aims to investigate the hydraulic losses and performance degradation mechanism of the centrifugal volute pump considered in this study handling non-Newtonian emulsions using the entropy production method, focusing on the influence of emulsion type on the loss mechanism. The influence of pump size on fluid's non-Newtonian behavior and energy loss in the centrifugal pump is also investigated by comparing the entropy distribution in two geometrically similar pumps. The flow field and entropy production are predicted by computational fluid dynamics (CFD) based on the Reynolds-averaged Navier-Stokes (RANS) equations presented in Chapter 3 (section 3.1). In this chapter, three different emulsions were considered, corresponding to an emulsion of each region presented previously (table 3.3), namely a water-continuous emulsion having 40% oil volume fraction, an oil-water mixture corresponding to the inversion region having 70%O-30%W, an oil-continuous emulsion having 20% water cut.

4.1 Governing equations

Entropy production refers to thermodynamic irreversibility and energy loss in a system. In centrifugal pumps, the impeller's kinetic energy is transformed into pressure energy, and this transfer is accompanied by an irreversible energy loss and an increase in entropy due to the viscosity of the working fluid, the turbulent flow regime and the high Reynolds stress. According to the second law of thermodynamics, flow losses are energy losses that can be assessed by determining the production of entropy. This is especially the case since the working fluid has a complex rheological behavior and other methods (analytical methods) of quantifying losses have proven to be limited [34, 52, 147]. This method is therefore used to explain the mechanism of the different energy losses in two similar pumps handling non-Newtonian fluids. The specific entropy S, a state variable, for an incompressible single-phase flow is given by Equation 4.1 [129].

$$\rho\left(\frac{\partial S}{\partial t}+u\frac{\partial S}{\partial x}+v\frac{\partial S}{\partial y}+w\frac{\partial S}{\partial z}\right)=-\operatorname{div}\left(\frac{\vec{q}}{T}\right)+\frac{\Phi}{T}+\frac{\Phi_{\Theta}}{T^2} \tag{4.1}$$

The negative term $-\operatorname{div}\left(\frac{\vec{q}}{T}\right)$ is the reversible heat transfer. $\frac{\Phi}{T}$ and $\frac{\Phi_{\Theta}}{T^2}$ represent the entropy production caused by dissipation and heat transfer respectively.

According to the time-averaged Reynolds process, the specific entropy in turbulent flow is separated into the time-averaged component $\bar{S}$ and the fluctuating part s'. The entropy transport equation wihin the pump is then provided by Equation 4.2 since the flow is assumed to be isothermal without heat transfer.

$$\rho\left(\frac{\partial \bar{S}}{\partial t}+\bar{u}\frac{\partial \bar{S}}{\partial x}+\bar{v}\frac{\partial \bar{S}}{\partial y}+\bar{w}\frac{\partial \bar{S}}{\partial z}\right)=\overline{-\operatorname{div}\left(\frac{\vec{q}}{T}\right)}-\rho\left(\overline{\frac{\partial u's'}{\partial x}}+\overline{\frac{\partial v's'}{\partial y}}+\overline{\frac{\partial w's'}{\partial z}}\right)+\overline{\frac{\Phi}{T}} \tag{4.2}$$

The viscous dissipation function for the incompressible flow is defined in Equation 4.3 [148].

$$\Phi = 2\mu\left[\left(\frac{\partial u}{\partial x}\right)^2+\left(\frac{\partial v}{\partial y}\right)^2+\left(\frac{\partial w}{\partial z}\right)^2\right]+\mu\left[\left(\frac{\partial u}{\partial y}+\frac{\partial v}{\partial x}\right)^2+\left(\frac{\partial u}{\partial z}+\frac{\partial w}{\partial x}\right)^2 + \left(\frac{\partial v}{\partial z}+\frac{\partial w}{\partial y}\right)^2\right] \tag{4.3}$$

From the time-averaged Reynolds process, the specific entropy production for the main flow (Equation 4.4) is divided into time-averaged part $\dot{s}_{pro,VD}$, which is caused by viscous dissipation, and fluctuating terms $\dot{s}_{pro,TD}$ which are caused by turbulence. The entropy production rate by viscous dissipation given by Equation 4.5 is directly calculated from CFD. While the entropy production caused by turbulence given by Equation 4.6 cannot be determined directly from the CFD since the RANS model does not solve fluctuating velocities. This quantity is however directly related to the chosen turbulence model and is determined using Equation 4.7 [149], where ϵ stands for the turbulent dissipation rate.

$$\overline{\left(\frac{\Phi}{T}\right)} = \dot{s}_{pro,VD}+\dot{s}_{pro,TD} \tag{4.4}$$

$$\dot{s}_{pro,VD} = \frac{\mu}{T}\left\{2\left[\left(\frac{\partial \bar{u}}{\partial x}\right)^2+\left(\frac{\partial \bar{v}}{\partial y}\right)^2 + \left(\frac{\partial \bar{w}}{\partial z}\right)^2\right]+\left(\frac{\partial \bar{u}}{\partial y}+\frac{\partial \bar{v}}{\partial x}\right)^2+\left(\frac{\partial \bar{u}}{\partial z}+\frac{\partial \bar{w}}{\partial x}\right)^2+\left(\frac{\partial \bar{v}}{\partial z}+\frac{\partial \bar{w}}{\partial y}\right)^2\right\} \tag{4.5}$$

$$\dot{s}_{\mathrm{pro,TD}} = \frac{\mu}{T}\left\{2\left[\left(\frac{\partial u}{\partial x}\right)^2+\left(\frac{\partial v'}{\partial y}\right)^2 + \left(\frac{\partial w'}{\partial z}\right)^2\right]+\left(\frac{\partial u}{\partial y}+\frac{\partial v'}{\partial x}\right)^2+\left(\frac{\partial u}{\partial z}+\frac{\partial w'}{\partial x}\right)^2+\left(\frac{\partial v'}{\partial z}+\frac{\partial w'}{\partial y}\right)^2\right\} \tag{4.6}$$

$$\dot{s}_{pro,TD} = \frac{\rho\varepsilon}{T} \tag{4.7}$$

In addition to the previously mentioned entropy generation, there is also entropy generation at the walls. This is because rotating fluid machines' blade surfaces have high velocity and pressure gradients, which cause a strong wall effect in the flow field and nontrivial irreversible flow losses [129]. The following expression is used to compute the entropy produced at the walls of the grid's first layer.

$$\dot{s}_{\mathrm{pro},\,W} = \frac{\vec{\tau}\cdot\vec{v}}{T} \tag{4.8}$$

where v is the fluid velocity at the first grid close to the wall and τ represents the wall's shear stress. In the end, the total energy loss (TEL) is the product of the surface integral of the entropy production at the walls (Equation 4.9) and the volume integral of the local entropy production rate due to viscous and turbulent dissipation.

$$T_{EL} = \int_V \left(\dot{s}_{pro,TD}+\dot{s}_{pro,TD}\right)\mathrm{d}V + \int_A \dot{s}_{\mathrm{pro},W}\,dA \tag{4.9}$$

4.2 Results and discussion

4.2.1 Analysis of energy losses by local entropy production

Figure 4.1 compares the volumetric TEL ($W/(m^3 \cdot K)$) per volume of the two centrifugal pumps handling different non-Newtonian emulsions versus flow rate.

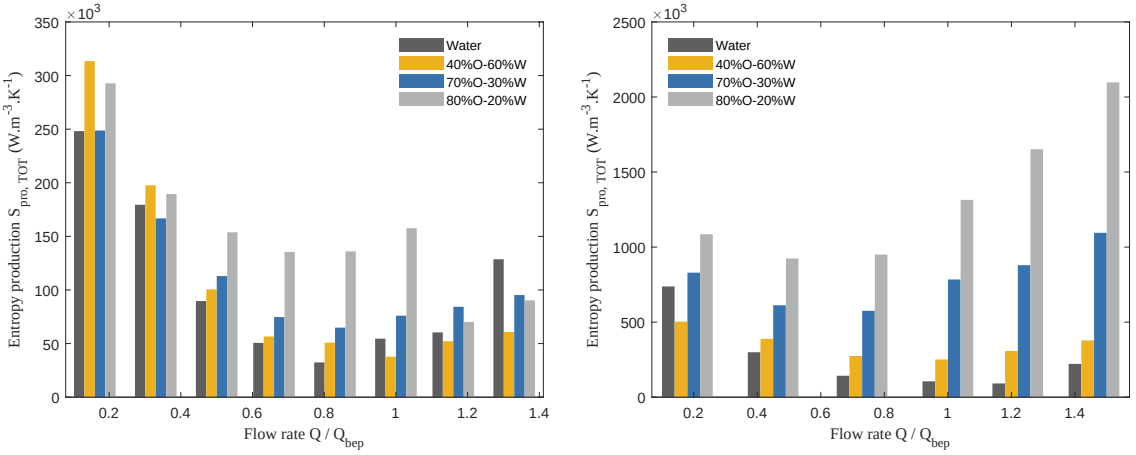

Figure 4.1: Total entropy production of the large size pump (left) and scaled-down model (right) handling different emulsions versus flow rate

It can be observed that the TEL per volume in both pumps increases with the volume fraction of the oil phase, which is consistent with the increase in fluid viscosity. When operating with water, the trend of the entropy production versus flow rate is the same in both pumps regardless of their size, but the amplitude is almost three times higher in the small-size pump. As expected, the TEL of the centrifugal pumps increases as the flow rate deviates from the design point. It increases slightly under overload conditions and increases more importantly as the flow rate decreases. This indicates that the hydraulic losses caused by the secondary vortex structure and recirculation zones increase. Similar observations were reported in previous studies [148].

However, for non-Newtonian mixtures, the influence of the pump size on the energy loss is more prominent. With the emulsion's concentration changing, the entropy production in the large-size pump varies in a similar trend to that of water, except for the 80%O-20%W emulsion for witch the TEL decreases at overload conditions. This can be explained by the viscous forces that overcome the convective forces due to the higher viscosity of this emulsion, so the flow becomes less turbulent in all parts of the pump. The entropy caused by turbulence, which is predominant here decreases significantly, resulting in a decrease in total entropy. However, for the small size pump, the evolution of hydraulic losses for different emulsions seems to show an opposite trend. Namely, the increase in the oil concentration i.e., the increase in fluid's viscosity, results in a slight increase in entropy generation at partial operating conditions and a significant increase as the flow rate increases. This implies firstly that the hydraulic losses caused by turbulence and vortex structure when operating with non-Newtonian fluid are more significant in the large-size pump under partial operating conditions, relatively to the total losses. Secondly, in the small-size pump, as the flow rate increases, the hydraulic losses become more significant as the viscosity of the emulsions increases, and can probably be attributed to incidence and shock losses. These types of losses

are indeed the most dominant at high flow rates. Moreover, the difference between the entropy generated for water and the different emulsions is larger in the reduced model. This explains the more pronounced performance degradation in the small-size pump observed previously when the fluid is non-Newtonian. Hereof, it can be concluded that the losses will be different in two geometrically similar pumps depending on the non-Newtonian behavior of the mixture. To further investigate this point, a detailed analysis of the different losses in the two pumps is given in the next section.

4.2.2 Effect of pump size and non-Newtonian rheology on entropy distribution in the impeller and volute

To clarify the mechanism of energy loss in two geometrically similar pumps handling non-Newtonian fluids, the TEL distribution in both domains, namely impeller and volute as a function flow rate is presented in Figure 4.2 for each fluid.

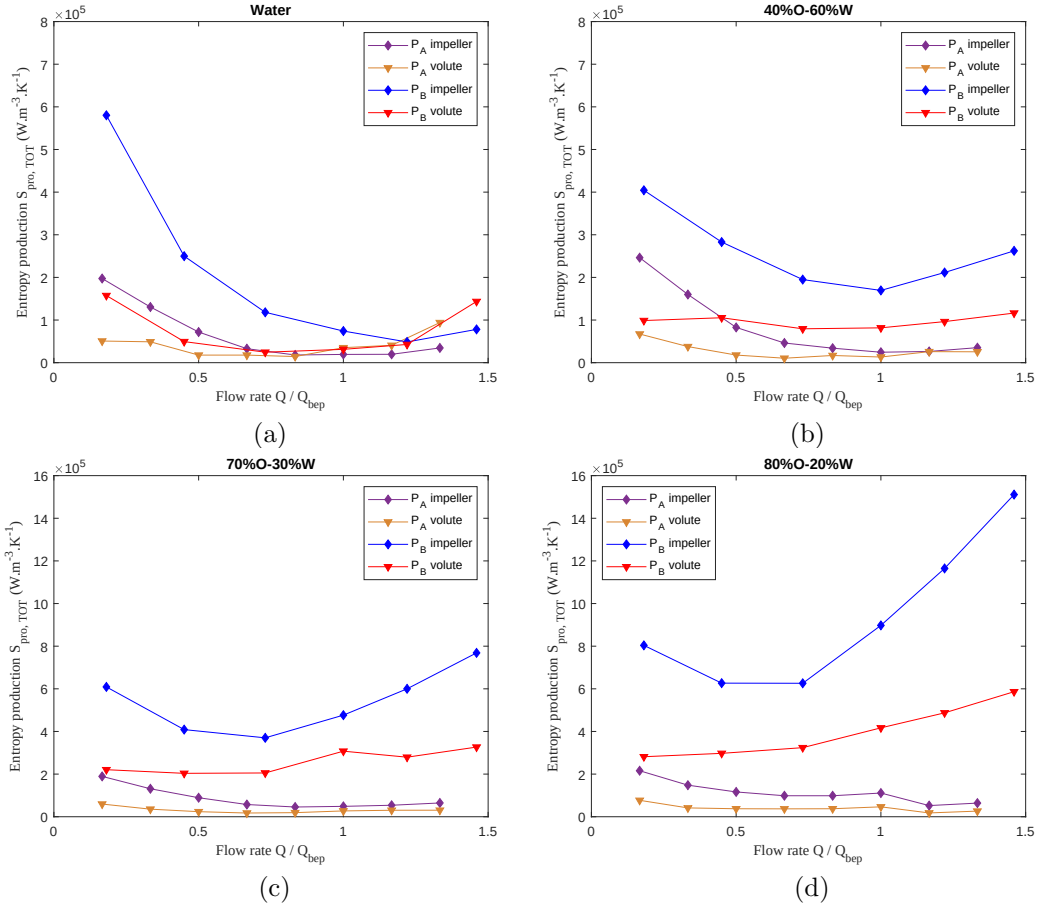

Figure 4.2: Influence of the emulsion type on the entropy production in the different parts of the large-size pump (P_A) and the scaled model (P_B). (a) Water, (b) 40%O-60%W, (b) 70%O-30%W, (b) 80%O-20%W

The predominance of losses within parts of a centrifugal volute pump depends on the fluid viscosity and pump size as observed in the figure. Before the design flow rate, the TEL in the impeller is higher than the one in the volute for both pumps when handling water, but it becomes larger in the volute

at overload conditions. As for emulsions, it is more dominant in the impeller than in the volute over the whole flow range and for both pumps. This difference in entropy generation in different parts of the pumps can be explained by the high rotational speed of the impeller, which generates more kinetic energy. As expected, the energy loss occurs mainly in the rotor region of centrifugal pumps. Both parts of the large-size pump (P_A) are weekly affected by the variation of the non-Newtonian rheology, where a similar level of entropy production in the impeller as well as in the volute is observed for all emulsions. On the other hand, the influence of emulsion type on entropy production is well observed in the different parts of the small-size pump. The TEL in the impeller shows a sharp increase with the flow rate as the oil volume fraction increases in the emulsion. At the same time, the increasing rate of TEL in the volute exhibit a lower slope as the flow rate increases, in comparison to the impeller. As shown above, pump size significantly affects the non-Newtonian behavior of emulsions and the associated losses.

Figure 4.3 and Figure 4.4 show the fraction of each type of entropy produced in the pump domains relative to the total entropy at different operating condition i.e 0.5 Q_{bep} and Q_{bep}. Water and concentrated emulsion 80%O-20%W have been chosen as reference fluids for the presentation of these results.

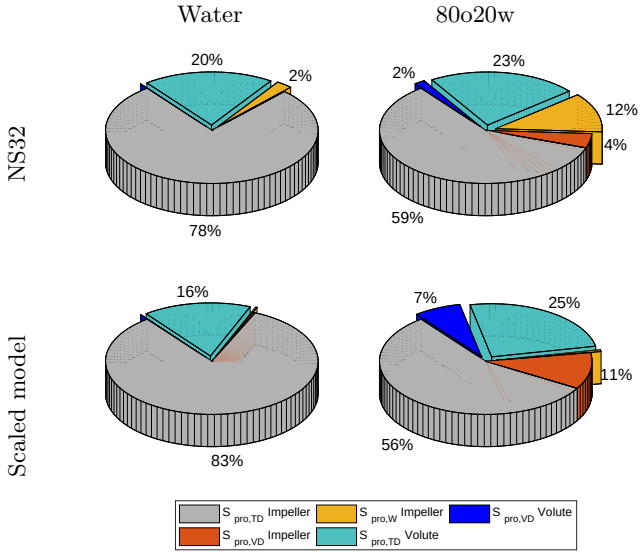

Figure 4.3: Fraction of each entropy production in the two domains of the two pumps versus the handled fluid in partial operation condition 0.5 Q_{BEP}

At partial operating conditions, the rate of energy loss caused by turbulence decreases in the impeller as the oil volume fraction increases in the emulsion. On the other hand, in the volute, the rate of energy loss caused by turbulence increases as the oil volume fraction in the emulsion increases. In addition, this type of entropy production is relatively more important in the impeller of the small-size pump than in the large-size pump when operating when water, and is smaller when operating with emulsions. This can be explained by the vortex zones that can be very large in the impeller of centrifugal pumps under partial operating conditions, generating a higher energy loss than in the volute. Moreover, the size of the vortex area depends on the pump size and is inversely proportional to the viscosity of the emulsions as mentioned in section 3.2.2. Where the study showed larger recirculation zones in the inter-blade space of the small-size pump when handling water at low flow rates, compared to the large pump. On the other hand, when handling emulsions, smaller recirculation zones appear in the inter-blade space compared to

the large-size pump. In both pumps, the percentage rate of energy loss caused by turbulence increases in the volute and decreases in the impeller as the flow rate increases for all fluids.

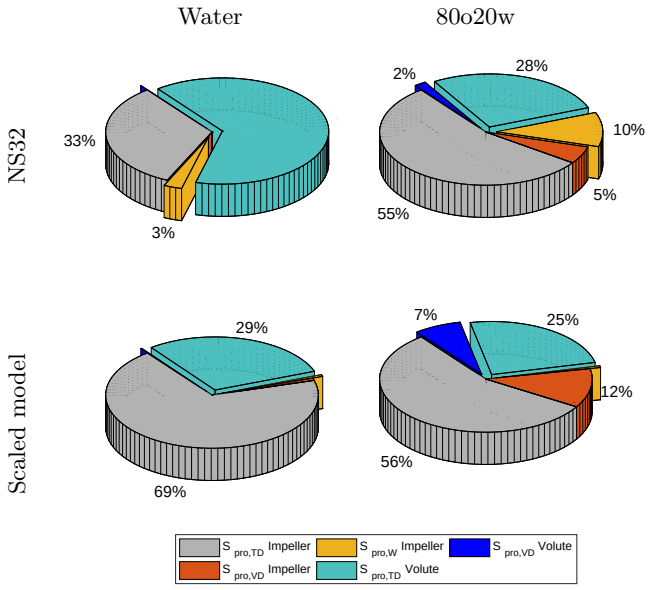

Figure 4.4: Fraction of each entropy production in the two domains of the two pumps versus the handled fluid at design condition Q_{BEP}

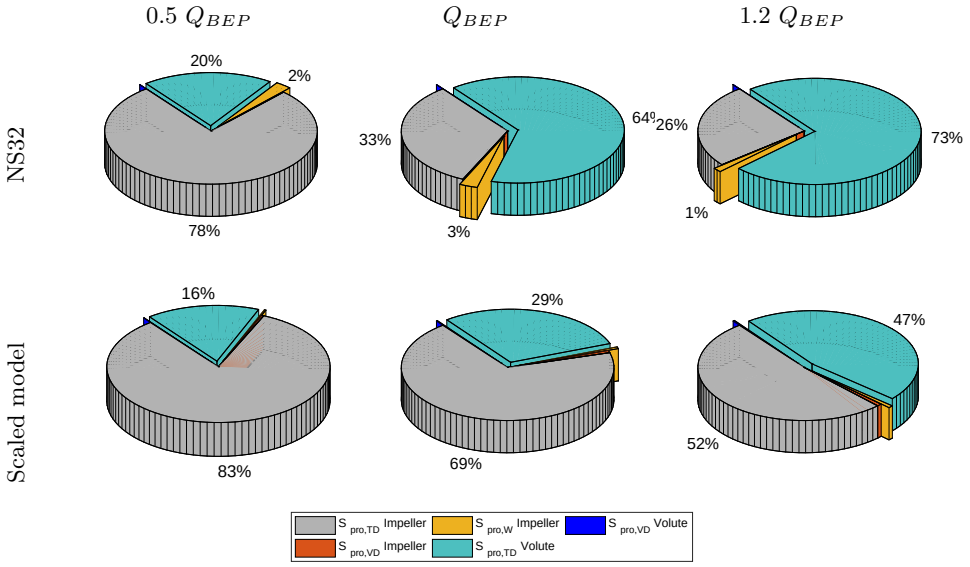

Figure 4.5: Fraction of each entropy production in the two domains of the two pumps when operating with water under three different operating conditions.

At the best efficiency point, the distribution of the different losses in the volute and the impeller is almost similar in both pumps when the fluid is non-Newtonian. However, when the fluid is water, the energy loss in the large-size pump occurs mainly in the volute, while in the small-size pump, the

energy loss occurs mainly in the impeller. The entropy generation becomes increasingly important in the volute as the flow rate increases regardless of pump size but has a high fraction in the large-size pump as illustrated in Figure 4.5, which shows the fraction of each entropy production in the two domains of the two pumps when operating with water under three different operating conditions.

It should be noted that the method of calculating entropy production based on the CFD results depends on the turbulence model and the mesh resolution. A comparison of the results obtained in this study for water with previous studies that have used the same approach for loss visualization and energy loss determination reveals the accuracy and reliability of the method. Using the same method for loss estimation, the study of Lai et al [150] on a volute centrifugal pump with a specific speed of 1579, a TEL in the main flow of 75W is obtained at 0.5 Q_{bep}, which gradually decreases with increasing flow rate to reach its minimum value of 50W at the design point. The TEL then gradually increases with the increase in flow rate to 60W. Comparing these results with the small-size pump considered in this study that has approximately the same specific speed (1605), a TEL of 115W is obtained at 0.5 Q_{bep}, which decreases to 80W at the design point, and increases slightly at higher flow rates.

The results show that the amount of entropy created by direct dissipation is significantly less than that produced by turbulent dissipation in both pumps, especially when water is the working fluid. This result is consistent with earlier research [151, 129] in which the authors concluded that the majority of the total entropy produced by the pump is due to turbulent dissipation entropy. For emulsions, the rate of energy loss by direct dissipation increased in the impeller and volute of both pumps with increasing oil concentration in the emulsion for all operating points. This is because when oil content rises, the emulsions' viscosity increases, promoting a rise in frictional losses while lowering secondary and recirculation losses. It should be noted that the method of calculating entropy production based on the CFD results depends on the turbulence model and the mesh resolution. A turbulence model is used to drive the numerical simulation to assess the impact of turbulence fluctuation on the mean fluid flow. A finer mesh would increase the entropy production by viscous dissipation, which is directly computed, and correspondingly decrease the entropy production by turbulence, which is modeled.

4.2.3 Analysis of the local distribution of entropy loss

To comprehensively understand the effect of non-Newtonian behavior on the energy loss mechanism in two similar pumps, the distribution of normalized entropy production coefficient (EPC) calculated using Equation 4.10 [133] is used to compare the locations of high dissipation values within the two pumps. Figure 4.6 (11-12) show the entropy distribution for all studied fluids under 0.5 Q_{bep}, Q_{bep}, and 1.2 Q_{bep} operating points at the midspan plane.

$$\Phi^* = \frac{(\Phi_{\bar{D}} + \Phi_{D'})\, D_2}{\omega^2 \rho Q} \tag{4.10}$$

As analyzed previously, the hydraulic losses in centrifugal pumps operating with non-Newtonian fluids depend on the pump size. In average, the small-size pump generates higher entropy loss compared to the large-size one, relatively to the pump volume.

Figure 4.6 shows the entropy distribution for all studied fluids under partial conditions at the midspan plane. The losses are concentrated at the impeller inlet, spiral volute part particularly in contact with impeller outlet, impeller inter-blade passage, and volute nozzle regions of both pumps at underload

conditions. On the contrary to the impeller passage, the losses in the volute increased with increasing emulsion viscosity. In both pumps, the energy loss occurring at the impeller inlet increases with the concentration of oil in the emulsion. In addition, this energy loss is higher in the small-size pump, mainly when operating with high viscous emulsions. This entropy production at the impeller inlet probably results from the difference between the fluid inlet angle and the blade inlet angle, generating impact losses. Thus, shock losses increase as the viscosity of the fluid increases and as the pump size is reduced.

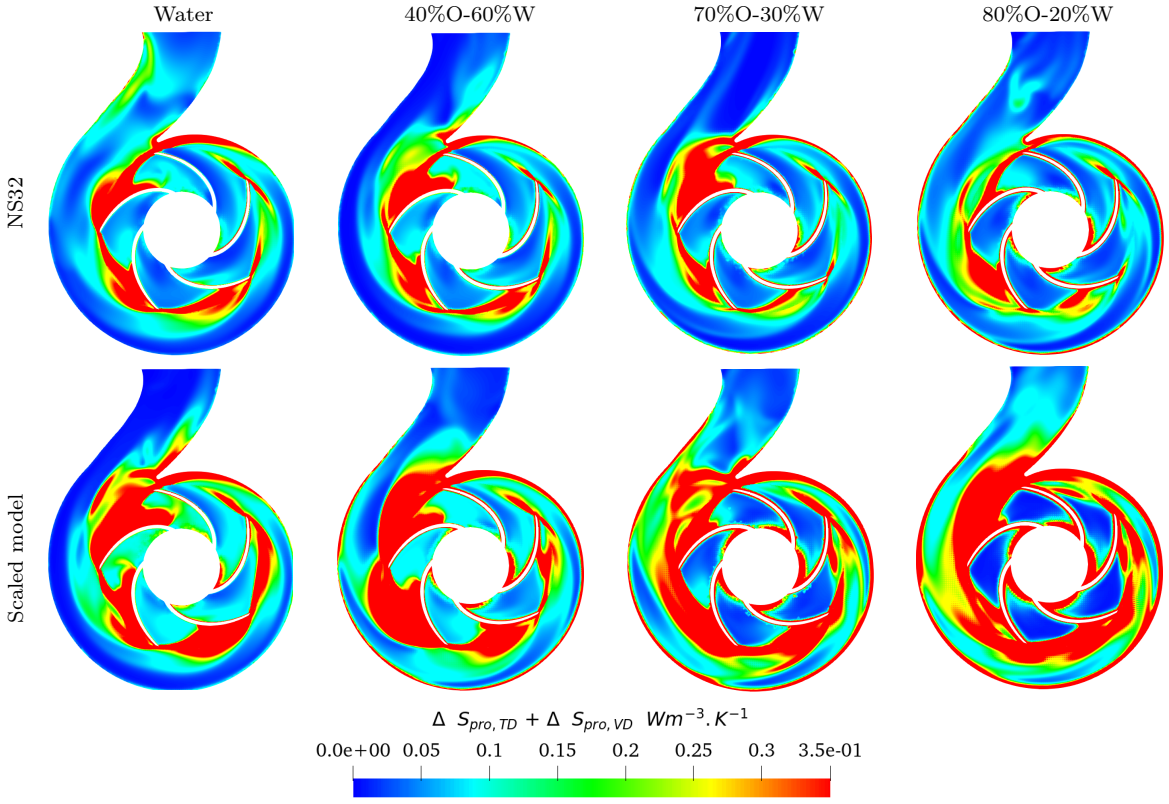

Figure 4.6: Entropy production distribution at underflow condition 0.5 Q_{BEP}

The losses occurring at the inter-blade space of the impeller decrease with oil concentration, and this decrease is more pronounced in the small-size pump. These areas of high entropy losses correspond to recirculation zones observed in the velocity field and streamlines within impeller inter-blade space (Figure 3.21 in section 4.2.3). Figure 4.6 shows high entropy regions near the pressure side of the impeller blades in contact with the volute tongue in both pumps that correspond to the vortex area. This vortex decreases as the volume fraction of the oil phase of the emulsions increases. In addition, this vortex is larger in the small-size pump than in the large-size one when handling water and is smaller when handling emulsions. These areas of recirculation and change of fluid direction cause the fluid to lose kinetic energy, which is the source of hydraulic losses, leading to an increased entropy generation. Regarding the losses at the spiral volute part, this last one is more significant in the reduced model and increases with increasing emulsions viscosity. These flow losses correspond to the flow entering the volute with a velocity angle that can deviate from that of the volute on which is superimposed a tangential velocity vortex opposite to the movement of the impeller [110]. This change in flow direction

inevitably involves hydraulic losses. This suggests that the energy loss generated by recirculation zones will be smaller in a small-size pump than in a large-size pump when handling non-Newtonian fluid, and inversely for the volute diffusion losses. This results highlight that the volute diffusion losses are the predominant losses in both pumps.

At the design point, the entropy produced decreases as expected in the whole pump, and high-loss regions are mainly located in the impeller inlet, in the wake of the trailing edges, the volute's tongue, and the divergent as shown in Figure 4.7. Compared to underload conditions, the entropy generated at the impeller inlet decreases in the large-size pump for all fluids, however, in the small-size pump, this entropy decreases for water and less viscous emulsion. Moreover, the energy dissipation of the emulsion is more pronounced in the small pump as shown in the figure. After the nominal flow rate (Figure 4.9), the entropy generated in the inter-blade space decreases, and the entropy generated in the wake of the trailing edges is constantly high, especially for the small-size pump. Figure 4.8 shows significant entropy generation regions at the tip and divergent of the volute. By analyzing the flow field and velocity streamlines within these regions (comparing Figure 4.9 (a) with Figure 4.9 (b)), we recognize a vortex zone near the volute tongue of the large-size pump that develops and moves toward the volute divergent as the fluid viscosity increases. For the scaled-down model, a small vortex zone appears in the volute divergent for 70%O-30%W emulsion. At overload conditions, a large recirculation zone appears in the divergent part of the volute and decreases as the oil volume fraction increases. This undesirable flow pattern produces the relatively high entropy loss observed previously. Regarding the entropy produced at the impeller inlet, we observe that it increased at overload conditions and with emulsion concentration. These results are consistent with the impact loss model, for which previous studies [89, 147] have shown that this loss loss decreases with increasing flow rates to reach its minimum at nominal flow rates, and increases as the flow rate increases above this point.

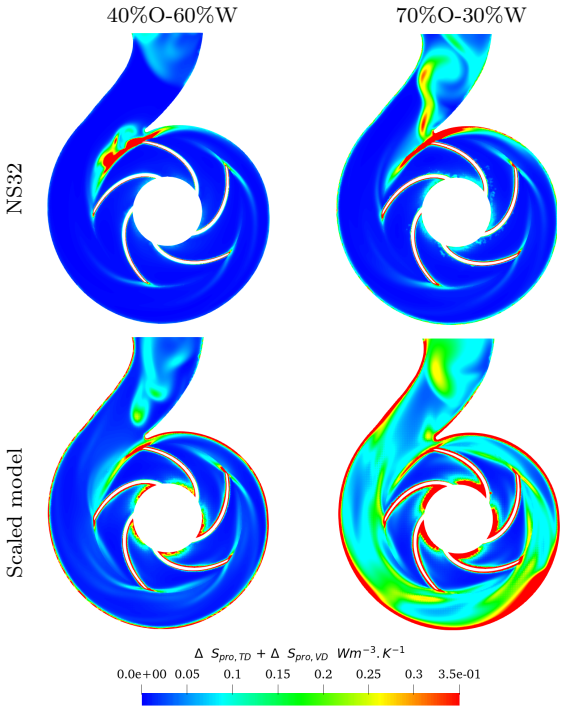

Figure 4.7: Entropy production distribution at design condition Q_{BEP}

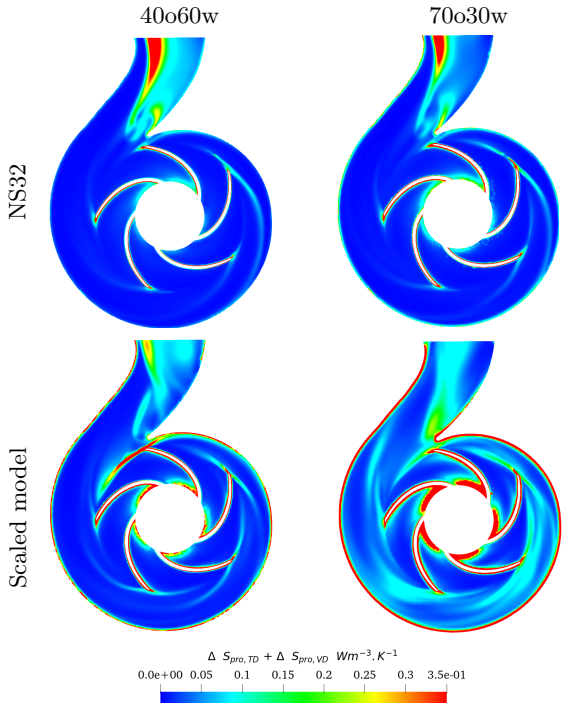

Figure 4.8: Entropy production distribution at overload condition 1.2 Q_{BEP}

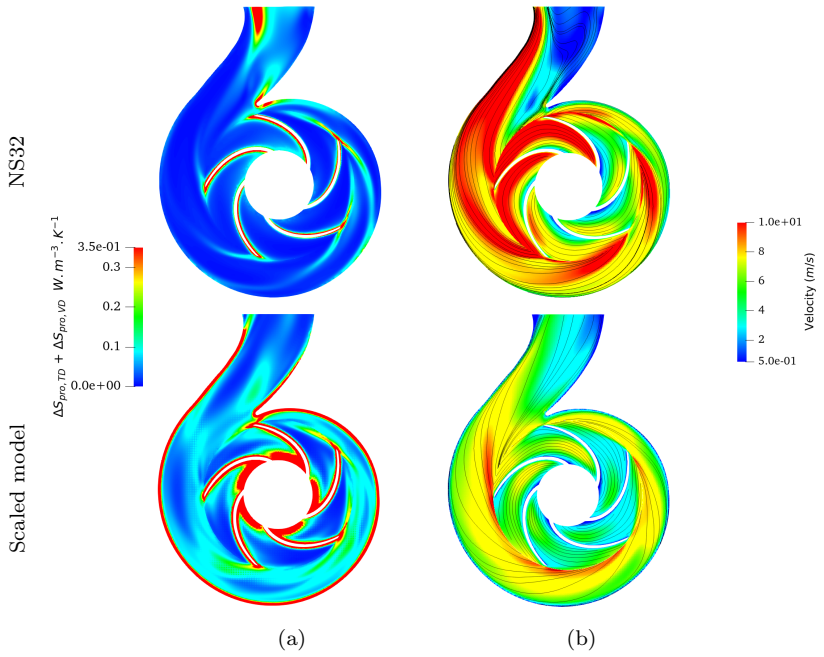

Figure 4.9: Entropy production distribution (a) and the velocity streamlines (b) at overload condition 1.2 Q_{BEP}

Conclusion

Based on the entropy generation method, the influence of non-Newtonian fluid rheology on the internal flow fields of a volute centrifugal pump is numerically investigated. A dependency between the non-Newtonian rheological behavior and the energy loss mechanism in a volute centrifugal pump has been highlighted. Furthermore, the influence of the pump size on the non-Newtonian behavior and entropy production is investigated by comparing the energy performance of two geometrically similar pumps handling non-Newtonian fluids. The analysis is performed both quantitatively and qualitatively, and supported by general integrated quantities and observation of local flow features. Based on the analysis of the results, the following findings and conclusions are drawn :

- The internal flow field of the centrifugal volute pump is affected by non-Newtonian rheology, which also contributes significantly to hydraulic losses and entropy generation in pumps. The entropy generation increases significantly as the lower limit of non-Newtonian viscosity increases and energy loss occurs primarily in the impeller, regardless of pump size and flow rate.
- The pump size influences the non-Newtonian behavior of the fluid, and thus the flow structure and magnitude of losses. The smaller the pump size, the greater the entropy generation relative to the volume.
- The predominance of losses in centrifugal volute pumps operating with non-Newtonian fluids depends on the size of the pump. More entropy production is generated at the leading and trailing edges of the smaller pump's impeller than the larger pump. Concluding that shock and change of direction losses will be more significant in a small-size pump, and the recirculation losses less prominent compared to a large-size pump when the fluid is non-Newtonian.
- The energy loss increases with the concentration of oil in the emulsion and is predominantly experienced at the impeller inlet of the small-size pump as the flow rate rises. In contrast, in the large pump, the energy loss at the impeller inlet is generally small compared to that of the small pump, especially when comparing emulsions with high concentrations, but the difference remains insignificant for water and emulsions with low oil concentrations. In conclusion, pump size affects shock losses for highly viscous emulsions, but insignificantly for water and low viscosity emulsions.

CHAPTER 5

Comparative assessment of single non-Newtonian and two-phase approaches for predicting the performance of pumps handling emulsions

Contents

Introduction and motivation

As previously mentioned, the work in the literature on the operation and performance of centrifugal pumps handling emulsions and oil-water mixtures is sparse and has mainly focused on experimental studies that have revealed that most emulsions have complex non-Newtonian rheology. In addition, few numerical analyses have been performed on this topic due to the complexity of modeling emulsions. These analyses are usually performed using two-phase approaches. In these approaches, several assumptions are made regarding emulsion flow, given the complexity of multiphase models and the physics underlying emulsion flow. Among the assumptions made is the neglect of the non-Newtonian behavior of the emulsion, which is observed experimentally and is a benefit to pump performance in some cases. Therefore, the first part of this thesis examined the effect of the rheological properties of the emulsion on the performance of volute centrifugal pumps. Oil-water mixtures were modeled and simulated as a single-phase fluid exhibiting shear thinning behavior while neglecting the two-phase character. However, emulsions are two-phase in nature. In comparison to single-phase flows, the presence of liquid droplets in multiphase flows can significantly affect the behavior of the fluid flow. Thus, assuming a single-phase fluid leads to setting several simplifying assumptions and neglecting the interactions between the coexisting phases.

This chapter aims to comparatively evaluate single-phase non-Newtonian and two-phase approaches to model emulsion flow within centrifugal pumps. In addition, it aims to conclude on the necessity to simulate two-phase fluid for accurate performance prediction. This comparative study of single-phase non-Newtonian and two-phase approaches for emulsion flow uses the experimental data of a multistage pump from the literature to evaluate the numerical results. The outcome of this chapter will provide a better understanding of the effect of the different interphase force terms on the mixture distribution and their effect on the pump performance. From another point of view, the study demonstrates the accuracy and feasibility of modeling emulsions as a single phase with non-Newtonian behavior.

This chapter will be structured as follows:

Firstly, the theory outlining the models of the two-phase approach will be presented. Then, the comparative study between the single-phase non-Newtonian approach and the two-phase approach will be carried out for a multistage electrical submersible pump (ESP) and will be compared to the experimental results from the literature. Finally, the comparative study will be conducted on the centrifugal volute pump (NS32) studied in the previous chapters.

5.1 Multiphase modeling methodologies

A detailed understanding of multiphase phenomena is crucial for the choice of the two-phase model which depends on the morphology of the flow (segregated, dispersed...) and on the physics which governs it. Currently, two approaches for the numerical calculation of multiphase flows exist, the Euler-Lagrange (E-L) approach and the Euler-Euler approach. In the Euler-Euler (E-E) approach, the different phases are treated mathematically as interpenetrating continua and the concept of phasic volume fraction is introduced since the volume of a phase cannot be occupied by the other phases. In the Euler-Lagrange approach, the fluid phase is treated as a continuum by solving the Navier-Stokes equations, while the dispersed phase is solved by tracking the dispersed phase particles through the calculated flow field. This chapter will not provide a comprehensive framework on the E-L approach as it is outside the purview of this study. Instead, the general concept underlying models of the E-E approach will be described.

5.1.1 VOF model

The volume of fluid (VOF) model attempts to simulate the motion of the fluid interface by tracking the motion of the phases in a single set of conservation equations for the mixture [25]. Thus, it solves a single conservation of mass and momentum equation (Equation 5.1 and Equation 5.2) [152] with an additional surface tension force (Fs) acting at the interface separating the phases.

$$\frac{\partial}{\partial t}(\rho) + \nabla \cdot (\rho \overline{\mathrm{u}}) = 0 \tag{5.1}$$

$$\frac{\partial \rho \overline{\mathbf{u}}}{\partial t} + \nabla \cdot (\rho \overline{\mathbf{u}} \otimes \overline{\mathbf{u}}) = -\nabla \cdot \bar{p}\mathbf{I} + \nabla \cdot \left(\overline{\mathbf{T}} + \mathbf{T}_{\mathrm{RANS}}\right) + \rho \mathbf{g} + \mathbf{F}_s \tag{5.2}$$

$\mathbf{T}$ and $\mathbf{T}_{\mathrm{RANS}}$ are viscous stress tensor and Reynolds stress tensor respectively. The surface force term (Fs) is given by Equation 5.3, where σ is the interfacial tension and $\kappa = -\nabla \cdot (\nabla\alpha/|\nabla\alpha|)$ is the local mean curvature of the interface [153].

$$\boldsymbol{F}_s = \sigma\kappa\nabla\alpha \tag{5.3}$$

α represents the volume fraction function defined such that $\alpha = 1$ in fluid 1 (dispersed phase) and $\alpha = 0$ in fluid 2 (continuous phase). The mixture properties, i.e density and viscosity are calculated as a function of the volume fraction, as shown in Equation 5.4 and Equation 5.5, respectively.

$$\rho = \sum_i \alpha_i \rho_i \tag{5.4}$$

$$\mu = \sum_i \alpha_i \mu_i \tag{5.5}$$

The VOF model uses a marker function (often the volume fractions) inside the control volume domain of the system to identify the different fluid phases. This model includes in addition an equation solving the interfaces given by Equation 5.6 [154].

$$\frac{\partial \alpha_i}{\partial t} + \nabla \cdot (\alpha_i \overline{\mathbf{u}}_{\text{mix}}) + \nabla \cdot [u_r \alpha_i (1 - \alpha_i)] = 0 \tag{5.6}$$

u_r is the compressive velocity counteracting numerical diffusion. Any discontinuity brought on by the lack of the other phases will be prevented if one has completely filled the control volume. This method is appropriate for inquiries that are interested in the form and fluid motion close to the interface. Although it provides superior resolution close to the interface, a dense dispersion phase greatly increases processing resources [25]. The third term in the volume fraction transport equation Equation 5.6 is a source term that reduces the solution smearing. This method is the most commonly used in the literature, but others exist.

5.1.2 Eulerian-Eulerian model

The pure Eulerian model introduces n sets of conservation equations, where n depends on the number of phases. The model describes multiphase flow as interpenetrating continua incorporating the concept of phasic volume fraction (α) [155]. With this approach, the fields of velocity and volumetric fractions are calculated individually, while the pressure field is shared between phases [156]. The continuity and momentum equations can be written as follow:

$$\frac{\partial \rho_i \alpha_i}{\partial t} + \nabla \cdot (\rho_i \alpha_i \overline{\mathbf{u}}_\mathbf{i}) = 0 \tag{5.7}$$

$$\frac{\partial \rho_i \alpha_i \overline{\mathbf{u}}_\mathbf{i}}{\partial t} + \nabla \cdot (\rho_i \alpha_i \overline{\mathbf{u}}_\mathbf{i} \otimes \overline{\mathbf{u}}_\mathbf{i}) = -\alpha_i \nabla \bar{p} + \nabla \cdot \left(\alpha_i \left(\overline{\mathbf{T}}_\mathbf{i} + \mathbf{T}_\mathbf{i}^{\text{RANS}}\right)\right) + \alpha_i \rho_i \mathbf{g} + (\mathbf{F}_\mathbf{int})_\mathbf{i} + \mathbf{M}_\mathbf{i} \tag{5.8}$$

In the above set of equation, ρ, α, and $\overline{\mathbf{u}}$ are the density, volumetric fraction, and velocity vector. $\mathbf{T}$ and $\mathbf{T}_{\text{RANS}}$ are viscous stress tensor and Reynolds stress tensor respectively. $\mathbf{M_i}$ and $(\mathbf{F_{int}})_\mathbf{i}$ represent the interfacial momentum transfer and internal forces respectively. The subscript i stands for the ith phase.

The Eulerian multiphase model is the most sophisticated multiphase flow model, because it has the strongest coupling between the continuous and dispersed phases [157]. Nonetheless, the Eulerian model is by far the most universal approach for solving multiphase flow issues [158] and is still recommended due to its general applicability for a wide range of volume fraction [100].

5.1.3 Mixture model

The mixture model is based on the single fluid approach that treats the phases as interpenetrating continua. This model solves a single set of mass-conservation and momentum equation for the mixture, given by the Equation 5.9 and Equation 5.10 respectively. It allows the phases to move at different velocities using the concept of slip velocities [159, 160].

$$\frac{\partial}{\partial t}(\rho_{mix}) + \nabla \cdot (\rho_{mix}\overline{\mathrm{u}_{mix}}) = 0 \tag{5.9}$$

$$\frac{\partial \rho_{mix}\overline{\mathbf{u}}_{mix}}{\partial t} + \nabla \cdot (\rho_{mix}\overline{\mathbf{u}}_{mix} \otimes \overline{\mathbf{u}}_{mix}) = -\nabla \cdot \bar{p}\mathbf{I} + \nabla \cdot \left(\overline{\mathbf{T}} + \mathbf{T}_{\mathrm{RANS}}\right) + \rho_{mix}\mathbf{g} + \mathbf{F} + \nabla \left(\sum_{i=1}^{n} \alpha_i \rho_i u_{\mathrm{dr},k} u_{\mathrm{dr},k} \right) \tag{5.10}$$

ρ_{mix} and u_{mix} are the the mixture density and velocity respectively, given as follow.

$$\rho_{\mathrm{mix}} = \sum_{k=1}^{n} \alpha_k \rho_k \tag{5.11}$$

$$u_{\mathrm{mix}} = \frac{\sum_{k=1}^{n} \alpha_k \rho_k u_k}{\rho_{\mathrm{m}}} \tag{5.12}$$

μ_{mix} is the viscosity of the mixture expressed as [159]:

$$\mu_{mix} = \sum_{k=1}^{n} \alpha_k \mu_k \tag{5.13}$$

F contains all the interaction forces of the related phase and $u_{\mathrm{dr},k}$ stands for the drift velocity for phase k.

This model is a good substitute for the full Eulerian multiphase model because it can perform a full multiphase simulation while solving for a smaller number of variables than the Eulerian approach and is less computationally expensive compared to the Eulerian approach. The essential approximation of this model is the local equilibrium assumption which states that the particles are accelerated instantaneously to terminal velocity. An algebraic formulation is used for the slip velocity which assumes of reaching a local equilibrium between the phases on a short spatial scale.

5.1.4 Population Balance Equation PBE

Generally, the modeling of multiphase dispersed fluids requires the assumption of uniform droplet size of the dispersed phase (as in the Eulerian-Eulerian model) which is a major simplification of the

physical state of multiphase systems. To aptly describe the different droplet sizes and the changes in the size distribution, population balance modeling (PBM) is increasingly being adopted in predicting the representative droplet size of the dispersed phase [105]. The ability of population balance modeling to consider the crucial kinetics of particle-particle interaction is one of its main features. PBM allows to better synthesize the behavior and the dynamic evolution of the discrete particle population of the dispersed phase. A system's PBE essentially serves as a count of the particles in the dispersed phase whose existence or occurrence controls the multiphase system's general behavior. These discrete elements' history is constantly dependent on birth and death processes, which cause the development of new discrete elements and the destruction of old ones in a limited or defined area [105, 102]. This model was developed at the end of the 18th century on the basis of the Boltzmann equation expressed in terms of the statistical distribution of molecules or particles in the state space. But it was in the middle of the 19th century that a general notion of population balance was first developed. The PBE coupling is only used with Eulerian-Eulerian methods, which in their initial formulation required the specification of the mean size of the dispersed phase droplets.

If we consider a particle size density function (PDF) $f(d, x, t)$, which depends on (i) internal variables d which designate the properties of the particles (droplet diameter of the dispersed phase in the case of emulsions), (ii) external variables $\vec{x}$ which correspond to the coordinates of the physical space, (iii) the time t; the general form of the PBE equation is [102, 161]:

$$\frac{\partial f(d;\vec{x},t)}{\partial t} + \vec{u}\cdot\nabla f(d;\vec{x},t) - \nabla\cdot(\Gamma_t \nabla f(d;\vec{x},t)) = S_b + S_c \tag{5.14}$$

The PDF represents the number of droplets with size range from d to d+d(d) per unit volume. $\vec{u}$ stands for the velocity and Γ_t is the effective diffusion coefficient of the number density.

S_b and S_c represent the source terms due to breakup and coalescence. Each contributes to the birth and death of a droplet, and the source terms are written as follows:

$$S(b) = B^b(d,t) - D^b(d,t) \tag{5.15}$$

$$S(c) = B^c(d,t) - D^c(d,t) \tag{5.16}$$

$B^b(d,t)$ and $D^b(d,t)$ stand for *birth* and *death* rates of a particle of diameter d caused by the *breakup* phenomenon. $B^c(d,t)$ and $D^c(d,t)$ stand for *birth* and *death* rates of a particle of diameter d caused by the *coalescence* phenomenon.

The coupling of PBE with CFD to simulate the spatially heterogeneous evolution of size distributions or mean particle size has led to the adoption of two methods of solving PBE in CFD codes: the quadrature-based method of moments (QMOM) and the method of classes [162]. The population balance equation is reformulated in the QMOM as a collection of transport equations. Integral source terms are evaluated efficiently using Gaussian quadrature and only a small number of scalar fields needs to be considered [162]. The class method takes its name from the classification of features into groups. Here, the droplet size density function is divided into intervals, over ranges of particle volumes, with each group assigned a single representative particle volume. The droplet size density function can then be integrated over any sub-interval to obtain the number concentration of particles in the corresponding size group.

5.2 Comparison of single non-Newtonian and two-phase approaches

The ability of the two CFD approaches considered to accurately predict the performance of pumps handling emulsions is evaluated in this subsection. The first part compares the numerical head values of a multistage pump (ESP) with the corresponding experimental data from the literature [30]. The second part analyzes the results obtained by both approaches for the volute centrifugal pump (NS32) studied in the previous chapters.

5.2.1 Accuracy assessment of the two numerical approaches to predict the performance of a multistage pump ESP

As a reminder, the emulsions studied in this thesis are taken from the literature [30]. The authors performed an experimental study on the rheology and characterization of emulsions (composed of different fractions of water and oil) within a multistage pump. Afterward, the authors performed a two-phase CFD study of the performance of the pump handling the oil-water mixture and the emulsions studied experimentally. In this section of the thesis, the CFD study is performed on the same multistage pump, but with a non-Newtonian single-phase approach, in order to compare the two-phase approach and the non-Newtonian single-phase approach to the experimental results and assess which approach is more accurate.

5.2.1.1 Model geometry and simulation conditions

In this case study, the performance of the multistage pump was obtained with StarCCM+ using different multiphase modeling techniques [99] and a single-phase non-Newtonian model (present work). The multistage pump is composed of four stages and operates at 3450 rpm. The outer diameter of the impellers is 78.75 mm and the outer diameter of the diffusers is 80.30 mm. Test measurements for the multistage pump performance under emulsion flow have been taken from the literature. Readers are invited to consult paper [30] for details on the pump, the experimental procedure, and the results obtained. The simulation of the pump performance under oil-water mixtures was carried out by the same authors that carried out the experimental study using multiphase approaches. For this purpose, the authors used three approaches of the two-phase model, namely the VOF model, the E-E model, and the Eulerian model coupled with the PBE. The selection of the multiphase approach was made based on the emulsion morphology (see Figure 2.1) and the CFD software STAR-CCM+ v13.04 was used for the simulations. The description of the pump geometry, the mesh generation, the physical model as well as the numerical procedure of the two-phase simulation are detailed in [99].

In the present work, only single-phase simulations with non-Newtonian rheology were conducted on the ESP and compared to two-phase simulation previously carried out. According to the results of these simulations presented in [99], an emulsion of each region (refer to section 2.1 of chapter 2) was considered for the single-phase simulations having the following compositions: 80%O-20%W, 70%O-30%W, 50%O-50%W, and 10%O-90%W. The 3-D geometrical configuration of the multistage pump used for CFD simulations is shown in Figure 5.1. The Carreau and power-law models presented in Table 3.3 of Chapter 3 are employed for non-Newtonian behavior. The same numerical simulation procedure as well as the boundary conditions presented in [113] have been adopted for this study.

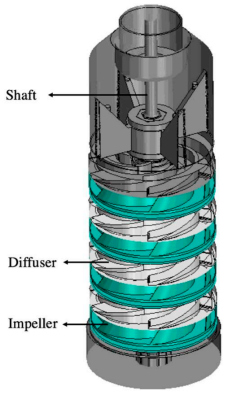

Figure 5.1: CFD model domains of the ESP [113]

5.2.1.2 Pump head

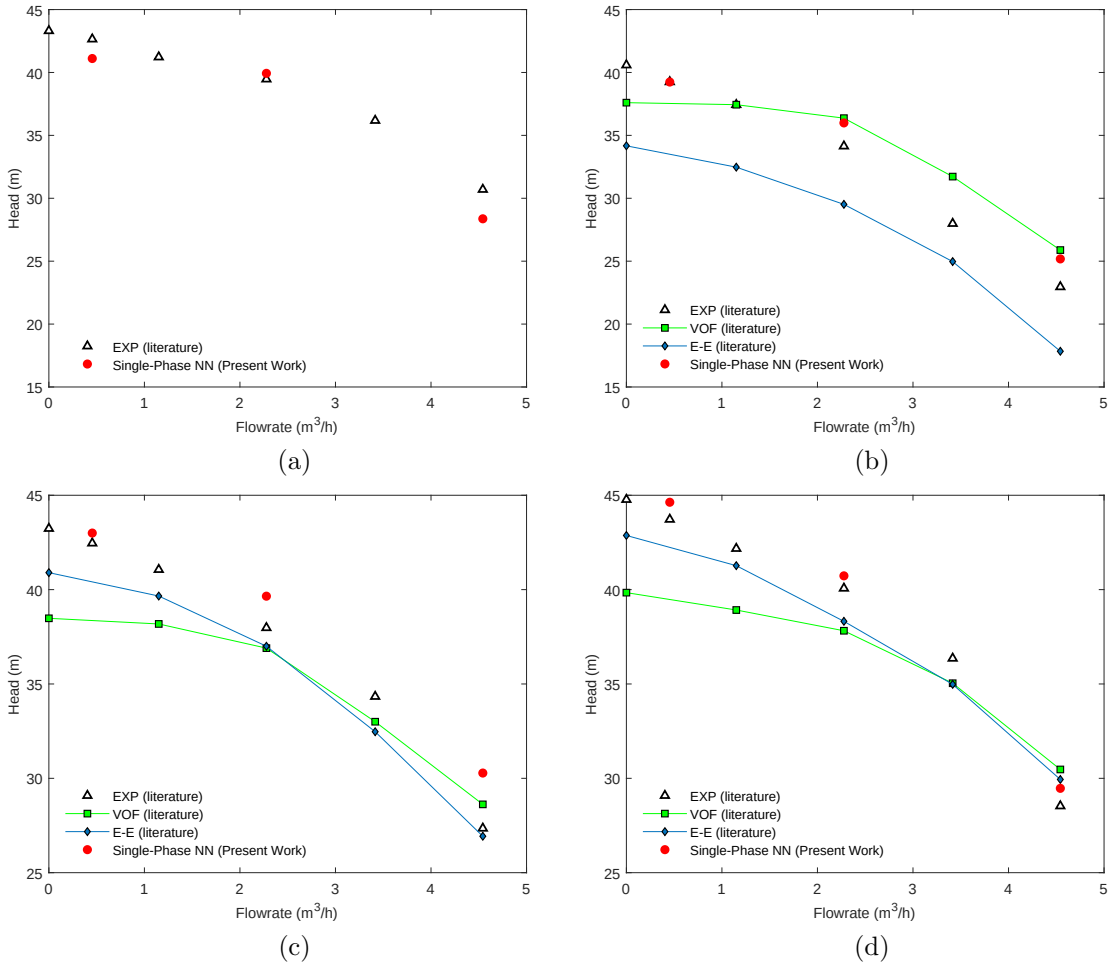

Figure 5.2: Comparison of the ESP pump head obtained by different multiphase models and the non-Newtonian single-phase model with experimental data for emulsions having oil volume fractions: (a) 80%, (b) 70%, (c) 50% and (d) 10%

Figure 5.2 compares the multistage pump head simulated using a single-phase non-Newtonian model (single-phase NN in the figures) (present work) and different two-phase models (data from [99]) with the experimental data (data from [30]). The results show the pump performance for emulsions selected from regions depicted in Figure 2.1 (chapter 2). The emulsions have the following oil volume fractions: 80%, 70%, 50%, and 10%.

For the region 1 emulsion with an oil volume fraction of 80% (Figure 5.2 (a)), the non-Newtonian single-phase model is in very good agreement with the experimental data. The model slightly underestimates the pump head, with a value ranging from 3% at low flow to 7% at high flow. Regarding the results of the two-phase simulations, the pumping head values obtained for this emulsion (i.e., 80% oil) were not reported in the reference paper [99]. However, the authors reported that the E-PBM model can approximate the experimental results with considerable accuracy for emulsions in Region 1. They indicated that the E-PBM model overestimated the pump head, and is the best-performing model compared to the VOF model.

For emulsion in region 2 having 70% oil, both the single-phase non-Newtonian model and the VOF model overestimate the pump head, with an approximate deviation of 7%. Pointing out that the single-phase non-Newtonian model approximates better the experimental data. On the other hand, the coupled two-phase E-PBM underestimates the pump performance with a difference of 13%. This emulsion has been previously shown to have the highest viscosity among oil-water mixtures and a strong shear-thinning property. Since the main losses in the single-phase model are related to the fluid's viscosity, the assumption of a non-Newtonian single-phase fluid that considers this rheology enables the numerical model to approximate better the experimental data. As the shear stress increases, the emulsion's viscosity decreases, which reduces losses and improves pump performance. In the VOF model, the properties of the two-phase system are calculated by a volume fraction average. Therefore, the model considers the average viscosity according to the volume fractions of oil and water, which contributes to the losses within the pump, along with other losses related to the interactions between the coexisting phases. The underestimation of the pump head by the E-PBM is attributed to the fact that the model does not account for the shear thinning behavior of the fluids and, as stated by Valdes et al. [99], due to the increase in the contact area between the two phases, produced by the concentrated dispersed phase fraction, the model predicts larger drag forces between the phases. The model may overestimate the interactions between the phases, which generates more losses and leads to an underestimation of the pumping head.

For emulsions in region 3 depicted in Figure 5.2 (c-d), the results of the non-Newtonian single-phase simulation are in good agreement with the experimental results. Regarding the emulsion with an oil volume fraction of 50%, the single-phase model overestimates the head by 3% at low flow rates, which increases to nearly 13% at high flow rates. Both two-phase models underestimate the pump head, except at high flow, where the VOF model overestimates it. Noting that the E-E model is more accurate than its VOF counterpart. Note that for this emulsion, the coupling between the Eulerian model and PBE has not been done since the morphology of the emulsion is multiple which makes the analysis of the particle size distribution inconsistent. Comparing the two approaches (non-Newtonian single-phase vs the E-E), the non-Newtonian model better approximates the experimental values at very low flow rates, and above a certain value, the E-E model gives better results. The shear-thinning character of this emulsion tends to reduce the pressure drop in the pump, and thus improve its performance. However, this emulsion has a low viscosity variation, as seen previously (figure 3.15). Therefore, the non-Newtonian character is not as relevant to this emulsion, and as mentioned in the reference article [99], the E-E two-phase model correctly accounts for phase interactions, such as drag forces, which better represents the physics of this

composition. In the single-phase model, we assume a virtual fluid with different physical properties, while the two-phase models include the interaction between the different phases. The latter better represents the physical character of this emulsion and the consideration of the interaction of the two phases in the simulation will be more obvious.

Considering emulsion having 10% oil, depicted in Figure 5.2 (d), the head predictions by the VOF and E-E models are very close to each other from a moderate flow rate (2.2 m^3/h) with an average deviation of 8%. At the shut-off point, the pump performance is well predicted by the E-E model compared to the VOF model. However, the single-phase non-Newtonian model gives better prediction compared to both two-phase models over the entire flow range. According to these results, the discrepancy obtained between the non-Newtonian single-phase simulation results and the experimental data decreases as the volume fraction of the dispersed phase decreases and the composition of the emulsion approaches the single-phase fluid.

To assess the effectiveness of the models in predicting the pump performance when handling emulsions, the comparison of the discrepancy obtained by the non-Newtonian single-phase simulations (present study) and those obtained by the two-phase models ([99]) with the experimental results are depicted in Figure 5.3.

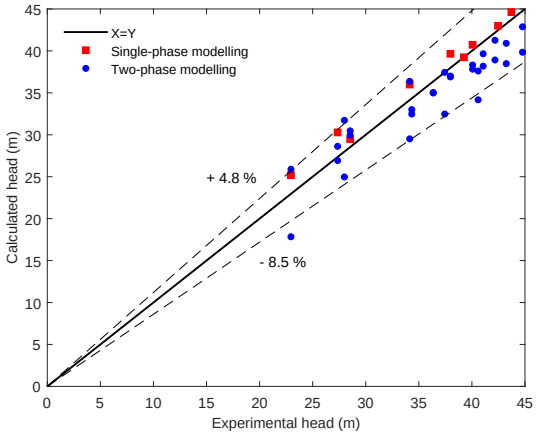

Figure 5.3: CFD versus experimental comparison of ESP pump head

The difference between the results obtained by the single-phase non-Newtonian models and the experimental data is on average 5.5%. It should be noted that the difference obtained by this model increases with increasing flow rate. The maximum error achieved corresponds to the emulsion in Region 3 at the nominal flow rate, which reached 13%. For two-phase modeling, the authors [99] reported an average deviation of 7% and 10% for the purely Eulerian/coupled PBM and VOF models, respectively. They also reported larger deviations of up to 14% for the PBM cases, particularly for Region 2.

In summary, compared to the experimental data, the coupled Eulerian-PBE model gives the most accurate results among the models for the emulsion with high dispersed phase composition (50%O-50%W). Nevertheless, the non-Newtonian single-phase model still represents an adequate estimate of the pump head. For other emulsions, with moderate to very low dispersed phase fraction (40%-10% v/v%), the single-phase non-Newtonian model performs better and gives a more accurate approximation of the pump performance. Since the two-phase models are not suitable for all emulsions, the non-Newtonian model is a very good substitute to show the behavior of emulsions in the pump and give an

approximation of its performance.

On one side, the two-phase models, and in particular the coupled E-PBM model, consider the interactions between the phases, such as coalescence and fragmentation. They are more realistic than the single-phase model in representing emulsions and dispersed oil-water fluids. In contrast, in the single-phase model, we have only a virtual fluid with appropriate rheology, which is one of the most important properties of fluids. Based on the results obtained and considering the computational efficiency of the non-Newtonian single-phase model compared to the two-phase model, which is not only time-consuming but also complicated to set up, especially regarding the emulsion closure relations, the non-Newtonian single-phase model can be recommended for applications where no prior experimental data is available and for the prediction of the overall pump performance.

5.2.1.3 Flow analysis

In this subsection, a flow field analysis is carried out to compare the flow behavior obtained with two-phase modeling and non-Newtonian single-phase modeling. The comparison is carried out for an emulsion from regions 1 and 3, while the region 2 emulsion corresponding to the phase inversion is not analyzed due to the lack of multiphase results from the reference paper [99].

Figure 5.4 - Figure 5.7 present the velocity vectors in the first and fourth stages of the impeller and diffuser of the ESP for emulsions having 50% and 80% oil volume fraction at shut-off point and BEP, respectively. The raw (a) shows the velocity vectors obtained by the single-phase non-Newtonian model and (b) the velocity vectors obtained by the two-phase model (figure from [99]).

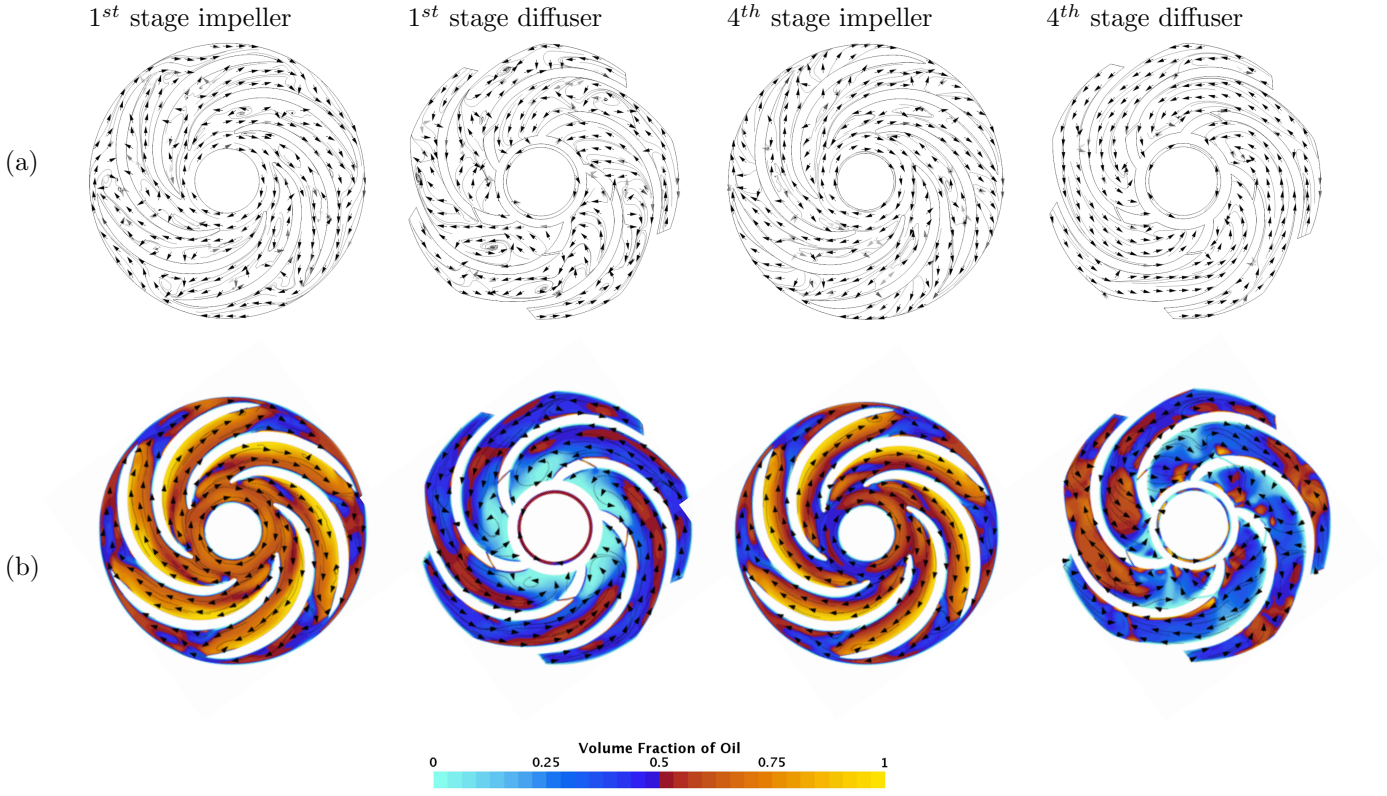

Figure 5.4: Velocity vectors and streamlines on a 0.5 span plane at the shut-off point calculated through: (a) non-Newtonian single phase model (present work) and (b) the Eulerian approach ([99]) for emulsion having 50% oil fraction.

At the shut-off point, larger recirculation regions and dead zones are obtained with the non-Newtonian single-phase model, compared to those obtained with the two-phase model. The latter are located only at the impeller outlet, whereas for the non-Newtonian model, the dead zones are located all along the impeller. These results could be attributed to the shear thinning behavior of this emulsion, where its viscosity will fluctuate and undergo changes according to the applied shear rate, influencing in return the flow pattern. For the recirculation zones that appear in Figure 5.4 (b), the authors [99] explained it by the high drag forces caused by the high concentration of the dispersed phase, which promotes the occurrence of unfavorable pressure gradients. The same flow behavior can be observed in the diffuser, large dead zones and chaotic flow are observed in both models, which are accentuated in the first stage of the diffuser and especially in the non-Newtonian modeling. In the fourth stage diffuser, a similarity can be observed between the flow behavior of the two modeling methods. The recirculation zones, located mainly at the outlet of the diffuser, are less accentuated and the flow better follows the diffuser profile.

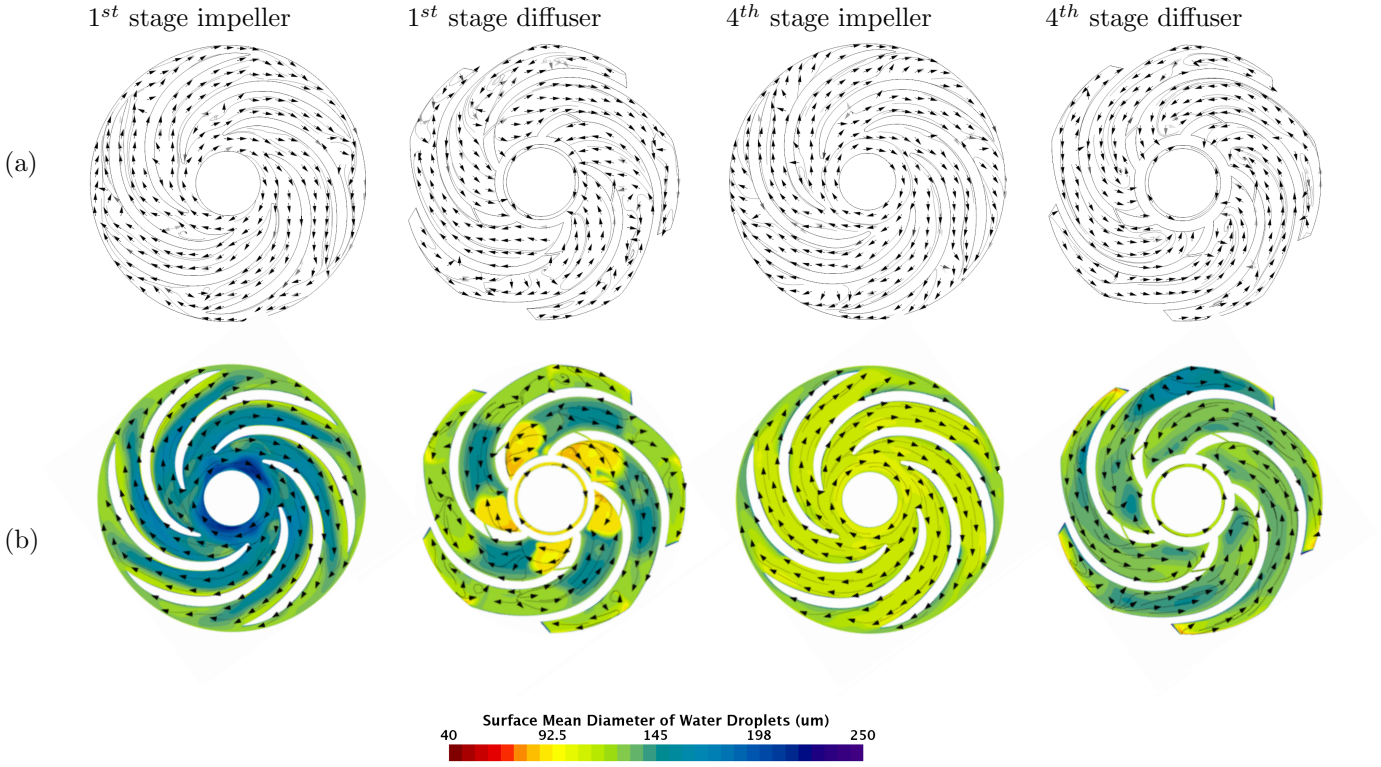

Figure 5.5: Velocity vectors and streamlines on a 0.5 span plane at the shut-off point calculated through: (a) non-Newtonian single phase model (present work) and (b) the Eulerian approach ([99]) for emulsion having 80% oil fraction.

For the emulsion with high oil concentration (80% v/voil), its flow field is represented by Figure 5.5 and Figure 5.7 at the shut-off and BEP points, respectively. The raw image (a) shows the velocity vectors obtained with the non-Newtonian single-phase modeling, while the raw image (b) corresponds to

the velocity vectors superimposed on the water droplet mean surface diameter distribution obtained by the E-PBM modeling. At low flow rates, the same observations on the flow behavior can be noted for this emulsion as for the emulsion with an oil volume fraction of 50%. Significant recirculation and vortex zones appear in the pump, which is more prominent in the non-Newtonian model than in the two-phase model, especially for the impeller.

Comparing the flow behavior between the two emulsions, one can note that the intensity of the recirculation zones is less important when increasing the oil volume fraction in the non-Newtonian model, except at the last stage diffuser. This observation is in agreement with previous results obtained for the volute centrifugal pump, where we observed that the recirculation zones decrease with increasing oil volume fraction and decreasing effective viscosity range of the emulsion. With the two-phase model, it is observed in the figures that the flow becomes less chaotic and that the vortices are less prominent in the emulsion with an oil fraction of 80% compared to the emulsion with an oil volume fraction of 50%. This is attributed to the higher concentration of the dispersed phase, which makes the contact area between the two phases larger and the drag force higher, leading to an unfavorable pressure gradient, as explained by Valdes et al [99].

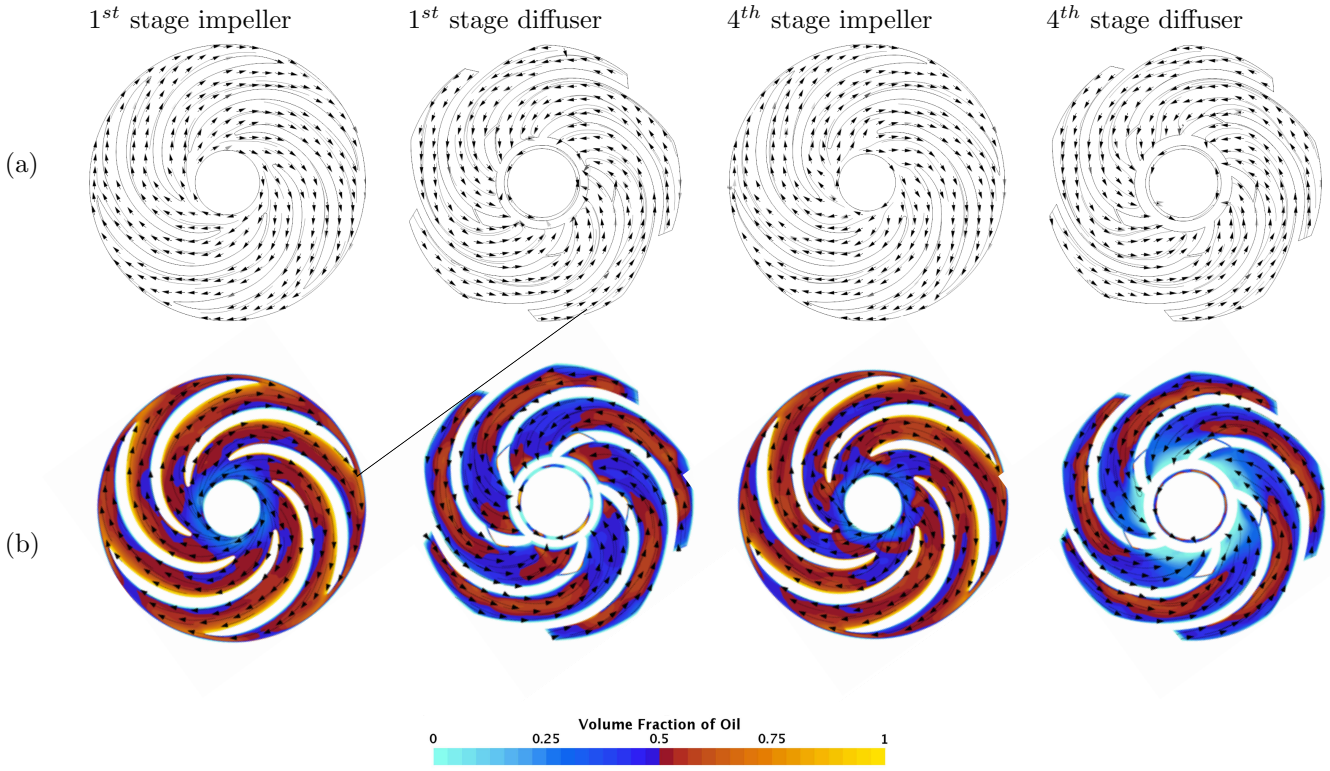

Figure 5.6: Velocity vectors and streamlines on a 0.5 span plane at the BEP calculated through: (a) non-Newtonian single phase model (present work) and (b) the Eulerian approach ([99]) for emulsion having 50% oil fraction.

At the BEP, no obvious recirculation or dead zone is observed within the pump stages for both emulsions (Figure 5.6 and Figure 5.7). In general, both modeling methods result in smooth flow inside the impellers and diffusers. However, a small area of recirculation is observed at the outlet of the fourth diffuser for both emulsions in Figure 5.6 and Figure 5.7, corresponding to the non-Newtonian behavior.

In this zone, we observe a low value of velocity, which causes an increase in the effective viscosity of the emulsion due to the tendency of shear thinning. This variation of the emulsion viscosity causes a weak pressure gradient and recirculation zones. The relative velocities at the impeller inlet obtained with the non-Newtonian modeling are relatively low for both emulsions compared to those of the partial flow, which means that impact losses are meaningless. Similarly, the hydraulic losses caused by recirculation become insignificant. The same observations can be deduced from the velocity vector directions and streamlines for two-phase modeling. At this point, the hydraulic losses decrease significantly and are dominated by frictional losses, which is consistent with the pump performance theory.

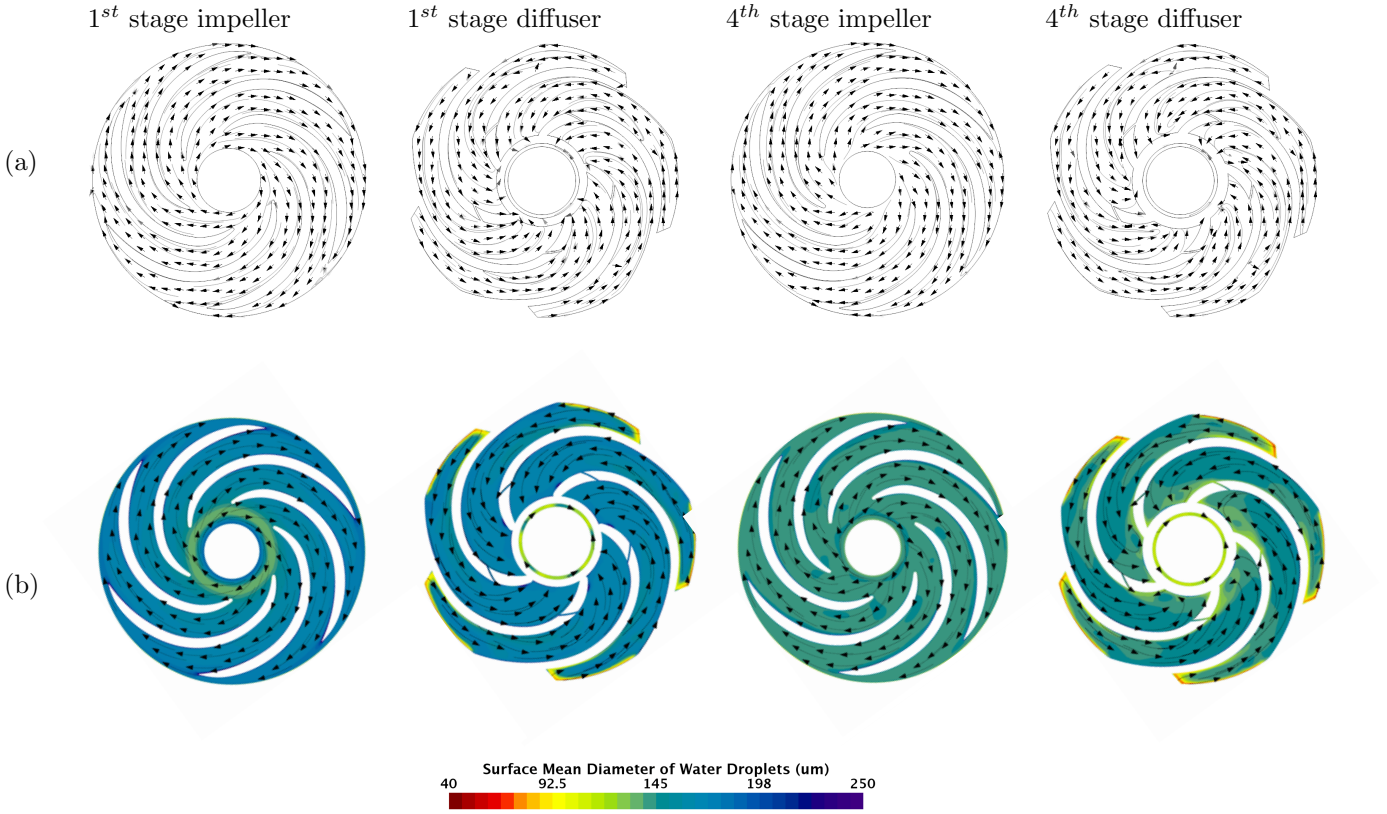

Figure 5.7: Velocity vectors and streamlines on a 0.5 span plane at the BEP calculated through: (a) non-Newtonian single phase model (present work) and (b) the Eulerian approach ([99]) for emulsion having 80% oil fraction.

In summary, the predominance of losses differs between the modeling methods since the physics governing the flow depends on the fluid properties. We have seen previously that the pump performance obtained by single-phase modeling is always superior to that obtained by two-phase modeling. From the internal flow analysis, the recirculation losses are higher in the non-Newtonian model than in the two-phase model. Therefore, it can be assumed that other losses such as friction due to drag forces and impact losses predominate over the recirculation loss and will be more important than in the non-Newtonian model. This is also evident from the additional losses governed by the interaction between the two phases associated with the two-phase model.

5.2.2 Comparison of single and two-phase approaches to predict the performance of a centrifugal volute pump (NS32)

In this subsection, the performance of the volute centrifugal pump carrying the emulsions is simulated using a two-phase model and compared to the non-Newtonian single-phase result presented in Chapter 3.

5.2.2.1 Numerical set-up

In this case study, the performance of the centrifugal pump handling emulsions was obtained using a multiphase modeling approach. For the issue being investigated, the Eulerian-Eulerian (pure Eulerian) model was applied for the URANS equations with a k-epsilon turbulence model, since it is the most general approach [163] and is more suitable for dispersed flows. The pure Eulerian modeling approach is based on ensemble-averaged mass and momentum equations governing the liquid-liquid phases, given in subsection 5.1.2. The phases are treated separately, and one set of conservation equations is solved for each phase. The flow field is assumed to be incompressible, inhomogeneous, isothermal, and without mass transfer between the phases. The dispersed phase was supposed to have a constant droplet diameter through the entire flow domain, so the change of size due to coalescence and breakup is not considered within this approach.

With this formulation, the momentum transfer between phases is duly considered. The interfacial forces related to momentum transfer of Equation 5.6 considered in this study are drag, lift, and turbulence dispersion. The drag forces, expressed by Equation 5.17, was modelled using the Schiller Naumann drag coefficient given by Equation 5.18:

$$F_D = \frac{1}{2} C_D \rho_C A \left| V_r \right| V_r \tag{5.17}$$

$$C_D = \frac{24}{Re} \left(1 + 0.15 Re^{0.687}\right) \tag{5.18}$$

$$C_D = \begin{cases} \frac{24}{Re_d} \left(1 + 0.15 Re_d^{0.687}\right) & 0 < Re_d \leq 1000 \\ 0.44 & Re_d > 1000 \end{cases} \tag{5.19}$$

C_D, ρ_c, A, and V_r stand for the drag coefficient, continuous phase density, projected area of the particle, and relative velocity between the phases respectively.

A lift force that is perpendicular to the direction of relative motion between phases acts on dispersed particles in a multiphase shear flow, mostly due to velocity gradients in the primary phase flow field. According to Drew and Lahey (1979), the force can be related to the relative velocity and the local liquid vorticity as follows [164]:

$$F_L = C_L \rho_C \left(\vec{u}_c - \vec{u}_d\right) \times \left(\nabla \times \vec{u}_d\right) \tag{5.20}$$

$$C_L = \sqrt{C_{L,\text{ low Re}}^2 + C_{\text{L, high Re}}^2} \tag{5.21}$$

$$C_{L,lowRe} = \frac{6}{\pi^2}\,\mathrm{Re}_\omega^{-0.5}\,\frac{2.55}{\left(1+0.2\frac{\mathrm{Re}_p^2}{\mathrm{Re}_\omega}\right)^{1.5}} \tag{5.22}$$

$$C_{L,highRe} = \frac{1}{2}\frac{1+16\,\mathrm{Re}_p^{-1}}{1+29\mathrm{Re}_p^{-1}} \tag{5.23}$$

$$\mathrm{Re}_p = \frac{\rho_c\,|\vec{u}_c - \vec{u}_d|\,d_p}{\mu_c} \tag{5.24}$$

$$\mathrm{Re}_\omega = \frac{\rho_c\,|\nabla \times \vec{u}_c|\,d_p^2}{\mu_c} \tag{5.25}$$

u_c and u_d are the velocity of the continuous phase and dispersed phase respectively.

The **TwoPhaseEulerFoam** solver used in this study is based on the Pressure Implicit Method for the Pressure-Linked Equations (PIMPLE) algorithm. For these two-phase simulations, the volumetric flow rate of each phase was defined as the input boundary condition, i.e., the flow rate of each phase was defined by calculating the volumetric contribution of each phase from the overall operating flow rate, assuming that the fluid is well mixed. All walls are smooth walls, with a no-slip velocity condition.

5.2.2.2 Pump head

The predicted pump characteristic, in terms of head, when handling an oil-water mixture, using Eulerian- Eulerian (E-E) model is presented in Figure 5.8. The pump head is predicted for an emulsion from each region having an oil concentration of 40%, 70%, and 80%. Several assumptions including monodispersed phase were set in this study. The results are compared to the pump head for water (presented in black triangle) and the simulated head for the same emulsion modeled as a single-phase non-Newtonian fluid exhibiting shear thinning behavior (results from Chapter 3).

As seen in Figure 5.8, a decrease in the pump head is obtained when handling emulsion compared to the pump head when handling water by both modeling methods (i.e., two-phase, and single-phase). However, the two-phase E-E model results in more degradation of the pump performance compared to the single-phase model for all emulsions.

Comparing the results obtained by the two approaches, a degradation of 21% at low flow is obtained with the E-E model, which rises to 49% at overflow for the emulsion with an oil volume fraction of 40%. On the other hand, single-phase modeling predicted a pumping head degradation ranging from 4% at low flow to 15% at overflow for the same emulsion. For the emulsion with an oil volume fraction of 70%, the Eulerian-Eulerian model predicts a pump head degradation ranging from 23% to 42% over the operating flow range. The single-phase modeling meanwhile, predicts a degradation ranging from 7% at low flow to 19% at high flow. Finally, for the Region 1 emulsion, which has an oil volume fraction of 80%, the E-E model predicts 22% degradation at low flow rates, rising to 41% at high flow rates. The non-Newtonian single-phase model predicted pump degradation ranging from 10% to 26% over the operating flow rate range.

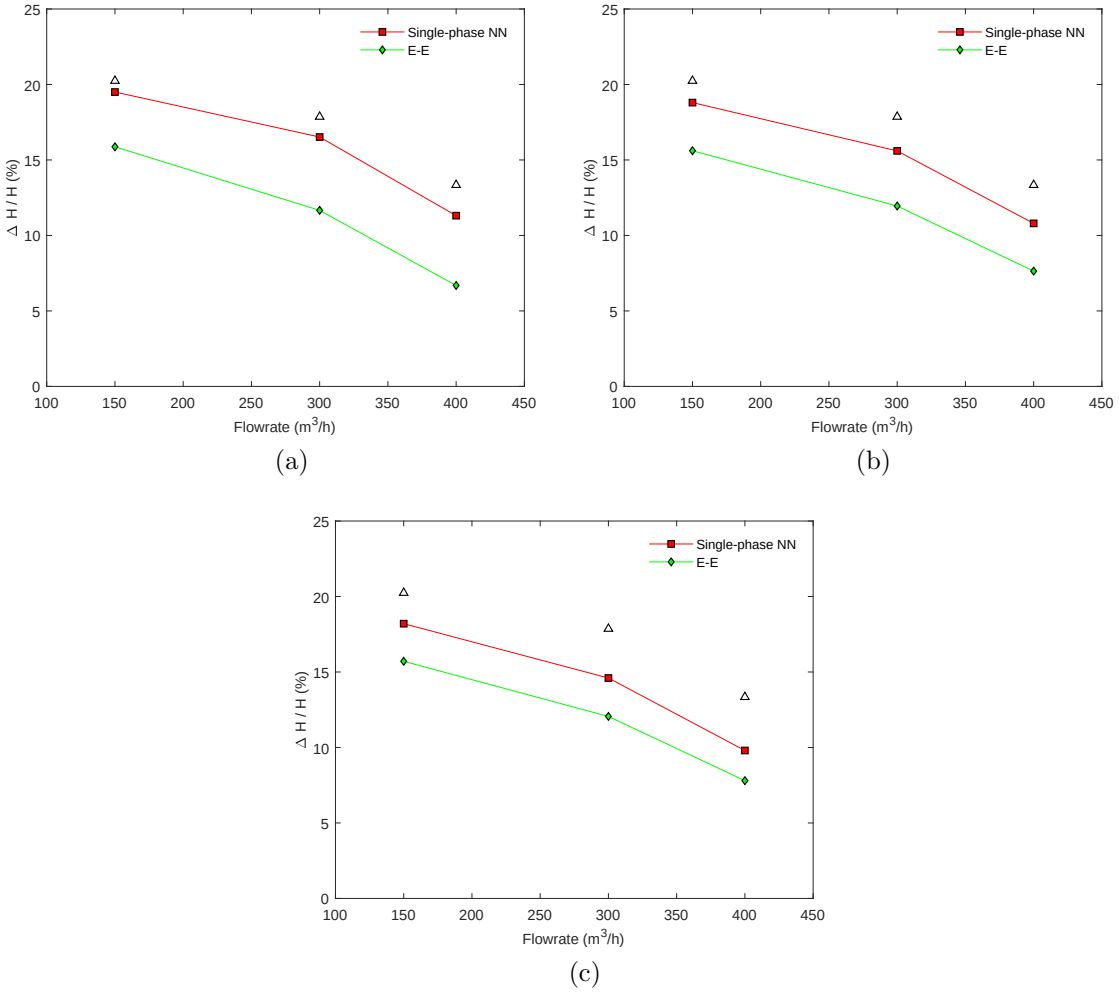

Figure 5.8: Comparison of pump head obtained by the E-E model and the non-Newtonian single-phase model for emulsion having (a) 40%, (b) 70% and (c) 80% oil volume fraction.

This higher degradation obtained by the two-phase model can be attributed to two main reasons. The first is the droplet-droplet interaction and the additional frictional effects of the coexisting phases, which the two-phase model considers compared to the single-phase model. The second is the shear-thinning behavior of the emulsion accounted for in the single-phase model, which is responsible for the performance improvement in the case of the single-phase model (as explained earlier in Chapter 3). Since this shear-thinning tendency is not accounted for by the E-E simulation, a higher head loss is expected for the emulsion. In the two-phase simulations, the main interfacial forces namely the drag, lift, and turbulent dispersion were considered. The results of the present study showed that the value of the lift force and turbulent dispersion have an insignificant effect on the pump performance relative to drag forces. This is in agreement with the results of previous studies in the literature, which suggested that lift and turbulent forces are negligible in emulsions [104]. Furthermore, two-phase numerical results showed that the simulation is quite sensitive to the initial droplet diameter value; which is reported also in the literature for gas-liquid simulations [165].

Given the lack of experimental data, no conclusion can be made on the accuracy of the two approaches. However, the relative difference between the pump head predicted by the two models is depicted in

Figure 5.9. For very low dispersed volume fractions, the numerical results obtained by both models are essentially close. The relative difference between the results of the two models varies from 10% to 26%. For higher volume fractions, the difference between the predictions of the single and two-phase models is noticeable. These results are consistent with those observed previously for the multistage pump. Furthermore, the difference between the two models increases with increasing flow rate.

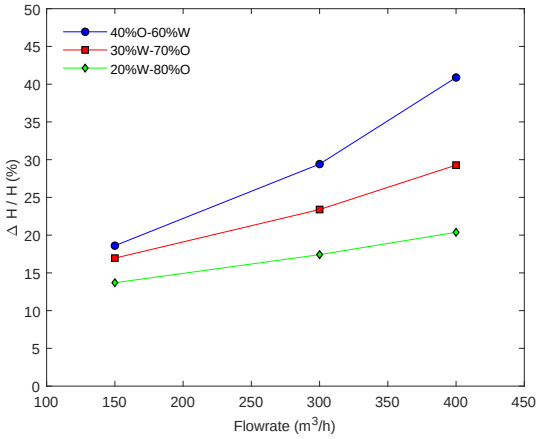

(c)

Figure 5.9: Relative difference between the pump head predicted by the two models for emulsion having (a) 40%, (b) 70% and (c) 80% oil volume fraction.

5.2.2.3 Internal flow analysis

A comparison of internal flow in the centrifugal pump obtained from the two CFD approaches is reported in this section. Figure 5.10 shows the velocity fields and streamlines in a cross-section of the impeller and volute obtained with the two modeling methods versus the flow rate. At low flow rates, recirculation zones appear in the inter-blade space of the impeller in both modeling approaches. In the case of two-phase modeling, several recirculation regions are observed at the impeller inter-blade space, compared to those obtained by single-phase modeling. This may be due to the strong pressure gradients, which are generally caused by the interfacial interactions between the two phases. Moreover, the recirculation zones appear in the inter-blade spaces before contact of the volute nozzle for the non-newtonian model. On the other hand, in the E-E two-phase model, these recirculation zones appear in the inter-blade spaces after contact of the volute nozzle. At the design flow and overflow, shown in Figure 5.10, the relative velocity streamlines are well guided through the impeller, while stagnant regions are observed primarily in the volute. The latter is more important in the case of two-phase modeling. The generation of more prominent vortices further aggravates the dispersed phase stagnation region in this part, resulting in an increased loss. The obtained flow field seems to follow the general flow principle of the centrifugal pump in both models, i.e. the magnitude of velocity increases along the blade passage and reaches the maximum at the impeller tip; recirculation zones appear in the inter-blade space at low flow rates and in the volute from the nominal flow rate.

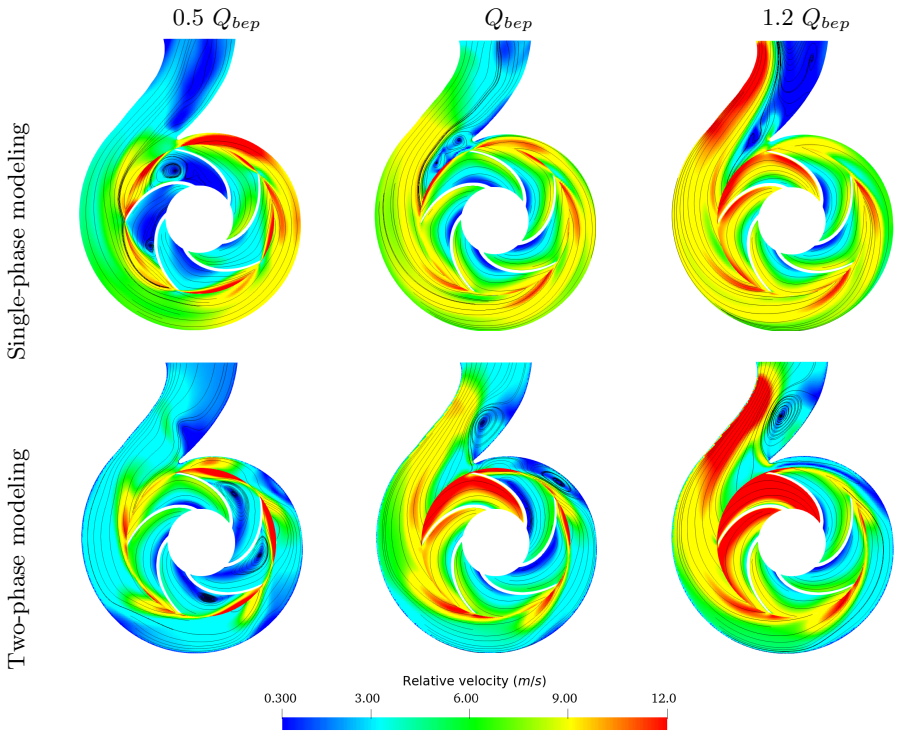

Figure 5.10: Comparison of the velocity field and streamlines obtained by the E-E model and the non-Newtonian single-phase model for the 40%O-60%W emulsion

Figure 5.11 shows the distribution of oil volume fraction on the half span of the impeller and volute. As shown in the figure, the oil phase is prone to accumulate near the pressure side of the impeller blades. However, the heterogeneity of the distribution remains relatively small. The mechanisms of oil accumulation inside rotating centrifugal pumps are caused by the force balance on oil droplets as a result of interfacial momentum transfer, wherein the drag force and turbulent dispersion force play the dominant roles.

Figure 5.11: Effect of different interphase forces on the volume fraction field of the dispersed phase of the 40%O-60%W emulsion at BEP

Conclusion

This chapter investigates the accuracy of single-phase and two-phase models in predicting pump performance under emulsion flow. The study was performed for two centrifugal pumps (ESP and NS32) and emulsions of different compositions. The validity of each model was examined based on the experimental data of the ESP pump. The results showed that for an emulsion with complex morphology (multiple emulsion), the coupled E-PBE model produced the most accurate results among the models. All models achieve almost the same degree of accuracy for emulsions in the inversion zone. The non-Newtonian single-phase model is more accurate in simulating an emulsion with simple morphology than the experimental data. In general, the two-phase models slightly underestimate the pump performance and the non-Newtonian single-phase model slightly overestimates the pump head. However, both approaches provide accurate pump performance results. The two-phase model can provide a better view of the physics of the emulsion since the two liquids are considered separately. However, the equations governing the single-phase model are less complicated and time-consuming. Therefore, single-phase modeling with the correct representation of non-Newtonian fluid behavior can be a more accurate and simpler method for predicting the performance of rotating machines under complex fluid flow conditions.

Conclusion

This thesis concerns the analysis of the hydrodynamic behavior of centrifugal volute pumps handling two-phase liquid-liquid fluids. Several methods were used in this study to investigate the behavior of the pump conveying emulsions of different compositions, namely an analytical approach, a single-phase CFD study, and a two-phase CFD study. The analytical approach used to predict the performance of the centrifugal pump is based on a mechanistic model for the determination of the viscosity of the emulsions, coupled with the model of the pressure losses inside the pump. The numerical model is based on the solution of the Navier-Stokes equations, where two models have been adopted. The first one models the emulsions as a single-phase fluid with non-Newtonian rheology and neglects the two-phase character. The second one is based on a two-phase model in which the interactions between the two phases are taken into account. Numerical predictions of the pump performance by the single-phase model and the different two-phase models are evaluated by comparison with experimental data.

The analysis of the obtained results led to the following conclusions:

- The rheological mechanistic model proposed in the literature gives a good approximation of the emulsion viscosity outside the phase inversion zone (difference less than 9%) after fitting the exponents to the experimental data. The analytical model for pump head prediction is semi-empirical and finds its limits when the fluid is highly viscous. In addition, the viscosity of the fluid is only considered in the friction loss equations, which therefore neglects the effect of the fluid rheology on the other losses.

- Pump performance progressively deteriorated as the oil volume fraction increased in the emulsion, except for the composition in the inversion zone. Despite the high effective viscosity of this composition, the strong tendency of the fluid to shear-thinning and the high shear rates of the pump resulted in a sharp viscosity decrease. Thus, the emulsion shear-thinning behavior is beneficial to the pump in some cases (e.g., the pump head obtained for this emulsion compared to that obtained for pure oil).

- The internal flow field of the centrifugal volute pump is affected by the non-Newtonian rheology, which also contributes significantly to hydraulic losses and entropy generation in pumps. Entropy generation increases significantly as the lower limit of non-Newtonian viscosity increases and energy loss occurs primarily in the impeller, regardless of pump size and flow rate. For instance, the smaller the value of ν_0, the less frictional loss the fluid will experience, and conversely, the larger the ν_∞, the less recirculation loss the fluid will experience.

- The performance degradation of a small-size pump is greater than that of a large-size pump relatively to its size. The size of the pump influences the non-Newtonian behavior of the fluid, and thus the flow structure, the magnitude, and the predominance of the losses. The small-size pump has been shown to reduce slippage when handling fluids with shear thinning behavior. However, it leads to an increase in frictional losses which results in increased performance degradation. In

addition, pump size affects losses for highly viscous emulsions, but insignificantly for water and low viscosity emulsions.

- The coupled Eulerian-PBE model gives the most accurate results than the non-Newtonian single-phase model for the emulsion with highly dispersed phase composition (50%O-50%W). Nevertheless, the non-Newtonian single-phase model still represents an adequate estimate of the pump head. For emulsions, having a moderate to very low dispersed phase fraction (40% to 10% v/v%), the single-phase non-Newtonian model performs better and gives a more precise approximation of the pump performance. Since two-phase models are not suitable for all emulsions, the non-Newtonian model is a very good alternative to show the behavior of emulsions in the pump and give an approximation of its performance. Moreover, due to the lack of a universal multiphase model for the simulation of emulsions and multiphase fluids, the single-phase model is a substitute to overcome the technological lock for the simulation of multiphase fluids, where the two-phase approach finds its limits.

The present work and the results suggest many perspectives.

- First, regarding the analytical analysis, the losses comparison between the numerical solution and analytical models yields more possible future work. It has been seen that some losses determined from CFD depend on the viscosity of the fluid (e.g., impact losses or slippage), and that their analytical counterpart does not consider. Therefore, an improvement of the loss models is needed where the viscosity of the fluid is considered by replacing the empirical factors that appear in the loss models with correlations that depend on the rheology of the fluid and the operating conditions of the pump, in order to universalize the correlations and to allow the analysis of a larger number of pumps and fluids with the same equation. Therefore, future work can focus on improving the pump's internal losses.

- Conduct experimental studies on two-phase oil-water systems with different compositions in a volute centrifugal pump and assess the influence of the mixtures on the pump performance and investigate the behavior and rheology of the emulsions.

- Carry out experimental studies on the centrifugal volute pump with stable emulsion systems, considering multiple surfactants and assessing the influence of the emulsion's stability in the rheological properties and the pump's performance.

- Achieve a better understating of the inversion phenomenon within volute centrifugal pumps for both stable and unstable emulsions through experiments and CFD modeling.

- Study multimodal distribution models that better represent the DSD within centrifugal pumps, which are implemented in CFD codes through PBM to better model the emulsion numerically.

- Investigate mechanistic models that predict final average and maximum droplet sizes, taking into account the effects of turbulence and shear to determine a relationship between droplet size and pump operating conditions.

- Study the effect of temperature simultaneously with the operating conditions of the pump on the rheological properties of the emulsions and their influence on the mesoscopic plane.

- Conduct a visualization study on phase regimes developed when changing the phase composition of the emulsion in the volute pump.
- Propose and develop computational models which can account for the emulsion's rheology and non-Newtonian characteristics in turbulent regimes together with / or depending on the two-phase character and the different interactions between the phases.

Bibliography

[1] A. A. Umar, I. B. M. Saaid, A. A. Sulaimon, and R. B. M. Pilus, "A review of petroleum emulsions and recent progress on water-in-crude oil emulsions stabilized by natural surfactants and solids," *Journal of Petroleum Science and Engineering*, vol. 165, pp. 673–690, 2018. [Online]. Available: https://doi.org/10.1016/j.petrol.2018.03.014

[2] M. Khalil, S. Kassab, A. Ismail, and I. Elazab, "Centrifugal pump performance under stable and unstable oil-water emulsions flow," *Twelfth International Water Technology Conference*, no. January, pp. 687–702, 2008. [Online]. Available: http://scholar.google.com/scholar?hl=en{&}btnG=Search{&}q=intitle:CENTRIFUGAL+PUMP+PERFORMANCE+UNDER+STABLE+AND+UNSTABLE+OIL-WATER+EMULSIONS+FLOW{#}0

[3] N. A. V. Bulgarelli, J. L. Biazussi, W. Monte Verde, C. E. Perles, M. S. de Castro, and A. C. Bannwart, "A novel criterion based on slip ratio to assess the flow behavior of W/O emulsions within centrifugal pumps," *Chemical Engineering Science*, vol. 247, p. 117050, 2022. [Online]. Available: https://doi.org/10.1016/j.ces.2021.117050

[4] J. C. Vielma, "Rheological behavior of oil-water dispersion flow in horizontal pipes," Ph.D. dissertation, Citeseer, 2006.

[5] J. Plasencia, B. Pettersen, and O. Jørgen, "Pipe flow of water-in-crude oil emulsions : Effective viscosity , inversion point and droplet size distribution," *Journal of Petroleum Science and Engineering*, vol. 101, pp. 35–43, 2013. [Online]. Available: http://dx.doi.org/10.1016/j.petrol.2012.11.009

[6] M. F. Ali and M. H. Alqam, "Role of asphaltenes, resins and other solids in the stabilization of water in oil emulsions and its effects on oil production in Saudi oil fields," *Fuel*, vol. 79, no. 11, pp. 1309–1316, 2000.

[7] N. Aske, H. Kallevik, and J. Sjöblom, "Water-in-crude oil emulsion stability studied by critical electric field measurements. Correlation to physico-chemical parameters and near-infrared spectroscopy," *Journal of Petroleum Science and Engineering*, vol. 36, no. 1-2, pp. 1–17, 2002.

[8] S. Kokal, "Crude-oil emulsions: A state-of-the-art review," pp. 5–12, 2005.

[9] E. M. Ofuchi, J. M. Cubas, H. Stel, R. Dunaiski, T. S. Vieira, and R. E. Morales, "A new model to predict the head degradation of centrifugal pumps handling highly viscous flows," *Journal of Petroleum Science and Engineering*, vol. 187, no. May 2019, p. 106737, 2020. [Online]. Available: https://doi.org/10.1016/j.petrol.2019.106737

[10] M. Zhang, R. Dabirian, R. S. Mohan, and O. Shoham, "Effect of Shear and Water Cut on Phase Inversion and Droplet Size Distribution in Oil-Water Flow," *Journal of Energy Resources Technology, Transactions of the ASME*, vol. 141, no. 3, pp. 1–9, 2019.

[11] S. A. Bellary, M. H. Siddique, A. Samad, J. S. Sangwai, and B. Chon, "Effects of crude oil-water emulsions at various water-cut on the performance of the centrifugal pump," *International Journal of Oil, Gas and Coal Technology*, vol. 16, no. 1, pp. 71–88, 2017.

[12] D. Croce and E. Pereyra, "Study of oil/water flow and emulsion formation in electrical submersible pumps," *SPE Production and Operations*, vol. 35, no. 1, pp. 26–36, 2019.

[13] M. T. Ghannam, "Water-in-crude oil emulsion stability investigation," *Petroleum Science and Technology*, vol. 23, no. 5-6, pp. 649–667, 2005.

[14] Q. Zhu, Y. Pan, X. Jia, J. Li, M. Zhang, and L. Yin, "Review on the Stability Mechanism and Application of Water-in-Oil Emulsions Encapsulating Various Additives," pp. 1660–1675, 2019.

[15] Sweeta Akbari and Abdurahman Hamid Nour, "Emulsion types, stability mechanisms and rheology: A review," *International Journal of Innovative Research and Scientific Studies*, vol. 1, no. 1, pp. 14–21, 2018.

[16] F. Y. Ushikubo and R. L. Cunha, "Stability mechanisms of liquid water-in-oil emulsions," *Food Hydrocolloids*, vol. 34, pp. 145–153, 2014. [Online]. Available: http://dx.doi.org/10.1016/j.foodhyd.2012.11.016

[17] S. R. Derkach, "Rheology of emulsions," *Advances in Colloid and Interface Science*, vol. 151, no. 1-2, pp. 1–23, 2009. [Online]. Available: http://dx.doi.org/10.1016/j.cis.2009.07.001

[18] S. A. Raya, I. Mohd Saaid, A. Abbas Ahmed, and A. Abubakar Umar, "A critical review of development and demulsification mechanisms of crude oil emulsion in the petroleum industry," *Journal of Petroleum Exploration and Production Technology*, vol. 10, no. 4, pp. 1711–1728, 2020. [Online]. Available: https://doi.org/10.1007/s13202-020-00830-7

[19] D. P. Ortiz, E. N. Baydak, and H. W. Yarranton, "Effect of surfactants on interfacial films and stability of water-in-oil emulsions stabilized by asphaltenes," *Journal of Colloid and Interface Science*, vol. 351, no. 2, pp. 542–555, 2010. [Online]. Available: http://dx.doi.org/10.1016/j.jcis.2010.08.032

[20] R. Morales, E. Pereyra, S. Wang, and O. Shoham, "Droplet formation through centrifugal pumps for oil-in-water dispersions," *SPE Journal*, vol. 18, no. 1, pp. 172–178, 2013.

[21] A. Y. Tjoeng and R. Loro, "Viscosity modelling of pyrenees crude oil emulsions," *Society of Petroleum Engineers - SPE Asia Pacific Oil and Gas Conference and Exhibition 2016*, no. October, pp. 25–27, 2016.

[22] A. Mosayebi and R. Abedini, "Using demulsifiers for phase breaking of water/oil emulsion," *Petroleum and Coal*, vol. 55, no. 1, pp. 26–30, 2013.

[23] L. Barrios, M. Rojas, G. Monteiro, and N. Sleight, "Brazil field experience of ESP performance with viscous emulsions and high gas using multi-vane pump MVP and high power ESPs," *Society of Petroleum Engineers - SPE Electric Submersible Pump Symposium 2017*, no. July 2009, pp. 38–48, 2017.

[24] N. Brauner and A. Ullmann, "Modeling of phase inversion phenomenon in two-phase pipe flows," *International Journal of Multiphase Flow*, vol. 28, no. 7, pp. 1177–1204, 2002.

[25] K. Ngan, "Phase Inversion in dispersed liquid-liquid pipe flow," *Chemical Engineering*, no. October, pp. 1 – 232, 2010.

[26] J. Hapanowicz, "Phase inversion in liquid-liquid pipe flow," *Flow Measurement and Instrumentation*, vol. 21, no. 3, pp. 284–291, 2010. [Online]. Available: http://dx.doi.org/10.1016/j.flowmeasinst.2010.03.001

[27] B. Hu, P. Angeli, O. K. Matar, and G. F. Hewitt, "Prediction of phase inversion in agitated vessels using a two-region model," *Chemical Engineering Science*, vol. 60, no. 13, pp. 3487–3495, 2005.

[28] B. Yaqob, "EXPERIMENTALLY INVESTIGATION THE EFFECT OF OIL-WATER PHASE," no. July 2011, 2017.

[29] N. A. V. Bulgarelli, J. L. Biazussi, M. S. De Castro, W. M. Verde, and A. C. Bannwart, "Experimental study of phase inversion phenomena in electrical submersible pumps under oil water flow," *Proceedings of the International Conference on Offshore Mechanics and Arctic Engineering - OMAE*, vol. 8, pp. 1–8, 2017.

[30] J. P. Valdés, M. Asuaje, and N. Ratkovich, "Study of an ESP's performance handling liquid-liquid flow and unstable O-W emulsions Part I: Experimental," *Chemical Engineering Science*, vol. 223, 2020.

[31] H. Banjar and H. Q. Zhang, "Experiments and emulsion rheology modeling in an electric submersible pump," *International Petroleum Technology Conference 2019, IPTC 2019*, 2019.

[32] J. M. Maffi, G. R. Meira, and D. A. Estenoz, "Mechanisms and conditions that affect phase inversion processes: A review," *Canadian Journal of Chemical Engineering*, vol. 99, no. 1, pp. 178–208, 2021.

[33] A. Kumar, S. Li, C. M. Cheng, and D. Lee, "Recent Developments in Phase Inversion Emulsification," *Industrial and Engineering Chemistry Research*, vol. 54, no. 34, pp. 8375–8396, 2015.

[34] N. A. V. Bulgarelli, J. L. Biazussi, W. Monte Verde, C. E. Perles, M. S. de Castro, and A. C. Bannwart, "Experimental investigation on the performance of Electrical Submersible Pump (ESP) operating with unstable water/oil emulsions," *Journal of Petroleum Science and Engineering*, vol. 197, p. 107900, 2021. [Online]. Available: https://doi.org/10.1016/j.petrol.2020.107900

[35] L. Prieto, A. Pinilla, D. Becerra, P. Pico, J. P. Valdes, E. Pereyra, and N. Ratkovich, "Phase inversion correlations analysis for oil–water flow in horizontal pipes," *Industrial & Engineering Chemistry Research*, vol. 58, no. 31, pp. 14 436–14 445, 2019.

[36] M. Nädler and D. Mewes, "Flow induced emulsification in the flow of two immiscible liquids in horizontal pipes," *International journal of multiphase flow*, vol. 23, no. 1, pp. 55–68, 1997.

[37] I. K. Hong, S. I. Kim, and S. B. Lee, "Effects of hlb value on oil-in-water emulsions: Droplet size, rheological behavior, zeta-potential, and creaming index," *Journal of industrial and engineering chemistry*, vol. 67, pp. 123–131, 2018.

[38] S. Tcholakova, N. D. Denkov, and T. Danner, "Role of surfactant type and concentration for the mean drop size during emulsification in turbulent flow," *Langmuir*, vol. 20, no. 18, pp. 7444–7458, 2004.

[39] D. P. de Moraes, F. G. Antes, J. S. Pereira, M. d. F. P. dos Santos, R. C. Guimaraes, J. S. Barin, M. F. Mesko, J. N. Paniz, and E. M. Flores, "Microwave-assisted procedure for salinity evaluation of heavy crude oil emulsions," *Energy & Fuels*, vol. 24, no. 4, pp. 2227–2232, 2010.

[40] Y. Zhou, D. Yin, W. Chen, B. Liu, and X. Zhang, "A comprehensive review of emulsion and its field application for enhanced oil recovery," pp. 1046–1058, 2019.

[41] F. Goodarzi and S. Zendehboudi, "A Comprehensive Review on Emulsions and Emulsion Stability in Chemical and Energy Industries," *Canadian Journal of Chemical Engineering*, vol. 97, no. 1, pp. 281–309, 2019.

[42] L. Achour, M. Specklin, I. Belaidi, and S. Kouidri, "Numerical Assessment of the Hydrodynamic Behavior of a Volute Centrifugal Pump Handling Emulsion," *Entropy*, vol. 24, no. 2, 2022.

[43] A. Einstein, "Eine neue bestimmung der moleküldimensionen," Ph.D. dissertation, ETH Zurich, 1905.

[44] G. I. Taylor, "The viscosity of a fluid containing small drops of another fluid," *Proceedings of the Royal Society of London. Series A, Containing Papers of a Mathematical and Physical Character*, vol. 138, no. 834, pp. 41–48, 1932.

[45] H. C. Brinkman, "The viscosity of concentrated suspensions and solutions," *The Journal of chemical physics*, vol. 20, no. 4, pp. 571–571, 1952.

[46] H. P. Ronningsen, "Correlations for predicting viscosity of w/o-emulsions based on north sea crude oils," in *SPE International Symposium on Oilfield Chemistry*. OnePetro, 1995.

[47] R. Pal, "A novel method to correlate emulsion viscosity data," *Colloids and Surfaces A: Physicochemical and Engineering Aspects*, vol. 137, no. 1-3, pp. 275–286, 1998.

[48] R. Pal, "Viscosity–concentration equation for emulsions of nearly spherical droplets," *Journal of colloid and interface science*, vol. 231, no. 1, pp. 168–175, 2000.

[49] D. Dan and G. Jing, "Apparent viscosity prediction of non-Newtonian water-in-crude oil emulsions," *Journal of Petroleum Science and Engineering*, vol. 53, no. 1-2, pp. 113–122, 2006.

[50] J. Guo, Y. Yang, D. Zhang, W. Wu, Z. Yang, and L. He, "A general model for predicting apparent viscosity of crude oil or emulsion in laminar pipeline at high pressures," *Journal of Petroleum Science and Engineering*, vol. 160, pp. 12–23, 2018.

[51] W. P. Do Carmo, M. K. Lenzi, E. K. Lenzi, M. Fortuny, and A. F. Santos, "A fractional model to relative viscosity prediction of water-in-crude oil emulsions," *Journal of Petroleum Science and Engineering*, vol. 172, pp. 493–501, 2019.

[52] J. Zhu, H. Zhu, G. Cao, H. Banjar, J. Peng, Q. Zhao, and H. Q. Zhang, "A new mechanistic model for oil-water emulsion rheology and boosting pressure prediction in electrical submersible pumps ESP," *Proceedings - SPE Annual Technical Conference and Exhibition*, vol. 2019-Septe, no. January, 2019.

[53] N. A. V. Bulgarelli, J. L. Biazussi, W. Monte Verde, C. E. Perles, M. S. de Castro, and A. C. Bannwart, "Relative viscosity model for oil/water stable emulsion flow within electrical submersible pumps," *Chemical Engineering Science*, vol. 245, p. 116827, 2021. [Online]. Available: https://doi.org/10.1016/j.ces.2021.116827

[54] D. Wang and L. S. Fan, *Particle characterization and behavior relevant to fluidized bed combustion and gasification systems*, 2013.

[55] R. Clift, J. R. Grace, and M. E. Weber, "Bubbles, drops, and particles," 2005.

[56] R. M. Perissinotto, W. Monte Verde, J. L. Biazussi, N. A. V. Bulgarelli, W. D. P. Fonseca, M. S. de Castro, E. d. M. Franklin, and A. C. Bannwart, "Flow visualization in centrifugal pumps: A review of methods and experimental studies," *Journal of Petroleum Science and Engineering*, vol. 203, no. January, p. 108582, 2021. [Online]. Available: https://doi.org/10.1016/j.petrol.2021.108582

[57] R. M. Perissinotto, W. Monte Verde, C. E. Perles, J. L. Biazussi, M. S. de Castro, A. C. Bannwart, R. Marcilli, W. Monte, C. Eduardo, J. Luiz, M. Souza, D. Castro, and A. Carlos, "Experimental analysis on the behavior of water drops dispersed in oil within a centrifugal pump impeller," *Experimental Thermal and Fluid Science*, vol. 112, no. August 2019, p. 109969, 2020. [Online]. Available: https://doi.org/10.1016/j.expthermflusci.2019.109969

[58] R. M. Perissinotto, W. Monte Verde, M. S. de Castro, J. L. Biazussi, V. Estevam, and A. C. Bannwart, "Experimental investigation of oil drops behavior in dispersed oil-water two-phase flow within a centrifugal pump impeller," *Experimental Thermal and Fluid Science*, vol. 105, no. February, pp. 11–26, 2019. [Online]. Available: https://doi.org/10.1016/j.expthermflusci.2019.03.009

[59] R. M. Perissinotto, W. Monte Verde, M. Gallassi, G. F. N. Gonçalves, M. S. de Castro, J. Carneiro, J. L. Biazussi, A. C. Bannwart, W. M. Verde, M. Gallassi, G. F. N. Gonçalves, M. Souza, D. Castro, J. Carneiro, J. Luiz, and A. Carlos, "Experimental and numerical study of oil drop motion within an ESP impeller," *Journal of Petroleum Science and Engineering*, vol. 175, no. July 2018, pp. 881–895, 2019. [Online]. Available: https://doi.org/10.1016/j.petrol.2019.01.025

[60] E. Michaelides, *Particles, bubbles & drops: their motion, heat and mass transfer*. World Scientific, 2006.

[61] J. N. Carneiro, A. Patil, S. T. Johansen, G. F. Gonçalves, and M. Gallassi, *Drop Breakup and Size Evolution in Oil and Gas Production: A Review of Models and Mechanisms*, 2018.

[62] R. M. Perissinotto, W. M. Verde, J. L. Biazussi, M. S. de Castro, and A. C. Bannwart, "Experimental analysis on the velocity of oil drops in oil-water two-phase flows in electrical submersible pump impellers," *Journal of Offshore Mechanics and Arctic Engineering*, vol. 141, no. 4, 2019.

[63] P. Schmitt, M. W. Hlawitschka, and H. J. Bart, "Centrifugal Pumps as Extractors," *Chemie-Ingenieur-Technik*, vol. 92, no. 5, pp. 589–594, 2020.

[64] J. O. Hinze, "Fundamentals of the hydrodynamic mechanism of splitting in dispersion processes," *AIChE Journal*, vol. 1, no. 3, pp. 289–295, 1955.

[65] S. N. Kale and S. L. Deore, "Emulsion Micro Emulsion and Nano Emulsion : A Review," vol. 8, no. 1, pp. 39–47, 2017.

[66] A. Morozova and A. Eskin, "Centrifugal Pump Effect on Average Particle Diameter of Oil-Water Emulsion," *IOP Conference Series: Materials Science and Engineering*, vol. 262, no. 1, 2017.

[67] M. Zhang, R. Dabirian, R. Mohan, O. Shoham, and S. Wang, "Effect of gear-pump shear rate on oil/water dispersion," *SPE Production and Operations*, vol. 34, no. 3, pp. 536–550, 2019.

[68] M. Zhang, S. Wang, R. S. Mohan, O. Shoham, and H. Gao, "Shear Effects of Gear Pump on Oil-Water Flow," pp. 18–20, 2015.

[69] A. W. Nienow, "Break-up, coalescence and catastrophic phase inversion in turbulent contactors," *Advances in Colloid and Interface Science*, vol. 108-109, pp. 95–103, 2004.

[70] R. Mohan, "Evaluation of Models for Droplet Shear Effect," no. 1949, pp. 1–11, 2018.

[71] S. Y. Ibrahim and I. E. Maloka, "Emulsification of secondary oil/water dispersions using a centrifugal pump," *Petroleum Science and Technology*, vol. 24, no. 5, pp. 513–522, 2006.

[72] P. B. Kowalczuk and J. Drzymala, "Physical meaning of the Sauter mean diameter of spherical particulate matter," *Particulate Science and Technology*, vol. 34, no. 6, pp. 645–647, 2016.

[73] N. A. Vieira Bulgarelli, "Experimental Study of Electrical Submersible Pump (ESP) Operating with Water / Oil Emulsion Estudo Experimental de Bomba Centrífuga Submersa (BCS) Operando com Emulsão Água / Óleo Experimental Study of Electrical Submersible Pump (ESP) Operating wit," p. 135, 2018.

[74] C. Vasquez, E. Pereyra, and K. Sambath, "Analysis and review of fluid-particle-size predictive models for pipe flow," *SPE Production and Operations*, vol. 34, no. 4, pp. 781–798, 2019.

[75] D. Moura, "EXPERIMENTAL STUDY OF WATER-OIL TWO-PHASE FLOW IN AN 8-STAGE ELECTRICAL SUBMERSIBLE PUMP," 2016.

[76] S. W. Lee and H. C. No, "Droplet size prediction model based on the upper limit log-normal distribution function in venturi scrubber," *Nuclear Engineering and Technology*, vol. 51, no. 5, pp. 1261–1271, 2019. [Online]. Available: https://doi.org/10.1016/j.net.2019.03.014

[77] A. Rajapakse, "Drop Size Distributions and Interfacial Area in Reactive Liquid-Liquid Dispersions," no. May, pp. 1–15, 2007.

[78] V. G. Levich and C. W. Tobias, "Physicochemical hydrodynamics," *Journal of The Electrochemical Society*, vol. 110, no. 11, p. 251C, 1963.

[79] J. T. Davies, "Drop sizes of emulsions related to turbulent energy dissipation rates," *Chemical Engineering Science*, vol. 40, no. 5, pp. 839–842, 1985.

[80] C. Desnoyer, O. Masbernat, and C. Gourdon, "Experimental study of drop size distributions at high phase ratio in liquid-liquid dispersions," *Chemical Engineering Science*, vol. 58, no. 7, pp. 1353–1363, 2003.

[81] E. J. Pereyra, *Modeling of integrated Compact Multiphase Separation System(CMSS (c))*, 2011, vol. 72, no. 07.

[82] B. Sajjadi, A. A. A. Raman, R. S. S. R. E. Shah, and S. Ibrahim, "Review on Applicable breakup/coalescence models in turbulent liquid-liquid flows," *Reviews in Chemical Engineering*, vol. 29, no. 3, pp. 131–158, 2013.

[83] W. G. Li, "A method for analyzing the performance of centrifugal oil pumps," *Journal of Fluids Engineering, Transactions of the ASME*, vol. 126, no. 3, pp. 482–485, 2004.

[84] KSB, "Régulation de pompes / Automatisation de pompes," vol. 4, 2009. [Online]. Available: http://www.ksb.com/linkableblob/ksb-fr/998936-38292/data/Savoir-faire{_}Automatisation-{_}regulation{_}12-data.pdf

[85] J. F. Gülich, "Pumping highly viscous fluids with centrifugal pumps - Part 1," *World Pumps*, vol. 1999, no. 395, pp. 30–34, 1999.

[86] H. Institute, "Effects of liquid viscosity on rotodynamic (centrifugal and vertical) pump performance," *ANSI-HI 9.6. 7-2010*, 2010.

[87] M. Asuaje, F. Bakir, S. Kouidri, F. Kenyery, and R. Rey, "Numerical Modelization of the Flow in Centrifugal Pump: Volute Influence in Velocity and Pressure Fields," *International Journal of Rotating Machinery*, vol. 2005, no. 3, pp. 244–255, 2005.

[88] M. A. El-Naggar, "A one-dimensional flow analysis for the prediction of centrifugal pump performance characteristics," *International Journal of Rotating Machinery*, vol. 2013, 2013.

[89] T. S. Vieira, J. R. Siqueira, A. D. Bueno, R. E. Morales, and V. Estevam, "Analytical study of pressure losses and fluid viscosity effects on pump performance during monophase flow inside an ESP stage," *Journal of Petroleum Science and Engineering*, vol. 127, pp. 245–258, 2015. [Online]. Available: http://dx.doi.org/10.1016/j.petrol.2015.01.014

[90] J. Zhu, H. Zhu, G. Cao, J. Zhang, J. Peng, H. Banjar, and H. Q. Zhang, "A new mechanistic model to predict boosting pressure of electrical submersible pumps ESPs under high-viscosity fluid flow with validations by experimental data," *Society of Petroleum Engineers - SPE Gulf Coast Section Electric Submersible Pumps Symposium 2019, ESP 2019*, no. January, 2019.

[91] H. M. Banjar, *Experiments, CFD simulation and modeling of oil viscosity and emulsion effects on ESP performance.* The University of Tulsa, 2018.

[92] G. H. Yeoh and J. Tu, *Computational techniques for multiphase flows.* Butterworth-Heinemann, 2019.

[93] G. H. Yeoh, C. P. Cheung, and J. Tu, *Multiphase flow analysis using population balance modeling: bubbles, drops and particles.* Butterworth-Heinemann, 2013.

[94] A. M. Shuard, H. B. Mahmud, and A. J. King, "Comparison of two-phase pipe flow in openFOAM with a mechanistic model," *IOP Conference Series: Materials Science and Engineering*, vol. 121, no. 1, 2016.

[95] H. Pouraria, J. K. Seo, and J. K. Paik, "Numerical modelling of two-phase oil-water flow patterns in a subsea pipeline," *Ocean Engineering*, vol. 115, pp. 135–148, 2016. [Online]. Available: http://dx.doi.org/10.1016/j.oceaneng.2016.02.007

[96] S. Subramaniam, "Lagrangian-Eulerian methods for multiphase flows," *Progress in Energy and Combustion Science*, vol. 39, no. 2-3, pp. 215–245, 2013.

[97] C. Wei, C. Williams Kenneth, and G. Jones Mark, "Application of neumerical modelling in pneumatic conveying," *Pneumatic conveying design guide*, vol. 3, pp. 521–552, 2016.

[98] D. Becerra, D. Rozo, J. P. Valdés, M. Asuaje, and N. Ratkovich, "Experimental and CFD study of an Electrical Submersible Pump's (ESP) operating under Two-Phase Liquid-Liquid Flow and Water-Oil emulsions," *10th International Conference of Multiphase Flow, Rio de Janeiro, Brasil*, vol. (1), no. July, p. 51, 2019.

[99] J. P. Valdés, M. Asuaje, and N. Ratkovich, "Study of an ESP's performance handling liquid-liquid flow and unstable O-W emulsions part II: Coupled CFD-PBM modelling," *Journal of Petroleum Science and Engineering*, vol. 198, no. November 2020, p. 108227, 2021. [Online]. Available: https://doi.org/10.1016/j.petrol.2020.108227

[100] H. Banjar, J. Zhu, and H. Q. Zhang, "CFD simulations of oil viscosity and emulsion effects on ESP stage performance," *Society of Petroleum Engineers - Abu Dhabi International Petroleum Exhibition and Conference 2020, ADIP 2020*, 2020.

[101] E. Guerrero, F. Muñoz, and N. Ratkovich, "Comparison between eulerian and vof models for two-phase flow assessment in vertical pipes," *CTyF - Ciencia, Tecnologia y Futuro*, vol. 7, no. 1, pp. 73–84, 2017.

[102] D. Ramkrishna, *Population Balances Theory and Applications to Particulate Systems in Engineering.* ACADEMIC PRESS, 2000.

[103] T. T. Nguyen, F. Laurent, R. O. Fox, and M. Massot, "Solution of population balance equations in applications with fine particles: Mathematical modeling and numerical schemes," *Journal of Computational Physics*, vol. 325, pp. 129–156, 2016.

[104] S. Fathi Roudsari, G. Turcotte, R. Dhib, and F. Ein-Mozaffari, "CFD modeling of the mixing of water in oil emulsions," *Computers and Chemical Engineering*, vol. 45, pp. 124–136, 2012. [Online]. Available: http://dx.doi.org/10.1016/j.compchemeng.2012.06.013

[105] G. H. Yeoh, C. P. Cheung, and J. Tu, *Multiphase Flow Analysis Using Population Balance Modeling: Bubbles, Drops and Particles*, 2014.

[106] T. Wennberg, *Transporting Highly Concentrated Slurries with Centrifugal Pumps*, 2010.

[107] S. L. Dixon and C. Hall, *Fluid mechanics and thermodynamics of turbomachinery.* Butterworth-Heinemann, 2013.

[108] A. Kara Omar, A. Khaldi, and A. Ladouani, "Prediction of centrifugal pump performance using energy loss analysis," *Australian Journal of Mechanical Engineering*, vol. 15, no. 3, pp. 210–221, 2017. [Online]. Available: http://dx.doi.org/10.1080/14484846.2016.1252567

[109] Natália Argene Lovate Pereira Fleischfresser, Jorge Luiz Biazussi, and Antonio Carlos Bannwart, "Correlations for the prediction of the head curve of centrifugal pumps based on experimental data," in *Proceedings of the 23rd ABCM International Congress of Mechanical Engineering*, no. August 2017, 2015.

[110] M. A. El-Naggar, "A one-dimensional flow analysis for the prediction of centrifugal pump performance characteristics," *International Journal of Rotating Machinery*, vol. 2013, no. 1, 2013.

[111] J. F. Gülich, *Centrifugal pumps*, 2014, vol. 9783642401.

[112] W. G. Li, "Blade exit angle effects on performance of a standard industrial centrifugal oil pump," *Journal of Applied Fluid Mechanics*, vol. 4, no. 3, pp. 105–119, 2011.

[113] J. P. Valdés, D. Becerra, D. Rozo, A. Cediel, F. Torres, M. Asuaje, and N. Ratkovich, "Comparative analysis of an electrical submersible pump's performance handling viscous Newtonian and non-Newtonian fluids through experimental and CFD approaches," *Journal of Petroleum Science and Engineering*, vol. 187, no. November 2019, 2020.

[114] M. Liu, L. Tan, and S. Cao, "Theoretical model of energy performance prediction and BEP determination for centrifugal pump as turbine," *Energy*, vol. 172, pp. 712–732, 2019. [Online]. Available: https://doi.org/10.1016/j.energy.2019.01.162

[115] F. Liu, "A thorough description of how wall functions are implemented in openfoam," *Proceedings of CFD with OpenSource Software*, vol. 34, 2016.

[116] F. Moukalled, L. Mangani, M. Darwish, F. Moukalled, L. Mangani, and M. Darwish, *The finite volume method*. Springer, 2016.

[117] J. H. Ferziger, M. Perić, and R. L. Street, *Computational methods for fluid dynamics*. Springer, 2002, vol. 3.

[118] X. He, W. Jiao, C. Wang, and W. Cao, "Influence of Surface Roughness on the Pump Performance Based on Computational Fluid Dynamics," *IEEE Access*, vol. 7, pp. 105 331–105 341, 2019.

[119] C. Wang, W. Shi, X. Wang, X. Jiang, Y. Yang, W. Li, and L. Zhou, "Optimal design of multistage centrifugal pump based on the combined energy loss model and computational fluid dynamics," *Applied Energy*, vol. 187, pp. 10–26, 2017. [Online]. Available: http://dx.doi.org/10.1016/j.apenergy.2016.11.046

[120] J. Zhu, H. Zhu, J. Zhang, and H. Q. Zhang, "A numerical study on flow patterns inside an electrical submersible pump (ESP) and comparison with visualization experiments," *Journal of Petroleum Science and Engineering*, vol. 173, no. October 2018, pp. 339–350, 2019. [Online]. Available: https://doi.org/10.1016/j.petrol.2018.10.038

[121] L. Achour, M. Specklin, I. Belaidi, and S. Kouidri, "Numerical Study of the Performance Loss of A Centrifugal Pump Carrying Emulsion," *E3S Web of Conferences*, vol. 321, p. 01010, 2021.

[122] Z. Li, Z. Wang, X. Wei, and D. Qin, "Flow similarity in the rotor–stator interaction affected region in prototype and model francis pump-turbines in generating mode," *Journal of Fluids Engineering*, vol. 138, no. 6, 2016.

[123] W. G. Li, "Effects of flow rate and viscosity on slip factor of centrifugal pump handling viscous oils," *International Journal of Rotating Machinery*, vol. 2013, no. November, 2013.

[124] F. J. Wiesner, "A review of slip factors for centrifugal impellers," *Journal of Engineering for Gas Turbines and Power*, vol. 89, no. 4, pp. 558–566, 1967.

[125] Y. D. Choi, J. Kurokawa, and J. Malsui, "Performance and internal flow characteristics of a very low specific speed centrifugal pump," *Journal of Fluids Engineering, Transactions of the ASME*, vol. 128, no. 2, pp. 341–349, 2006.

[126] W. G. Li, "Effects of flow rate and viscosity on slip factor of centrifugal pump handling viscous oils," *International Journal of Rotating Machinery*, vol. 2013, no. November, 2013.

[127] G. Fortuny, J. Herrero, D. Puigjaner, C. Olivé, F. Marimon, J. Garcia-Bennett, and D. Rodríguez, "Effect of anticoagulant treatment in deep vein thrombosis: a patient-specific computational fluid dynamics study," *Journal of Biomechanics*, vol. 48, no. 10, pp. 2047–2053, 2015.

[128] P. Thanapandi and R. Prasad, "Performance prediction and loss analysis of low specific speed submersible pumps," *Proceedings of the Institution of Mechanical Engineers, Part A: Journal of Power and Energy*, vol. 204, no. 4, pp. 243–252, 1990.

[129] L. Zhou, J. Hang, L. Bai, Z. Krzemianowski, M. A. El-emam, E. Yasser, and R. Agarwal, "Application of Entropy Production Theory for Energy Losses and other Investigation in Pumps and Turbines: A ReviewAPEN-D-21-11938," *Applied Energy*, vol. 318, no. December 2021, p. 119211, 2022. [Online]. Available: https://doi.org/10.1016/j.apenergy.2022.119211

[130] L. Ji, W. Li, W. Shi, H. Chang, and Z. Yang, "Energy characteristics of mixed-flow pump under different tip clearances based on entropy production analysis," *Energy*, vol. 199, p. 117447, 2020. [Online]. Available: https://doi.org/10.1016/j.energy.2020.117447

[131] J. Cao, J. Pei, Y. Gu, W. Wang, and S. Yuan, "Flow losses analysis in a mixed flow pump with annular volute by entropy production evaluation," *IOP Conference Series: Earth and Environmental Science*, vol. 240, no. 3, 2019.

[132] S. Shen, Z. Qian, and B. Ji, "Numerical analysis of mechanical energy dissipation for an axial-flow pump based on entropy generation theory," *Energies*, vol. 12, no. 21, 2019.

[133] Y. Gu, J. Pei, S. Yuan, W. Wang, F. Zhang, P. Wang, D. Appiah, and Y. Liu, "Clocking effect of vaned diffuser on hydraulic performance of high-power pump by using the numerical flow loss visualization method," *Energy*, vol. 170, pp. 986–997, 2019. [Online]. Available: https://doi.org/10.1016/j.energy.2018.12.204

[134] B. Yang, B. Li, H. Chen, and Z. Liu, "Entropy production analysis for the clocking effect between inducer and impeller in a high-speed centrifugal pump," *Proceedings of the Institution of Mechanical Engineers, Part C: Journal of Mechanical Engineering Science*, vol. 233, no. 15, pp. 5302–5315, 2019.

[135] Q. Deng, J. Pei, W. Wang, B. Lin, C. Zhang, and J. Zhao, "Energy loss and radial force variation caused by impeller trimming in a double-suction centrifugal pump," *Entropy*, vol. 23, no. 9, 2021.

[136] H. Chang, W. Shi, W. Li, and J. Liu, "Energy Loss Analysis of Novel Self-Priming Pump Based on the Entropy Production Theory," *Journal of Thermal Science*, vol. 28, no. 2, pp. 306–318, 2018.

[137] L. Ji, W. Li, W. Shi, F. Tian, and R. Agarwal, "Effect of blade thickness on rotating stall of mixed-flow pump using entropy generation analysis," *Energy*, vol. 236, p. 121381, 2021. [Online]. Available: https://doi.org/10.1016/j.energy.2021.121381

[138] B. Qian, J. P. Chen, P. Wu, D. Z. Wu, P. Yan, and S. Y. Li, "Investigation on inner flow quality assessment of centrifugal pump based on Euler head and entropy production analysis," *IOP Conference Series: Earth and Environmental Science*, vol. 240, no. 9, 2019.

[139] H. Hou, Y. Zhang, and Z. Li, "A numerical research on energy loss evaluation in a centrifugal pump system based on local entropy production method," *Thermal Science*, vol. 21, no. 3, pp. 1287–1299, 2017.

[140] X. Zhao, Z. Wang, Y. Xiao, and Y. Luo, "Thermodynamic analysis of energy dissipation and unsteady flow characteristic in a centrifugal dredge pump under over-load conditions," *Proceedings of the Institution of Mechanical Engineers, Part C: Journal of Mechanical Engineering Science*, vol. 233, no. 13, pp. 4742–4753, 2019.

[141] Y. Zhang, H. Hou, C. Xu, W. He, and Z. Li, "Application of entropy production method to centrifugal pump energy loss evaluation," *Paiguan Jixie Gongcheng Xuebao/Journal of Drainage and Irrigation Machinery Engineering*, vol. 35, no. 4, 2017.

[142] R. Gong, H. Wang, L. Chen, D. Li, H. Zhang, and X. Wei, "Application of entropy production theory to hydro-turbine hydraulic analysis," *Science China Technological Sciences*, vol. 56, no. 7, pp. 1636–1643, 2013.

[143] D. Li, Y. Qin, Z. Zuo, H. Wang, S. Liu, and X. Wei, "Numerical Simulation on Pump Transient Characteristic in a Model Pump Turbine," *Journal of Fluids Engineering, Transactions of the ASME*, vol. 141, no. 11, 2019.

[144] D. Li, R. Gong, H. Wang, G. Xiang, X. Wei, and D. Qin, "Entropy production analysis for hump characteristics of a pump turbine model," *Chinese Journal of Mechanical Engineering (English Edition)*, vol. 29, no. 4, pp. 803–812, 2016.

[145] M. M. Ghorani, M. H. Sotoude Haghighi, A. Maleki, and A. Riasi, "A numerical study on mechanisms of energy dissipation in a pump as turbine (PAT) using entropy generation theory," *Renewable Energy*, vol. 162, pp. 1036–1053, 2020. [Online]. Available: https://doi.org/10.1016/j.renene.2020.08.102

[146] A. Yu, Q. Tang, H. Chen, and D. Zhou, "Investigations of the thermodynamic entropy evaluation in a hydraulic turbine under various operating conditions," *Renewable Energy*, vol. 180, pp. 1026–1043, 2021.

[147] J. Zhu, H. Zhu, G. Cao, J. Zhang, J. Peng, H. Banjar, and H. Q. Zhang, "A new mechanistic model to predict boosting pressure of electrical submersible pumps under high-viscosity fluid flow with validations by experimental data," *SPE Journal*, vol. 25, no. 2, pp. 744–758, 2020.

[148] L. Ji, W. Li, W. Shi, F. Tian, and R. Agarwal, "Diagnosis of internal energy characteristics of mixed-flow pump within stall region based on entropy production analysis model," *International Communications in Heat and Mass Transfer*, vol. 117, p. 104784, 2020. [Online]. Available: https://doi.org/10.1016/j.icheatmasstransfer.2020.104784

[149] A. Mwesigye, T. Bello-Ochende, and J. P. Meyer, "Numerical investigation of entropy generation in a parabolic trough receiver at different concentration ratios," *Energy*, vol. 53, pp. 114–127, 2013. [Online]. Available: http://dx.doi.org/10.1016/j.energy.2013.03.006

[150] F. Lai, X. Zhu, and G. Li, "Numerical investigation of energy loss in a centrifugal pump through kinetic energy dissipation theory," *Proceedings of the Institution of Mechanical Engineers, Part C: Journal of Mechanical Engineering Science*, vol. 234, no. 19, pp. 3745–3761, 2020.

[151] F. Zhang, D. Appiah, F. Hong, J. Zhang, S. Yuan, K. A. Adu-Poku, and X. Wei, "Energy loss evaluation in a side channel pump under different wrapping angles using entropy production method," *International Communications in Heat and Mass Transfer*, vol. 113, no. February, p. 104526, 2020. [Online]. Available: https://doi.org/10.1016/j.icheatmasstransfer.2020.104526

[152] V. Oruganti, H. Grimler, and E. Ghahramani, "Implementation of cavitation models into the multiphaseeulerfoam solver," *Proc. of CFD with OpenSource Software*, 2017.

[153] K. Feigl, A. Baniabedalruhman, F. X. Tanner, and E. J. Windhab, "Numerical simulations of the breakup of emulsion droplets inside a spraying nozzle," *Physics of Fluids*, vol. 28, no. 12, p. 123103, 2016.

[154] M. Manafpour and H. Ebrahimnezhadian, "The multiphase capability of openfoam cfd toolbox in solving flow field in hydraulic structure," in *Proceedings of the 4th International Conference on Long-Term Behavior and Eco-Friendly Dams, Tehran, Iran*, 2017, pp. 17–19.

[155] N. Basha, A. Kovacevic, and S. Rane, "Analysis of oil-injected twin-screw compressor with multiphase flow models," *Designs*, vol. 3, no. 4, p. 54, 2019.

[156] J. Zhu and H.-Q. Zhang, "Numerical study on electrical-submersible-pump two-phase performance and bubble-size modeling," *SPE Production & Operations*, vol. 32, no. 03, pp. 267–278, 2017.

[157] E. A. Afolabi and J. Lee, "An eulerian-eulerian cfd simulation of air-water flow in a pipe separator," *The Journal of Computational Multiphase Flows*, vol. 6, no. 2, pp. 133–149, 2014.

[158] S. Shahid, A. Q. Hasan, M. S. Gadala *et al.*, "A review on electrical submersible pump head losses and methods to analyze two-phase performance curve," 2021.

[159] R. Tarodiya and B. K. Gandhi, "Numerical simulation of a centrifugal slurry pump handling solid-liquid mixture: Effect of solids on flow field and performance," *Advanced Powder Technology*, vol. 30, no. 10, pp. 2225–2239, 2019.

[160] C. Li and Q. Huang, "Rheology-based computational fluid dynamics modeling for de-oiling hydrocyclone efficiency," *Chemical Engineering & Technology*, vol. 39, no. 5, pp. 899–908, 2016.

[161] B. Tan, M. Lan, L. Li, Y. Wang, and T. Qi, "Drop size correlation and population balance model for an agitated-pulsed solvent extraction column," *AIChE Journal*, vol. 66, no. 8, p. e16279, 2020.

[162] R. Lehnigk, W. Bainbridge, Y. Liao, D. Lucas, T. Niemi, J. Peltola, and F. Schlegel, "An open-source population balance modeling framework for the simulation of polydisperse multiphase flows," *AIChE Journal*, vol. 68, no. 3, p. e17539, 2022.

[163] B. Andersson, R. Andersson, L. Håkansson, M. Mortensen, R. Sudiyo, and B. Van Wachem, *Computational fluid dynamics for engineers*. Cambridge university press, 2011.

[164] Y. Liu, "Two-fluid modeling of gas-solid and gas-liquid flows: solver development and application," Ph.D. dissertation, München, Technische Universität München, Diss., 2014, 2014.

[165] Q. Si, Q. Cui, K. Zhang, J. Yuan, and G. Bois, "Investigation on centrifugal pump performance degradation under air-water inlet two-phase flow conditions," *La Houille Blanche*, no. 3, pp. 41–48, 2018.

Lila ACHOUR

Modélisation du comportement hydrodynamique des pompes pour des fluides au comportement rhéologique complexe

Résumé : Les travaux de recherche de la thèse portent sur le pompage de fluides au comportement rhéologique complexe. L'objectif de la thèse est d'effectuer une analyse exhaustive des performances et des caractéristiques d'écoulement interne d'une pompe centrifuge à volute lors du traitement d'émulsions non newtoniennes complexes. Les applications industrielles dans ce domaine sont nombreuses et peuvent inclure le pompage d'émulsions de pétrole brut, le pompage d'eaux usées, et les émulsions cosmétiques et alimentaires. Deux éléments se combinent pour expliquer la complexité de ce problème scientifique : le premier concerne la pompe et sa géométrie tridimensionnelle avec un fort couplage avec la boucle. Le second concerne le comportement rhéologique non linéaire et instable du fluide pompé, en particulier lorsque la pompe transporte une fraction réduite de la phase continue. Ces écoulements concernent des fluides au comportement non newtonien et particulièrement instable. Les connaissances nécessaires à leur compréhension sont parfois à la limite de la chimie avec des approches à l'échelle moléculaire. Dans ce travail, plusieurs approches ont été utilisées pour étudier le comportement hydrodynamique de la pompe sous écoulement d'émulsion : une approche analytique, une simulation CFD monophasique et une simulation CFD diphasique. L'approche analytique est basée sur un modèle mécaniste pour la détermination de la viscosité de l'émulsion en fonction des conditions de fonctionnement de la pompe, qui est ensuite couplé à un modèle mécaniste basé sur les différentes pertes rencontrées dans les pompes à volute. La simulation monophasique est basée sur une étude CFD dans laquelle le comportement rhéologique des émulsions a été considéré en négligeant la nature diphasique du fluide, et l'étude diphasique qui considère les deux fluides et les différentes interactions entre les phases. Les approches adoptées appartiennent à deux catégories distinctes ; l'approche analytique permet de différencier les pertes au sein de la pompe centrifuge, ce qui n'est pas le cas pour la CFD. Cette lacune est toutefois compensée par l'analyse entropique, qui permet de localiser les pertes d'énergie. Enfin, la capacité des deux approches CFD considérées à prédire avec précision les performances des pompes véhiculant des émulsions est évaluée en comparant les résultats numériques d'une pompe multicellulaire (ESP) avec les données expérimentales correspondantes.

Mots clés : pompe centrifuge, fluide complexe, modélisation hydrodynamique, CFD, non-Newtonian